Antarctic ice-sheet expansions in the Middle Miocene and Pliocene

Dissertation zur Erlangung des
Doktorgrades der Naturwissenschaften
am Fachbereich Geowissenschaften
der Universität Bremen

vorgelegt von

Petra Langebroek

Oktober 2008

Betreuer und 1. Gutachter:	**Herr Prof. Dr. M. Schulz**
2. Gutachter:	**Herr Prof. Dr. R. Tiedemann**
1. Weiterer Prüfer:	**Herr Prof. Dr. H. Willems**
2. Weiterer Prüfer:	**Herr Prof. Dr. D. Hebbeln**
1. Weiteres Mitglied der Universität:	**Herr Dr. A. Paul**
2. Weiteres Mitglied der Universität:	**Frau L. Cristini (AWI, Bremerhaven)**
Tag des öffentlichen Kolloquiums:	**12.12.2008**

Name:	Petra Langebroek	Datum:	17. Oktober 2008
Anschrift:	Jahnstrasse 1 28201 Bremen Deutschland		

Erklärung

Hiermit versichere ich, dass ich

1. die Arbeit ohne unerlaubte fremde Hilfe angefertigt habe,

2. keine anderen als die von mir angegebenen Quellen und Hilfsmittel benutzt habe und

3. die den benutzten Werken wörtlich oder inhaltlich entnommenen Stellen als solche kenntlich gemacht habe.

Bremen, den 17. Oktober 2008

For my parents,
who always encouraged
my interest in the world.

Once, long ago, Sun was the ruler of all the earth. Next to him, the other spirits were as the sparrow beside the grizzly bear. So the spirits had a secret meeting and elected the water spirit to approach Sun, to persuade him to give up some of his power.

Water went to Sun, and formed a clear, deep pool at his feet. When Sun saw his own face reflected in the pool, he was so delighted that he promised Water anything she wanted. When she demanded some of his power, he realized he had been tricked, but according to his word, he gave power to all of the other spirits. Water, for her part, got more than anyone, and became, next to Sun, the most powerful force on earth.

As soon as the Water received her power, she went laughing and dancing through the hills, carrying pieces of land off to the sea until the landscape was filled with canyons of Water's making. Seeing that the rugged mountainous terrain Water sculpted made the world he created more beautiful, Sun became jealous and turned his face away from the earth.

Deprived of Sun's warmth, Water froze, her power locked in icy chains. Being very sly, Water allowed her icy form to build up in the high mountains, until slowly, slowly, the ice moved down the valleys, tearing the earth as it went. In this way, Water put the finishing touches on her mountain landscape, smoothing out the canyons into broad valleys. Seeing that Water had once more outwitted him, Sun relented and smiled again upon the earth.

Freed from the great age of ice, Water sang down the mountain faces and through her valleys once again. But, she kept some of her ice high in the mountains, safely out of reach of Sun. From one of these ice masses, she sent forth waterfalls to tumble with awesome power down the side of one of her valleys, reminding the world of her still-great power.

But even to this day, at the end of the summer, Sun begins to turn his face away to show Water that he is still ruler of all the earth. Water's flow decreases to hardly a trickle, and finally that freezes into an icy castle. Thus, although the mountain landscape was carved by Water, Sun still rules.

- *modified after Canada's Yoho National Park staff (written in ~1970)*

Contents

Acknowledgements

The financial support for this three-year project was provided by the Deutsche Forschungsgemeinschaft within the European Graduate College 'Proxies in Earth History' (EUROPROX). The work itself was carried out at the Geosciences Department of the University of Bremen, in Germany. I am grateful for the possibilities EUROPROX and the University of Bremen gave me to attend to several (international) courses, workshops and conferences.

The first time I arrived in Bremen was on a cold day in the beginning of the year 2005. That day, during the interview, two main things made me quickly accept the offer to start a PhD in the modeling research group of the University of Bremen: first, the enormous enthusiasm that Prof. Dr. Michael Schulz and Dr. André Paul showed for the project and second, the nice ambiance in the research group. These two factors luckily never changed.

Michael and André always continued to show large interest in my work. I would like to thank André especially for his daily support. Without his great knowledge of physic and good guidance with implementing these processes in a numerical model, the development of the model would have been a very hard, maybe even impossible, job. To Michael I am grateful for his broader supervision. His ability to identify important ideas or problems often let me see my work from a different perspective, thereby always largely improving the scientific content.

Also the ambiance in the research group continued to be very friendly and relaxed, thereby providing a great working environment. I would like to thank the entire 'palmod' group for all the interesting conversations, lively discussions and tasty cakes during lunches and coffee breaks. Many special thanks to Dr. Andreas Manschke, not only for solving many of my computer problems, but also for always being ready to help, normally accompanied with a smile (or a piece of apple). Dr. Matthias Prange I would like to thank for the nice cooperation and brilliant conversations, which resulted in a very interesting third manuscript.

During my PhD I also spend a few months working at the Institute for Marine and Atmospheric research Utrecht. I would like to thank my colleagues there for making these months so well spend, on a personal as well as scientific level. I am especially touched by the continuation of this support and guidance, even after I returned back to Bremen. Above all, I am grateful for the support of Prof. Dr. Hans Oerlemans. Although our contact was not very regular, his positive attitude and trust in my work always stimulated me. The course 'Ice sheets and glaciers in the climate system' organized by Hans and the IMAU, in the picturesque village of Karthaus, did not only give me the opportunity to learn from ice-sheet (modeling) experts, but also brought me in contact with many cryosphere scientists from all over the world.

It is not only in Bremen and Utrecht that I received scientific support. I also would like to acknowledge all the scientists I met at meetings, workshops and conferences that showed interest in my research and asked (provoking) questions. Their comments and discussions largely inspired me and broadened my scientific thinking.

Special thanks also to Markus Raitzsch, Martijn Deenen, Dr. Stijn De Schepper and Dr. David Heslop for helping me with the abstracts in this thesis.

All this work I could not have done without the friends I found here in Bremen. Thank you for all the 'last ones' and making Bremen a sunny city for me. Likewise, I would like to express my gratitude to my friends in the Netherlands. Despite the distance they were always there for me. Their support and faith in me means a lot to me.

Last I would like to thank my family. My parents always largely encouraged my curiosity in the world surrounding us. Even when my siblings and I were little, we traveled around the world, stimulating our interest in other countries and cultures. The story in the beginning of this thesis is a remnant of one of our travels in the Canadian Rocky Mountains. To thank them for all their love and support, I dedicate this thesis to them.

Petra Langebroek
Bremen, Germany
17. October 2008

Abstract

This study focuses on the interactions between climate and ice sheets in order to obtain a better understanding of the processes involved. Two periods in the geological past are explored; the Middle Miocene and the mid-Pliocene. For both periods, foraminiferal oxygen-isotope records from deep-sea sediment cores as well as stratigraphical data, suggest a global sea-level lowering. The magnitude of these reductions in sea level indicate large-scale ice-sheet build-up. However, the origin of these events and even the geographic locations of the ice sheets, are still under discussion.

The ice sheet-climate model developed in this study provides a tool to test some of the hypotheses brought forward to explain the ice-sheet expansion events. It describes the Antarctic ice sheet and is forced by a climate component based on energy and mass balances. Further more, the model computes the oxygen-isotopic composition of the ice-sheet, thereby providing the possibility to compare numerical results directly to deep-sea sediment records. Numerical experiments focus on the interactions between atmospheric CO_2, temperature, ice volume (sea-level equivalent) and the isotopic composition of sea water.

Among the proposed causes for the ice-sheet expansion in the Middle Miocene is a decrease in atmospheric CO_2, possibly in combination with orbital forcing. The ice-sheet sensitivity to atmospheric CO_2 was tested in several scenarios using either a constant or a decreasing CO_2 forcing. It is shown that orbital variations by themselves, without change in atmospheric CO_2, were insufficient to induce an Antarctic ice-sheet expansion in the Middle Miocene. Small, ephemeral ice sheets occurred under relatively high atmospheric CO_2 conditions; whereas a largely glaciated Antarctic existed under low CO_2. The atmospheric CO_2 threshold between the two ice-sheet states was approximately 400 ppm. Atmospheric levels likely crossed this threshold around 13.9 million years ago, where after a minimum in summer insolation produced the final trigger to initiate the large-scale ice-sheet expansion.

By including a description of oxygen isotopes in the ice sheet-climate model, the modeled isotopic composition of sea water could be compared to high-resolution benthic foraminiferal records. The modeled transition to a large ice sheet, induced by a drawdown of atmospheric CO_2, explains the entire increase in oxygen isotopes recorded by the sediment records during the Middle Miocene.

The simulation of ice-sheet volume and isotopic composition in a single model provides a unique opportunity to investigate the relationship between sea level and isotopic composition of sea water. The experiments confirm the validity of the often applied ratio of a 1 ‰ increase in oxygen-isotope composition for a global sea-level lowering of 100 m. Small (large) ice sheets, however, have a slightly smaller (larger) relative effect on the isotopic seawater composition, due to their less (more) depleted isotopic ratio of ice.

For the mid-Pliocene, the ice-sheet component was forced by temperatures and accumulation rates from a comprehensive climate model. The closure of the Panamanian gateway in the mid-Pliocene was found to induce an intensification of the meridional circulation with a cooling over Antarctica as result. In turn, this cooling forced the Antarctic ice-sheet to expand. The consequent global sea-level drop could explain up to 60 % of the proposed long-term sea-level lowering in the mid-Pliocene.

From the examples discussed in this study it can be concluded that changes in temperature, due to atmospheric CO_2 as well as due to tectonic forcing, have a large impact on the extent of the Antarctic ice sheet.

Zusammenfassung (German abstract)

Diese Arbeit konzentriert sich auf die Wechselwirkungen zwischen dem Klima und den Eisschilden, um ein besseres Verständnis von den daran beteiligten Prozessen zu bekommen. Es werden zwei Zeitabschnitte der geologischen Vergangenheit behandelt: das mittlere Miozän und das mittlere Pliozän. Beide Zeitabschnitte wurden von globalen Meeresspiegelabsenkungen begleitet, worauf stabile Sauerstoffisotope in Foraminiferen aus Tiefseesedimenten und stratigraphische Daten hindeuten. Das Ausmaß dieser Meerespiegelabsenkungen weist auf die Bildung von mächtigem Inlandeis hin. Jedoch werden der Ursprung dieser Ereignisse und sogar die geographische Lage der Eisschilde noch immer debattiert.

Das in dieser Studie entwickelte Eisschild-Klima-Modell bietet die Möglichkeit, einige der vorgebrachten Hypothesen über die Ausdehnungsereignisse der Eisschilde zu überprüfen. Es beschreibt die antarktische Eisdecke und wird durch eine auf Energie- und Massenbilanzierung basierende Klima-Komponente angetrieben. Weiterhin berechnet das Modell die Zusammensetzung der Sauerstoffisotope im Inlandeis und bietet damit die Möglichkeit, die numerischen Ergebnisse direkt mit den Datensätzen aus Tiefseesedimenten zu vergleichen. Die numerischen Experimente konzentrierten sich auf die Wechselbeziehungen zwischen atmosphärischem CO_2, Temperatur, Eisvolumen (gleichwertig mit Meeresspiegel) und der Isotopenzusammensetzung des Meerwassers.

Als Ursache für die Eisschildausdehnung im mittleren Miozän wurde unter anderem eine Abnahme des atmosphärischen CO_2 genannt, die möglicherweise mit orbitalen Schwankungen einherging. Die Empfindlichkeit des Inlandeises gegenüber atmosphärischem CO_2 wurde in mehreren Szenarien überprüft, indem der CO_2-Antrieb entweder konstant gehalten oder reduziert wurde. Es zeigt sich, dass orbitale Änderungen an sich ohne Änderungen der Kohlendioxidkonzentration nicht ausgereicht hätten, um die Ausdehnung des antarktischen Eisschildes im mittleren Miozän zu verursachen. Kleine Eisschilde von kurzer Lebensdauer traten bei verhältnismäßig hohen atmosphärischen CO_2-Bedingungen auf, wohingegen bei niedriger CO_2-Konzentration eine weitgehend vereiste Antarktis existierte. Der CO_2-Schwellenwert zwischen den beiden Eisschild-Zuständen beträgt ungefähr 400 ppm. Die Konzentration in der Atmosphäre hat wahrscheinlich diesen Schwellenwert vor ungefähr 13,9 Millionen Jahren überschritten und nach einem Minimum in der sommerlichen Sonneneinstrahlung letztendlich die umfangreiche Eisschildausdehnung ausgelöst.

Indem eine Beschreibung der Sauerstoffisotope in das Eisschild-Klima-Modell aufgenommen wurde, konnte die modellierte Isotopenzusammensetzung des Meerwassers mit hochauflösenden, auf Foraminiferen basierenden Datensätzen verglichen werden. In dem Modell könnte der Übergang zu einem großen Eisschild, der durch eine Abnahme der atmosphärischen Kohlendioxidkonzentration hervorgerufen wurde, den gesamten Anstieg des Sauerstoffisotopen verhältnisses im Sediment des mittleren Miozäns erklären.

Die Simulation von Eisschildvolumen und Isotopenzusammensetzung in einem einzelnen Modell bietet die einzigartige Möglichkeit, die Beziehung zwischen Meeresspiegel und der Isotopenzusammensetzung des Meerwassers zu untersuchen. Die Modellexperimente in dieser Arbeit bestätigen, dass das häufig verwendete Verhältnis von 1 ‰ Zuwachs zu einer globalen Meeresspiegelabsenkung von 100 m stichhaltig ist. Kleine (große) Eisschilde haben dennoch aufgrund ihrer geringeren (höheren) Verringerung des Isotopenverhältnisses einen geringfügig kleineren (größeren) relativen Effekt auf die Isotopenzusammensetzung des Meerwassers.

Für das mittlere Pliozän wurde die Eisschild-Komponente durch Temperatur und Akkumulationsraten aus einem umfassenden Klimamodell forciert. Es stellte sich heraus, dass die Schließung des zentralamerikanischen Seewegs im mittleren Pliozän die meridionale Zirkulation verstärkte, was eine Abkühlung über der Antarktis zur Folge hatte. Diese Abkühlung wiederum führte zur Ausdehnung des antarktischen Eisschildes. Der damit verbundene globale Meeresspiegelabfall könnte bis zu 60 % der langfristigen Meeresspiegelabsenkung im mittleren Pliozän erklären.

Aus den in dieser Arbeit diskutierten Beispielen kann gefolgert werden, dass infolge Änderungen des atmosphärischen Kohlendioxids als auch tektonischer Prozesse auftretende Temperaturänderungen großen Einfluss auf die Größe des antarktischen Eisschildes haben.

Samenvatting (Dutch abstract)

Dit onderzoek richt zich op de interactie tussen klimaat en ijskappen met de bedoeling een beter inzicht te krijgen in de achterliggende processen. Twee dynamische perioden uit het geologische verleden worden onderzocht: het Midden Mioceen (ongeveer 13.9 miljoen jaar geleden) en het Midden Plioceen ($\sim$ 3 miljoen jaar geleden). Variaties in zuurstofisotopen verhoudingen van benthische foraminifera en stratigrafische data wijzen erop dat in beide perioden een wereldwijde zeespiegeldaling heeft plaats gevonden. De magnitude van de zeespiegeldaling suggereert dat er grootschalige ijskappen moeten zijn opgebouwd. Desalniettemin is er nog veel discussie over de oorsprong en achterliggende processen van deze ijskap expansies.

Met het ijskap-klimaat model ontwikkeld tijdens dit onderzoek, is het mogelijk om hypothesen aangaande ijskap expansies te testen. Het model beschrijft de Antarctische ijskap en wordt geforceerd door een klimaatcomponent gebaseerd op energie en massa balansen. Daarnaast berekent het model de zuurstofisotopen compositie van de ijskap waardoor het mogelijk wordt om de gemodelleerde numerieke resultaten direct te vergelijken met waarden verkregen uit diepzee sedimentkernen. De model simulaties focussen op de interactie tussen atmosferische CO_2, temperatuur, ijsvolume (direct gelinkt aan het niveau van de zeespiegel) en de isotopen samenstelling van het zeewater.

Een voorgestelde oorzaak voor de ijskapgroei in het Midden Mioceen is een afname van atmosferische CO_2, al dan niet in combinatie met *orbital forcing* (variaties in de aardbaan ten opzichte van de zon). De gevoeligheid van de ijskap voor atmosferische CO_2 is aan de hand van verschillende scenarios (zowel een constante als een afnemende CO_2 forcering) getest. Hieruit bleek dat orbital forcing alleen, dus zonder variaties in atmosferische CO_2, niet voldoende was om de ijskap expansie op Antarctica in het Midden Mioceen te verklaren. Kleine, tijdelijke ijskappen konden bestaan onder relatief hoge atmosferische CO_2 condities, terwijl bij lage CO_2 waarden Antarctica grotendeels met een ijskap is bedekt. De drempelwaarde tussen voorgenoemde situaties ligt bij ongeveer 400 ppm. Atmosferische waarden moeten rond 13.9 miljoen jaar geleden onder deze grens zijn gedaald, waarna een minimum in zomer insolatie de ideale condities veroorzaakten om de ijskappen op grote schaal te laten uitbreiden.

Door het traceren van zuurstofisotopen in het ijskap-klimaat model was het mogelijk om de gemodelleerde isotopische samenstelling van het zeewater direct te vergelijken met de waarden die bekend zijn uit de foraminifera studies. De gemodelleerde overgang naar een ijskap expansie op Antarctica, veroorzaakt door een verlaagde atmosferische CO_2 waarde, kan de geobserveerde stijging in zuurstofisotopen van foraminifera uit het Midden Mioceen volledig verklaren.

Het simuleren van het ijskapvolume en de isotopische samenstelling van het ijs binnen een enkel model zorgt voor de unieke gelegenheid om het verband tussen zeespiegelniveau en de isotopische samenstelling van het zeewater te onderzoeken. De model experimenten bevestigen de alom gebruikte waarden van 1 ‰ stijging in de zuurstof-isotopen verhouding bij een zeespiegeldaling van 100 m. Kleine ijskappen hebben echter een relatief klein effect op isotopische compositie van het zeewater vanwege de zwaardere isotopische compositie van het ijs. Grote ijskappen zijn daarentegen relatief licht in zuurstofisotopische samenstelling en hebben een relatief groot effect op de isotopen verhouding van het zeewater.

Voor simulaties van de Midden Pliocene ijskap werd het model geforceerd door temperaturen en sneeuw-accumulatie verkregen uit een complex klimaat model. De sluiting van de Panama zeestraat in het Midden Plioceen veroorzaakte een meer intense meridionale circulatie. Dit leidde tot een afkoeling van het Antarctische continent en tot de expansie van de Antarctische ijskap. De zeespiegeldaling ten gevolge van deze expansie kan tot 60 % van de veronderstelde lange termijn zeespiegeldaling in het midden Plioceen verklaren.

Uit de voorbeelden die besproken worden in dit proefschrift kan worden geconcludeerd dat veranderingen in temperatuur als gevolg van zowel veranderingen in atmosferische CO_2 als tektonische forcering een groot effect hebben op de Antarctische ijskap.

Chapter 1

Introduction

1.1 Climate and ice sheets

The climate of the Earth is in a perpetual change. The long-term trend over the last 65 million years (65 Ma), the Cenozoic period, is dominated by a transition from a warm, ice-free greenhouse world into a colder, largely glaciated ice-house world (*Zachos et al.*, 2001, 2008). Extreme warm and cold periods override this gradual cooling in the Cenozoic. Climatic optima reigned the Eocene, but also occurred in the Miocene (Fig. 1.1). Abrupt cooling events dominate the later part of the Cenozoic, starting with the major step at the Eocene-Oligocene boundary, where large continental ice sheets started to evolve on Antarctica (*Shackleton*, 1986; *Zachos et al.*, 1994; *Lear et al.*, 2000; *Coxall et al.*, 2005). Northern Hemisphere ice sheets are in general assumed to appear more recent, from the Late Miocene onwards (e.g. *Zachos et al.*, 2001). In the mid-Pliocene a large global sea-level lowering (*Mudelsee and Raymo*, 2005) denotes one of the final stages of climatic cooling and expansion of ice sheets in the Northern as well as in the Southern Hemisphere.

In contrast to these past cooling events, modern climate is dominated by a global warming trend. Direct evidences for this warming are the increases in global air and ocean temperatures, the melting of snow and ice and the rising of the global sea level (*IPCC*, 2007). Also atmospheric concentrations of greenhouse gasses increased substantially over the last few centuries. Measurements of the partial pressure of atmospheric CO_2 ($p$$CO_2$), the most important anthropogenic greenhouse gas, show an increase of approximately 100 ppm over the last 250 years, from the pre-industrial value of $\sim$280 to 385 ppm in 2008 (*IPCC*, 2007; *Hansen et al.*, 2008). There exists high confidence that human activities are (partly) responsible for the observed global warming trend (*IPCC*, 2007). Future estimates from a range of emission scenarios predict a further warming of about 0.15 to 0.3 °C per decade. This is likely to induce further melting of snow and ice and associated rise of the global sea level.

In order to act appropriately it is important to improve the constraints on the predictions of temperature and sea-level rise. For this we need to understand the climate system and especially the interactions between temperature, greenhouse gases, ice sheets and global sea level. Since the early Miocene, the estimated $p$$CO_2$ levels range between 150 and 500 ppm, varying in time and depending on the proxy used (see overview by *Royer*, 2008). The minimum values are though to be associated with periods of increased global ice coverage as compared to today. The upper end of this range, levels of $p$$CO_2$ that most probably will be reached in the near future, coincide with geological periods when the Earth was covered by less continental ice than today. Investigating these periods in the past can help us to improve our understanding of the interactions between climate and ice sheets, and therefore better

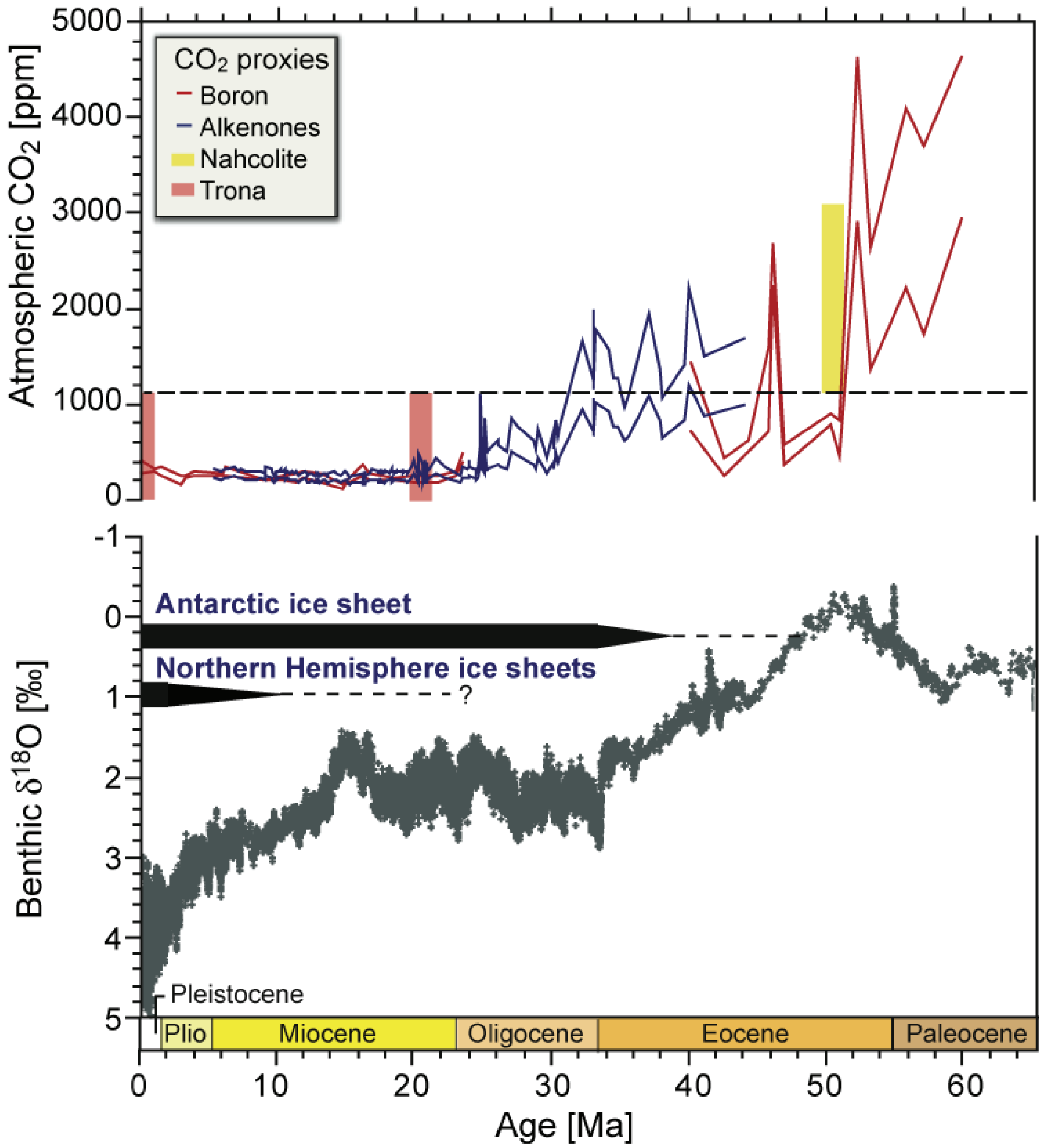

Figure 1.1: *Evolution of global climate in the Cenozoic (Zachos et al., 2008).* ***(a)*** *Compilation of atmospheric CO_2 from marine (see Royer (2006) for original references) and lacustrine (Lowenstein and Demicco, 2006) proxy records. The upper and lower colored lines indicate maximum and minimum estimates for pCO_2 derived from boron and alkenone proxies. The dashed horizontal line at 1125 ppm marks the minimum pCO_2 necessary to precipitate nahcolite (yellow bar) and the maximum value for stable trona (red bar) (Lowenstein and Demicco, 2006). This indicates a maximum pCO_2 level for the Neogene (Miocene to present) and a minimum value for the early Eocene.* ***(b)*** *Compilation of deep-sea benthic foraminferal oxygen-isotope records from over 40 Deep Sea Drilling Project and Ocean Drilling Program sites (Zachos et al., 2001).*

constrain the possible response of ice sheets to future global warming.

The most recent geological time period when pCO_2 levels were relatively similar (~380 ppm, *Kürschner et al.*, 1996; *Raymo et al.*, 1996) to today is the Pliocene (~5.3-1.8 Ma) (*Hill et al.*, 2007). In the midst of this dynamic period (~3.6-2.4 Ma), marine oxygen-isotope records indicate a significant continental ice-sheet expansion (e.g. *Zachos et al.*, 2001). The associated sea-level lowering of 40-50 m (*Mudelsee and Raymo*, 2005) is proposed to result from Northern Hemisphere Glaciation (NHG) (e.g. *Zachos et al.*, 2001). Several hypotheses aim to explain the NHG, ranging from tectonic mechanisms (closure of the Panamanian gateway, the restriction of the Indonesian Seaway or the uplift of mountain ranges) to climatic mechanisms (termination of a permanent El Nino, reduction of pCO_2 and/or variations in the Earths orbit) to even extraterrestrial causes (*Lunt et al.*, 2008a; *Raymo*, 1994b, and references therein). However, none of these hypothesis satisfactorily explain a sea-level drop in the order of 40-50 m.

Another period in which pCO_2 estimations range between 150 and 500 ppm is the Middle Miocene (Fig. 1.2). Statigraphical (*Miller et al.*, 1998, 2005) and proxy (*Holbourn et al.*, 2005; *Shevenell et al.*, 2004) data indicate a global sea-level lowering and large-scale cooling event at proximately 13.9 Ma. In order to explain this abrupt change, many different hypothesis have been proposed. These range from indirect causes such as the effect of ocean circulation and gateways (e.g. *Flower and Kennett*, 1995) and enhanced chemical weathering in combination with the burial of organic matter (e.g. *Raymo*, 1994a) to direct climate causes such as orbital forcing together with a decrease in pCO_2 (*Holbourn et al.*, 2005, 2007). The latter idea, orbital forcing in combination with pCO_2, form a basis for this work and these processes will be discussed in the following sections.

1.2 Atmospheric CO_2 in the Middle Miocene

An important factor which is proposed to have a large influence on the global climate and temperature is the partial pressure of atmospheric CO_2 (pCO_2), one of the main greenhouse gasses. The exact relationship between pCO_2 and temperature and more precisely their interaction is still under discussion. However, at least for the Cenozoic period, it is obvious that high and largely variable pCO_2 levels correspond to a warm climate and low, more constant levels to a cold, icehouse climate (Fig. 1.1). Whether pCO_2 drives the climate or vice versa depends on the time scale considered. On tectonic time scales it is thought that climate influences pCO_2 levels in the atmosphere. For example, according to the weathering hypothesis chemical weathering due to uplift of mountain ranges removes pCO_2 from the atmosphere and thereby cools the Earth (e.g. *Raymo*, 1994a). On the other hand, at shorter time scales pCO_2 is likely to affect the climate. Hence, the present-day and future rise of greenhouse gases will increase the part of the outgoing longwave radiation to be captured in the atmosphere and the global-mean temperature will continue to rise.

Unfortunately, it is not easy to retrieve paleo-pCO_2 which makes it difficult to resolve causes and consequences; leads and lags. For an Cenozoic overview and discussion of pCO_2 proxies see *Royer et al.* (2001), *Lowenstein and Demicco* (2006) and *Royer* (2008). Atmospheric

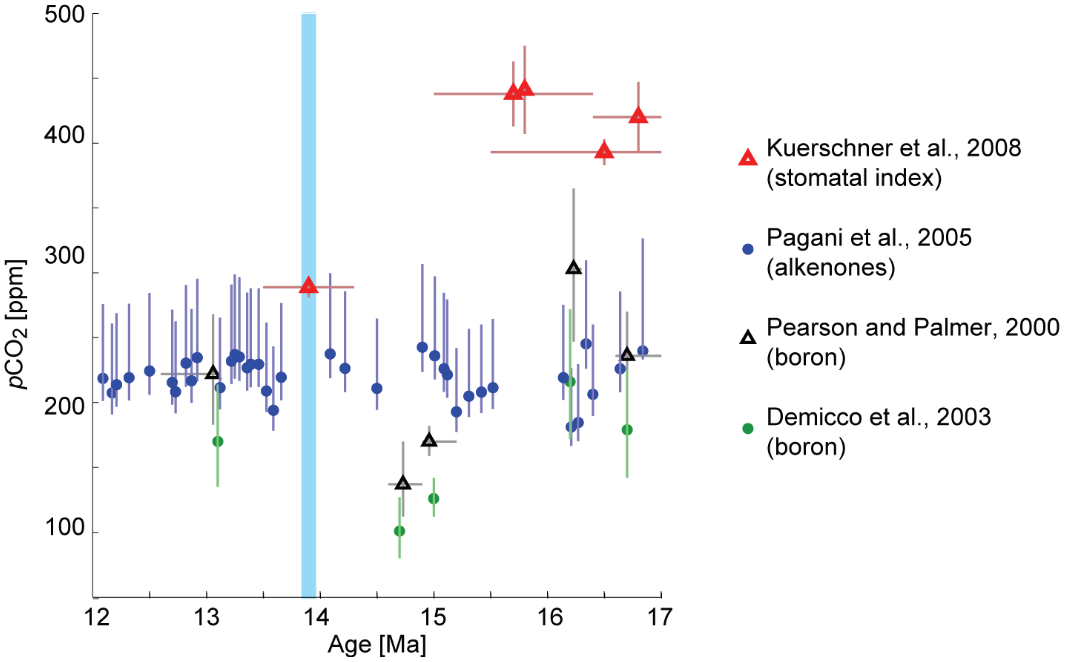

Figure 1.2: *Compilation of published atmospheric pCO_2 in the Middle Miocene. The stomatal method uses the inverse relationship between the stomatal density in plant and pCO_2 (Kürschner et al., 2008). Pagani et al. (2005) measured the stable carbon isotopic compositions of di-unsaturated alkenones extracted from deep-sea sediment cores. These isotopic values depend on the carbon isotopic fractionation that occurred during marine photosynthetic carbon fixation and gives an estimate of paleo-pCO_2. The third method uses boron-isotope ratios of planktonic foraminifer shells (also from marine deep-sea records) to estimate the pH of surface sea water. The pH is then used to reconstruct pCO_2 (Pearson and Palmer, 2000; Demicco et al., 2003).*

pCO_2 proxies applied to the Middle Miocene period are the $\delta^{13}C$ of long-chained alkenones in algae (*Pagani et al.*, 2005), $\delta^{11}B$ of marine carbonate (*Pearson and Palmer*, 2000; *Demicco et al.*, 2003) and stomatal densities and indices in plants (*Kürschner et al.*, 2008) (Fig. 1.2). The low temporal resolution and the large uncertainties in magnitude and age discourages to draw detailed conclusions concerning pCO_2 trends in this period. Nevertheless, from this available data, a maximum pCO_2 variation in the order of only 100 to 200 ppm can be interpreted. This relatively small decline in pCO_2 makes a large contrast to the Eocene-Oligocene transition, where the pCO_2 drawdown is thought to be almost an order of magnitude larger (Fig. 1.1, *Lowenstein and Demicco*, 2006; *Zachos et al.*, 2008).

1.3 Orbital parameters and insolation

The amount and distribution of solar energy (insolation) received by the Earth depends on the solar zenith angle. Three main orbital components influence the solar irradiation at 10^4-10^5 years time-scales: eccentricity, obliquity and precession (Fig. 1.3). The orbit of the Earth

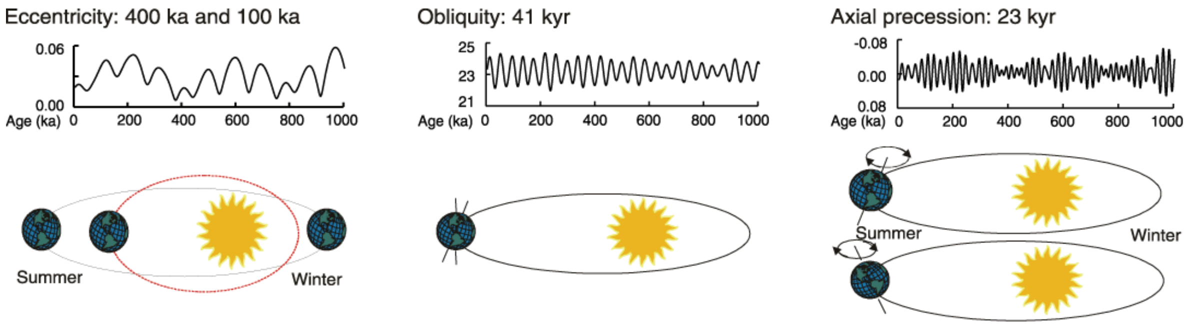

Figure 1.3: *Primary orbital components influencing solar irradiation on longer time scales (modified after Zachos et al., 2001).* ***(a)*** *Eccentricity describes the shape of the Earth's orbit around the Sun. Related periods are approximately 100 and 400 ka.* ***(b)*** *Obliquity (tilt) refers to the variations in the angle between the Earths rotation axis and the orbital plane. This angle varies between 22.1 and 24.5 ° with a period of 41 ka.* ***(c)*** *Axial precession describes the wobble of the Earth's rotation axis. It introduces the shortest periods, of 19 and 23 ka.*

around the Sun varies between near circular to elliptical. Eccentricity describes the extent of this circularity and the periods related to it ($\sim$ 100 and 400 ka). This change in orbit has a minor effect on annual mean insolation, only about 0.18% (e.g. *Hartmann*, 1994), but is still considered as an important process, because its frequencies are recovered from many paleoclimatic sequences. Obliquity or tilt refers to the variations in the angle between the Earth's rotation axis and the orbital plane. This angle varies between 22.1 and 24.5 ° and introduces a main period of 41 ka. An increase in obliquity (higher angle) enhances the seasonal contrast at the Earth (e.g. colder winters and warmer summers). This effect is the most profound at high latitudes and can produce up to $\sim$10 % variations in summer insolation (e.g. *Hartmann*, 1994). The direction of the Earth's rotation axis describes a circle of a period of 26 ka. It defines which hemisphere is closer to the Sun and therefore has the largest seasonal contrast. For example, today the rotation axis is directed towards the Sun during the summer solstice (the Earth is located close to the aphelion). Therefore, boreal summers are warm, whereas austral summers relatively cold. During the winter solstice, the Earth is located near the perihelion, and boreal winters are cold in contrast to the relatively warm austral winters. The effect of this axial precession is largest at the equator and decreases towards the poles. It is also strongly modulated by eccentricity of the orbit around the Sun. In a circular orbit, seasonal contrast is small, while in times of maximum eccentricity the precession cycle reaches its maximum impact. The combined effect of axial precession and eccentricity can explain variations in high-latitude summer insolation of $\sim$15 % (e.g. *Hartmann*, 1994) and are found in the paleoclimatic records as periods of $\sim$19 and 23 ka.

After solving the interplay of the three orbital parameters it is possible to compute the amount of insolation at a specific day and latitude (*Berger*, 1978a,b; *Laskar et al.*, 2004). This infinite set of time series needs to be simplified in order to be able to work with. Often insolation for a certain period and latitude is used as primary forcing mechanism. For example, in Quaternary ice-age studies, the summer insolation at 65 °N is taken as representative, because the Laurentide Ice Sheet was centered around this latitude.

In the Middle Miocene a special combination of minima in eccentricity and obliquity at $\sim$ 13.84 Ma (*Abels et al.*, 2005) resulted in a relatively constant and average-to-low January-February insolation at high southern latitudes (*Holbourn et al.*, 2005). This orbital situation has been proposed as one of the processes responsible for ice-sheet expansion on Antarctica (*Holbourn et al.*, 2005). Cold summer temperatures could prevent the ice and snow from melting in the following summer. Additionally, when the tilt angle is small the differential heating between the equator and poles is enhanced. This promotes meridional transport of moisture and therefore stimulates ice growth. Further investigation of the orbital parameters and resulting insolation in the Middle Miocene shows an even lower minimum in high-latitude summer insolation $\sim$40 ka earlier, around 13.88 Ma (Fig. 1.4). Obliquity is then in another minimum, but eccentricity has average values. The same hypothesis of glaciation inception during an obliquity minimum could also apply for this time. Note that the annual mean insolation lacks the precession frequency, the effect cancels out during the course of a year.

1.4 Oxygen isotopes

Disentangling processes in the past is complicated by the fact that from before the instrumental period ($\sim$ last 150 years) no direct information or measurement is available. Paleoclimatic studies therefore gather information by the use of proxies: variables that obtain a relation (approximation) to a climate-related parameter.

A commonly used proxy for past temperature and ice volume is the ratio of stable oxygen isotopes in water. Isotopes are variants of a chemical element with different atomic mass, due to a different number of neutrons in its nucleus. Three stable isotopes exist of oxygen (O) (Table 1.1), of which the ratio of the heaviest (^{18}O) and the lightest, most common isotope (^{16}O) are used as a proxy for the hydrological cycle (Fig. 1.5) and climate at a given time. For practical reasons the isotopic ratio R between ^{18}O and ^{16}O (^{18}O/ ^{16}O) is given as the relative deviation δ^{18}O of a sample with respect to a standard value R_{std}:

$$\delta^{18}\mathrm{O}[‰] = (\mathrm{R}_{\mathrm{sample}}/\mathrm{R}_{\mathrm{std}} - 1) \times 1000\,. \tag{1.1}$$

The accepted standard ratio for water samples is the Standard Mean Ocean Water of Vienna (V-SMOW), which has a value of 2005.2$\times10^{-6}$ (*Gonfiantini*, 1978).

Table 1.1: *Natural abundances of oxygen isotopes in water molecules (Gat et al., 2001)*

	^{16}O	^{17}O	^{18}O
Abundance (‰)	99.759	0.037	0.204

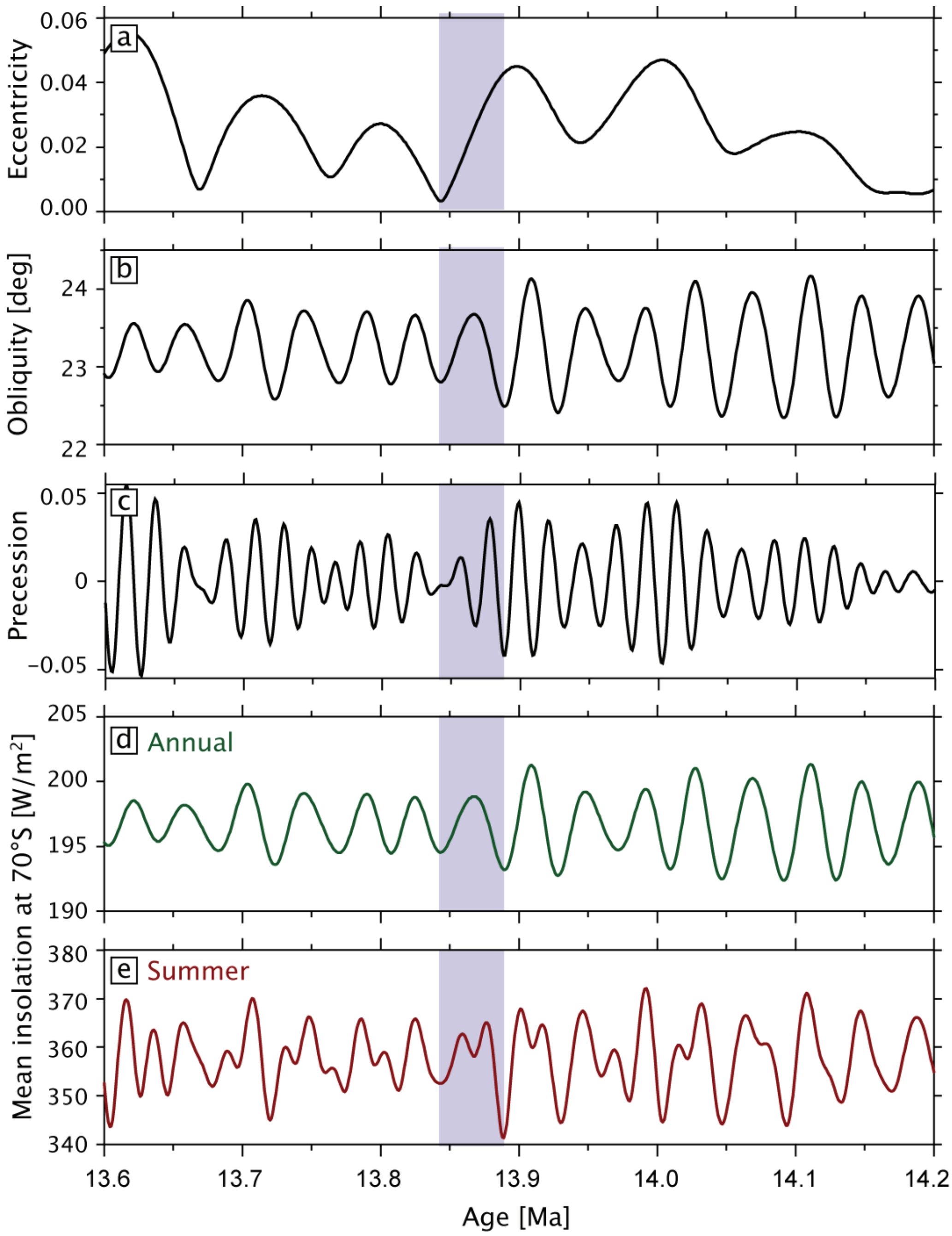

Figure 1.4: *Orbital elements and insolation over the Middle Miocene (Berger, 1978a,b; Laskar et al., 2004).* ***(a)*** *Eccentricity,* ***(b)*** *obliquity [°],* ***(c)*** *precession parameter (eccentricity (ϵ) modulated sine function of the longitude of the perihelion with respect to the moving vernal equinox (ω), $\epsilon sin(\omega)$),* ***(d)*** *annual mean insolation at 70 °S [W/m^2] and* ***(e)*** *summer mean insolation at 70 °S [W/m^2]. The blue rectangle encompasses the Middle Miocene glaciation period as infered from oxygen-isotope records (cf. Shevenell et al., 2004; Holbourn et al., 2005; Raffi et al., 2006).*

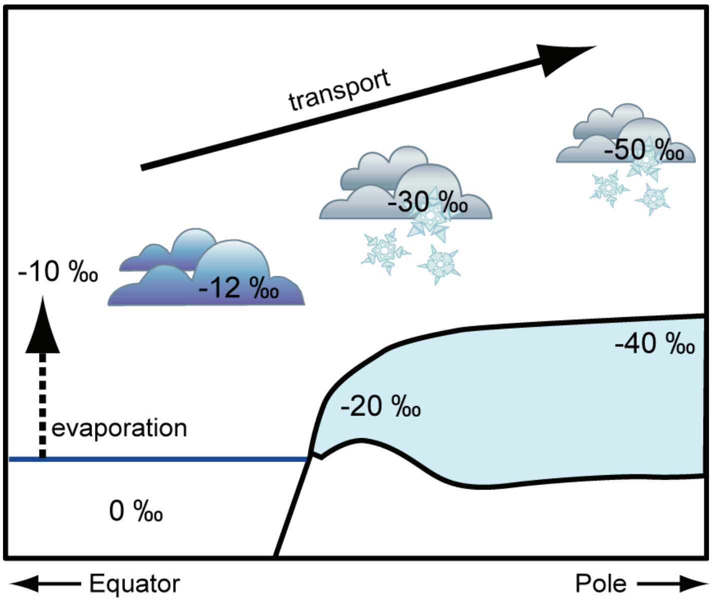

Figure 1.5: *Schematic overview of oxygen isotopes in the hydrological cycle. Due to the large distance from the source (the ocean) and the high elevation, the most depleted precipitation is found inland on Antarctica.*

Figure 1.5 shows schematically the observed global distribution of annual mean $\delta^{18}O$ values in precipitation. Two main patterns towards isotopically lighter precipitation exist: the latitude and the altitude effect. Both have their origin in the same process of fractionation. Most water evaporates in subtropical regions. During this fractionation process, the lighter ^{16}O is preferentially evaporated, leaving the seawater enriched in heavier ^{18}O. The $\delta^{18}O$ in the poleward-moving vapor is further depleted by cooling and associated condensation processes, preferentially removing ^{18}O from the atmosphere. The moisture reaching the high latitudes accumulates as snow significantly depleted in ^{18}O. The altitude effect follows the same reasoning, where the fractionation occurs due to upward transport of moisture and leaving heavier ^{18}O in the rain or snow remaining at lower elevation. The combined effects of high latitudes and high altitudes result in the lowest concentrations of heavy isotopes in the snow falling on central Antarctica (today up to $\sim$ -50 ‰).

For mid- and high latitudes, this distribution of $\delta^{18}O$ in snow ($\delta^{18}O_{snow}$) strongly resembles the annual mean temperature distribution. Not surprisingly, the two parameters show a strong correlation (r >0.9, *Dansgaard*, 1964; *Giovinetto and Zwally*, 1997; *Masson-Delmotte et al.*, 2008). This present-day spatial relationship has often been used in climate reconstructions, approximating past temperatures from the $\delta^{18}O$ signal in ice cores. Bore hole paleothermometry, however, indicates that this approach can introduce large errors. For example, temperature reconstructions between present-day and the Last Glacial Maximum (LGM) in central Greenland from paleothermometry reveal temperature shifts twice as large as would be expected from the local calibration to $\delta^{18}O_{snow}$ (e.g. *Cuffey et al.*, 1995). However, atmospheric models for Antarctica suggest that the istopic-temperature slope remained valid for the LGM (e.g. *Delaygue et al.*, 2000). It is therefore considered conceivable to derive past $\delta^{18}O_{snow}$ from the present-day spatial distribution of $\delta^{18}O_{snow}$ corrected for local changes in surface elevation and changes in mean surface temperature of the ice sheet (*Cuffey*, 2000; *Lhomme*, 2004; *Lhomme et al.*, 2005).

The reconstructed $\delta^{18}O_{snow}$ or $\delta^{18}O_{ice}$ can be validated against direct measurements from the ice sheets. Unfortunately, ice-cores records only extent back to ∼800 ka (*EPICA community members*, 2004). However, the paleoclimate is also archived in marine sediments. Sediment cores normally have a much lower temporal resolution than ice cores, but they are more widely distributed and can span longer time periods. Over the past decades, a considerable number of sediment cores have been recovered by projects like the Deep Sea Drilling Project (DSDP) and the Ocean Drilling Program (ODP). These cores potentially capture long, continuous records useful for paleoclimate reconstructions. Many of the records contain fossil shells from marine organism. The oxygen-isotopic ratio within the calcite of the shells of (benthic) foraminifera ($\delta^{18}O_c$)[1] is a commonly used proxy for past temperatures and ice volume.

The interpretation of this proxy, however, is not as straightforward as the $\delta^{18}O_{ice}$ from ice-core records. The $\delta^{18}O_c$ in the calcite is set at the moment of the formation of the shell and depends on the temperature and the isotopic ratio of the seawater surrounding the foraminifera (*Shackleton*, 1974). The oxygen-isotope ratio of seawater ($\delta^{18}O_{sw}$) in turn, is related to the global ice volume (V_{ice}) and the isotopic composition of this ice ($\delta^{18}O_{ice}$). Additionally, local climatic processes, such as evaporation and precipitation, affect the $\delta^{18}O_{sw}$ and further complicate the reconstruction (*Waelbroeck et al.*, 2002). By stacking many sediment records from different locations (*Zachos et al.*, 2001; *Lisiecki and Raymo*, 2005) the local effects are thought to be reduced and the remaining $\delta^{18}O_c$ record can be used as a proxy for global ocean temperature and ice volume. Disentangling these two processes remains problematic and can only be achieved by independent information on either the seawater temperature or the $\delta^{18}O_{sw}$. The temperature effect can be addressed with the help of other temperature proxies, such as Mg/Ca (e.g. *Lear et al.*, 2000), where after global ice volume can be approximated, considering $\delta^{18}O_{ice}$ to be constant. However, all temperature proxies have their own uncertainties and additionally, questions arise about using a constant $\delta^{18}O_{ice}$.

To my knowledge, only four high-resolution $\delta^{18}O_c$ records, retrieved from deep-sea sediment cores, span the Middle Miocene (Fig. 1.6). All of these show an increase in $\delta^{18}O_c$ of approximately 0.5 ‰. No accompanying high-resolution temperature records exist. Studies using Mg/Ca from benthic foraminifera with a much lower resolution, claim that the major share (70-85 %) of the increase in $\delta^{18}O_c$ can be explained by the expansion of continental ice (e.g. *Lear et al.*, 2000; *Shevenell et al.*, 2008). This general idea is confirmed by a considerable sea-level fall depicted by stratigraphical methods (*Miller et al.*, 1998, 2005).

[1]The notation of $\delta^{18}O_c$ is similar to Eq. 1.1, whereby R_{std} is described by a known external standard. For an overview and discussion of these standards see *Coplen* (1996)

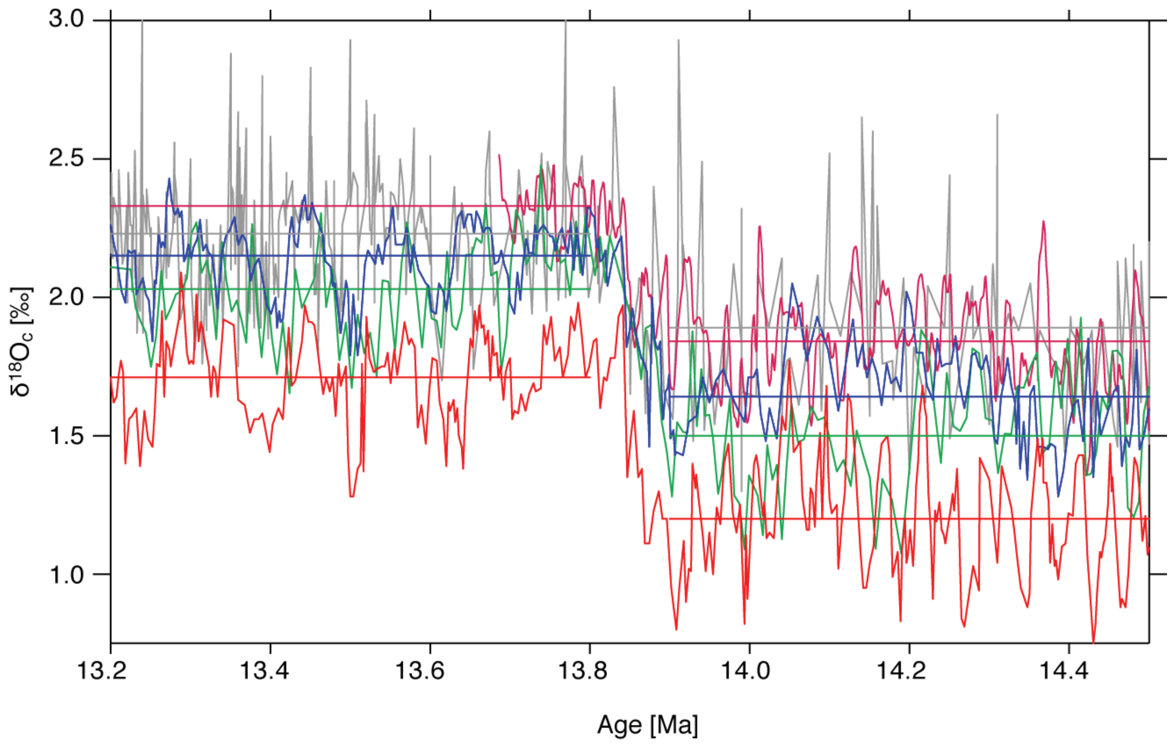

Figure 1.6: *Compilation of high-resolution benthic* $^{18}O_c$ *records for the Middle Miocene. The two records from Holbourn et al. (2005) are plotted in blue (Site 1237) and red (Site 1146). Another ODP record (Site 1171), at latitudes closer to Antarctica, is indicated in green-blue (Shevenell et al., 2004) on the same time scale. The record with the highest resolution only extends from ∼16.6 Ma to ∼13.7 Ma (purple Raffi et al., 2006). The compilation of over 40 records by Zachos et al. (2001) is shown in gray for comparison. The mean values for every records in the period before (13.9-14.5 Ma) and after (13.2-13.8 Ma) the transition are indicated in horizontal straight lines.*

1.5 Scientific objectives

The interactions between climate and ice sheets become very important if we consider the future rise of atmospheric CO_2. This study addresses two dynamic periods in the recent geological past where $p CO_2$ initially was at the same level as we expect for the near future. For both periods, the Middle Miocene and the mid-Pliocene, the available proxy and geological data strongly suggest an expansion of continental ice. In contrast to this widely accepted notion, the proposed origin of the glaciations is still under large discussion. The scarce, unsatisfactorily-constrained $p CO_2$ data and the lack of high-resolution independent temperature records further complicate the paleoclimate reconstructions and lead to many unsolved questions. The following of these questions will be discussed in this study:

1. Was orbital forcing by itself sufficient to cause the ice-sheet expansion in the Middle Miocene? Or was an additional reduction in atmospheric $p CO_2$ needed? And if a $p CO_2$ drawdown did occur, is it possible to constrain the timing and glaciation threshold of $p CO_2$ decrease?

2. To what extent is the $\sim$0.5 ‰ increase found in deep-sea oxygen-isotope records from the Middle Miocene due to continental ice build-up on Antarctica?

3. Is the assumption of a constant relationhip between ice volume (or sea level) and the oxygen-isotopic composition of sea water valid? Moreover, can the mean isotopic composition of ice sheets considered to be constant?

4. Did the closure of the Panamanian gateway have an effect on Antarctic ice-sheet expansion in the Pliocene? And if so, can it explain part of the mid-Pliocene sea-level fall?

1.6 Research approach and outline of this study

Numerical models can help to interpret and understand the processes underlying the proxy data from sediment cores. The best approach for investigating these processes would be to conduct transient experiments using an Ice Sheet Model (ISM) coupled to a Global Circulation Model (GCM), with a closed energy and hydrological cycle. For the objectives stated in the previous section, the ISM should also include computation of the isotopic ratio inside the ice layers. Unfortunately this is not simple considering the current computational speed of computers.

A model approach in that direction is the work of *DeConto and Pollard* (2003) and more recently *DeConto et al.* (2008). They coupled a thermo-mechanical ISM to an atmospheric GCM and conducted experiments spanning 10 Ma. A slow decrease in $p CO_2$ resulted in the expansion of the ice volume in the ISM, representing Antarctica over the Eocene-Oligocene boundary. From the point of view of this study, the disadvantages of the approach by *DeConto and Pollard* (2003) are the unrealistic treatment of the orbital parameters (they defined synthetic orbital parameters with minor-interfering periods), the missing daily climate feedbacks and the relatively high computation time.

Therefore, this work followed a different strategy. A complex ice-sheet model for Antarctica was developed (after the work of *Sima*, 2005; *Sima et al.*, 2006). The model was further expanded by a climate component. The resulting coupled ice sheet-climate model consists of three large-scale boxes covering the entire southern hemisphere. In the high latitude box the climate and ice-sheet the physical processes are resolved on a much smaller spatial grid. The complete model is forced by orbital parameters (insolation) and $p\mathrm{CO_2}$ only. In addition, $\delta^{18}\mathrm{O_{ice}}$ is computed.

This model is described and discussed in the following chapter (Chapter 2). It starts with the basic equations constituting the ice-sheet component and the numerical implementation of the grid and time steps. This is followed by a description of the climate and $\delta^{18}\mathrm{O}$ forcing. Whereafter the initial bedrock topography and other boundary condition will be discussed, as well as the validation of the model and its climate sensitivity.

Research Question 1 (see previous section) is addressed in Chapter 3, while Questions 2 and 3 are discussed in Chapter 4. Both chapters focus on the Antarctic ice sheet in the Middle Miocene. Chapter 5 deals with the Pliocene Antarctic ice sheet and examines Question 4.

Appendix A contains an extensive manual describing how to work with the ice sheet-climate model, including several example recipes.

Chapter 2

Ice sheet-climate model

The model consists of a large-scale climate component coupled to a high-resolution ice-sheet model (Fig. 2.1). The climate part is explained in Section 2.3 [1], but first the theory and numerics of the ice-sheet model (Sections 2.1 and 2.2) are described. The parameterizations of δ^{18}O are discussed in Section 2.4. Initial bedrock topography and other boundary conditions are examined afterwards (Sections 2.5 and 2.6), followed by some comments on the validation and climate sensitivity of the model (Section 2.7) and a list of all used constant parameters (Section 2.8).

2.1 Theory ice-sheet model

The ice-sheet model is zonally averaged and symmetric around the South Pole. A figure from pole to ocean captures therefore all relevant modelled geometrical features (Fig. 2.1). The current model is based on the thermomechanical ice-sheet model of *Sima* (2005) and *Sima et al.* (2006) and contains of 12 vertical ice layers. The total ice-sheet thickness H_{ice} at a specific latitude φ in time t is determined by the continuity equation (e.g. *Gallée et al.*, 1992):

$$\frac{\partial H_{\text{ice}}\,(\varphi)}{\partial t} = -\frac{1}{r(\varphi)}\frac{\partial}{\partial \varphi} r(\varphi) H_{\text{ice}}(\varphi) u_r(\varphi) + M\,, \tag{2.1}$$

where r is the distance from the ice divide, u_r the vertically-averaged horizontal (radial or meridional) velocity and M the mass balance.

The meridional velocity is deduced from Glen's nonlinear flow law for ice:

$$u_r(z) = -2\frac{(\rho_{\text{ice}}\, g)^n}{r_E^2}\left|\frac{\partial s}{\partial \varphi}\right|^{n-1}\frac{1}{r_E}\frac{\partial H_{\text{sfc}}}{\partial \varphi}\int_{H_{\text{sfc}}}^{z} A(T^\star)(H_{\text{sfc}} - z)^n dz + u_{\text{sld}}\ \ , \tag{2.2}$$

where z is the depth, ρ_{ice} is the density of ice, g is acceleration of gravity, n the flow law exponent, r_E is the radius of the Earth, H_{sfc} and H_{bed} the surface and bedrock elevation, respectively, and u_{sld} the sliding velocity.

The stiffness of ice deformation is defined by an Arrhenius-type function:

$$A(T^\star) = EAr_0 e^{-\frac{Q}{RT^\star}}\,, \tag{2.3}$$

[1]This is published as the Appendix of Langebroek, P.M., Paul, A. and Schulz, M. (2008), Constraining atmospheric CO_2 content during the Middle Miocene Antarctic glaciation using an ice sheet-climate model, *Clim. Past Discuss. 4*, 859-89.

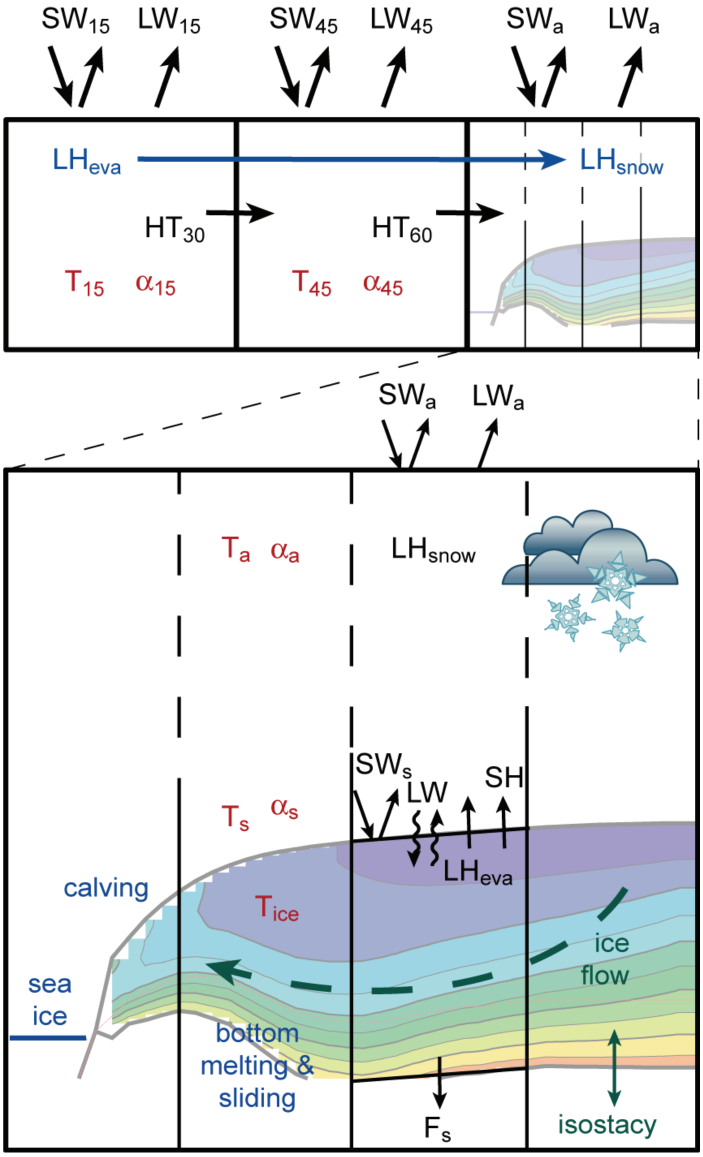

Figure 2.1: *Set-up of the model.* ***Upper:*** *Large-scale box model consisting of low (0-30° S), middle (30-60° S) and high (60-90° S) latitude cells. Each compartment is forced by shortwave (SW) and longwave (LW) radiation at the top of the atmosphere and sensible heat transport by eddies (HT), as well as latent heat transport induced by evaporation and snowfall (LH). The two lower latitude boxes are described by one general temperature (T) and albedo (α).* ***Lower:*** *The high-latitude, Antarctic box is subdivided into smaller grid cells with a resolution of 0.5° latitude. For each cell the energy and mass balances are solved for surface and atmospheric temperatures (T_s and T_a, respectively). Fluxes include incoming and outgoing shortwave radiation at the top of atmosphere (SW_a) and at the land/ice/snow surface (SW_s); reflected longwave radiation at the top of atmosphere (LW_a); longwave (LW), sensible heat (SH) and latent heat of evaporation (LH_{eva}) fluxes between the surface and atmosphere; latent heat of snowfall in atmosphere (LH_{snow}); heat flux into underlying bedrock (F_s). In all boxes ice flow velocities and ice height are computed, depending on the mass balance, local temperature (T), albedo (α) and isostasy.*

where E is a flow-enhancement factor accounting for the effects of crystal anisotropy and impurities on the bulk-ice deformation (*Marshall et al.*, 2000), A_0 is a constant coefficient, Q the creep activation energy and R the universal gas constant. $T^\star$ is the absolute temperature of the ice, corrected for deviations from this value due to pressure:

$$T^\star = T - T_{\text{pmp}} + T_0 \,, \tag{2.4}$$

$$T_{\text{pmp}} = T_0 - \rho_{\text{ice}} g \Phi (H_{\text{sfc}} - z) \,. \tag{2.5}$$

Here, T_0 and T_{pmp} are the temperatures of the triple point of water and of the pressure melting point, respectively and Φ is the rate of change of the melting-point temperature with pressure.

The sliding velocity u_{sld} is only non-zero when the basal ice temperature T_{base} is equal to T_{pmp}:

$$u_{\text{sld}}(H_{\text{sfc}}) = -B \rho_{\text{ice}} g H_{\text{ice}} \frac{\partial H_{\text{sfc}}}{\partial r(\varphi)} \qquad \text{if} \qquad \mathrm{T}_{\text{base}} = \mathrm{T}_{\text{pmp}} \,, \tag{2.6}$$

where B is a free parameter. Basal temperatures below T_{pmp} indicate frozen bedrock and resulting sliding velocities are zero. When T_{base} exceeds T_{pmp}, this energy is used for bottom melting and the T_{base} is reset to T_{pmp}. The melt rate S is computed as:

$$S = \frac{C_{\text{ice}}}{\lambda_{\text{ice}}} (T_{\text{base}} - T_{\text{pmp}}) \frac{\Delta z_{\text{base}}}{\Delta t} \,, \tag{2.7}$$

where C_{ice} and λ_{ice} are the specific and latent heat capacities of ice, respectively. Here Δz_{base} is the thickness of the basal layer and Δt the timestep.

Using the condition that ice is incompressible, vertical velocities w can be derived from the meridional velocities:

$$w(z) = -\int_{H_{\text{bed}}}^{z} \frac{\partial u_r}{\partial r(\varphi)} dz \,. \tag{2.8}$$

Vertical velocities are the boundary conditions at the surface and bottom of the ice sheet, derived from the net mass balance at the ice surface and the melt or ablation at the ice base.

Local isostasy, using a local lithosphere deflection and relaxed asthenosphere, is used for bedrock adjustments:

$$\frac{\partial h}{\partial t} = \frac{1}{\tau_b} (H_{\text{eq}} - H_{\text{bed}} - \frac{\rho_{\text{ice}} H_{\text{ice}}}{\rho_{\text{bed}}}) \,, \tag{2.9}$$

where τ_b is a characteristic timescale for bedrock relaxation, H_{eq} the equilibrium bedrock elevation with respect to present-day sea level (initial bedrock topography) and ρ_{bed} the density of the bedrock. The ice-free, initial bedrock elevation is discussed in Section 2.5.

Within the ice sheet, ice temperature is computed for every vertical layer, using vertical diffusion, horizontal and vertical advection and frictional heat generation terms:

$$\frac{\partial T}{\partial t} = \frac{k_{\text{ice}}}{\rho_{\text{ice}} c_{\text{ice}}} \frac{\partial^2 T}{\partial z^2} - u_r \frac{\partial T}{\partial r} - w \frac{\partial T}{\partial z} + \frac{\tau_{rz}}{\rho_{\text{ice}} c_{\text{ice}}} \frac{\partial u_r}{\partial z}\,, \tag{2.10}$$

where k_{ice} is the thermal conductivity and c_{ice} the specific heat capacity of ice.

The ratio of oxygen isotopes of the ice layers is computed as a passive tracer, following the same advection scheme as ice temperature. Naturally, no diffusion or melting is affecting the isotopic ratio. By using $\delta^{18}\text{O}_{\text{ice}}$ rather than the mass ratios of ^{16}O and ^{18}O reduced the number of (tracer) computations. The truncation of this equation only introduced a negligible conservation error (*Sima*, 2005).

The conditions forcing the ice tracers are described in the Section 2.3 (for temperature and mass balance) and Section 2.4 (for the surface distribution of oxygen isotopes). Boundary conditions for diffusion and advection within the ice sheet are given in Section 2.6.

2.2 Numerical implementation

The ice-sheet model is solved with a finite-difference approach on a staggered grid in both, vertical and horizontal, directions. Tracers (T_{ice} and $\delta^{18}\text{O}_{\text{ice}}$) are solved on the T-grid, whereas fluxes and velocities are computed exactly in between, on the U-grid. The horizontal resolution is 0.5° latitude. In the vertical σ-coordinates are used (e.g. *Payne and Dongelmans*, 1997) and the grid is stretched in 12 layers with uneven thicknesses decreasing towards the base of the ice sheet. A first-order upwind scheme is used for advection and a second-order scheme for heat diffusion. For the vertical upwinding, the relative vertical velocity of ice with respect to the down- or uplift of the grid point is used, with the surface mass balance and bottom melting as boundary conditions. The integration in time is computed by an Eulerian-forward scheme. Most equations (continuity, velocities and tracers) are solved in a one year time step, occasionally reduced to a minimum of 0.05 year in periods of extreme melting or ablation. The energy and mass balance equations, however, are solved with a daily time step.

2.3 Climate forcing

The ice sheet-climate model is controlled by energy and mass balances. Orbital elements are derived following the work of *Laskar et al.* (2004). They drive the daily solar radiation at the top of the atmosphere (*Berger*, 1978a,b) and define, together with the $p\text{CO}_2$, the amount of energy entering the entire climate system.

2.3.1 Energy and temperature balances

The model consists of three large-scale boxes covering the entire southern hemisphere: a low (0-30° S), middle (30-60° S) and high (60-90° S) latitude box (Fig. 2.1). Within the climate system energy is conserved and changes in time are described by (*Pollard*, 1983a; *Hartmann*, 1994):

$$\frac{\partial E_{\mathrm{ao}}}{\partial t} = R_{\mathrm{TOA}} + \Delta F_{\mathrm{ao}} + LH\,, \tag{2.11}$$

where E_{ao} is the total energy in the system, t the time of year, R_{TOA} the net incoming solar radiation on the top of the atmosphere, ΔF_{ao} the divergence of the meridional energy transport in the ocean as well as in the atmosphere, and LH the latent heat added to the atmosphere after condensation and freezing of water vapor. The net incoming radiation is the sum of the incoming short-wave radiation (SW_p) and the outgoing short- and long-wave radiation (LW_p):

$$R_{TOA} = SW_p^{\downarrow} - SW_p^{\uparrow} - LW_p^{\uparrow}\,. \tag{2.12}$$

Radiation fluxes in the two *lower latitude* boxes (0-30° S and 30-60° S) are parameterized as:

$$SW_p^{\downarrow} - SW_p^{\uparrow} = Q(1-\alpha_p) \tag{2.13}$$

$$LW_p^{\uparrow} = \varepsilon_p \sigma T_a^4 + f_{\mathrm{CO_2}} \tag{2.14}$$

where Q is the solar insolation at the top of the atmosphere, α_p the planetary albedo, ε_p the planetary emissivity and σ the Stefan-Boltzmann constant. T_a is interpreted as the near-surface air temperature and $f_{\mathrm{CO_2}}$ as the effect of the atmospheric CO_2 content (cf. *Myhre et al.*, 1998):

$$f_{\mathrm{CO_2}} = -4\frac{\ln(\frac{\mathrm{CO_2}}{280})}{\ln(2)} \approx 2.8 - 0.7\ln(\mathrm{CO_2})\,. \tag{2.15}$$

Therefore, a doubling of $p\mathrm{CO_2}$ from 280 ppm (pre-industrial conditions) to 560 ppm accounts for a reduction of 4 W/m^2 in the outgoing longwave radiation of the two lower latitude boxes.

The physical processes in the *high latitude* box are deciphered in much higher resolution and complexity. For every 0.5° latitude energy and mass balances for the atmosphere and for the surfaces are simultaneously solved. Atmospheric temperature (T_a) is described by:

$$C_a\frac{dT_a}{dt} = R_a + LW + SH + LH_{\mathrm{eva}} + LH_{\mathrm{snow}} \tag{2.16}$$

and surface temperature (T_s) by:

$$C_s\frac{dT_s}{dt} = R_s - LW - SH - LH_{\mathrm{eva}} - F_s - F_m\,, \tag{2.17}$$

where $C_{a,s}$ is the heat capacity for the atmosphere and surface, respectively.

The incoming energy at the top of the atmosphere and at the surface is represented as (*Jentsch*, 1987; *Wang and Mysak*, 2000):

$$\begin{aligned} R_a &= SW_a^{\downarrow} - SW_a^{\uparrow} - LW_a^{\uparrow} \\ &= Q(1-\alpha_a)(1-\tau)(1+\tau\alpha_s) - [\varepsilon_2\sigma T_a^4 + (1-\varepsilon_1)\sigma T_s^4] \end{aligned} \tag{2.18}$$

$$\begin{aligned} R_s &= SW_s^{\downarrow} - SW_s^{\uparrow} \\ &= \tau Q(1-\alpha_a)(1-\alpha_s) \end{aligned} \tag{2.19}$$

where τ is the atmospheric transmissivity of solar radiation, $\alpha_{a,s}$ the atmospheric and surface albedos, ε_2 an emissivity constant and ε_1 a term describing the greenhouse effect (see below).

The longwave and sensible heat fluxes between the atmosphere and surface are parameterized as:

$$LW = \sigma T_s^4 - \varepsilon_1 \sigma T_a^4 \tag{2.20}$$

$$SH = \lambda(T_s - T_a) \tag{2.21}$$

where λ is a heat exchange coefficient which in principle depends on wind speed, atmospheric density and heat capacity, but is taken to be constant. The heat flux into the subsurface soil or upper ice layer F_s is given by:

$$F_s = \frac{2k_1}{\Delta z_1}(T_s - T_a)\,, \tag{2.22}$$

where k_1 is the thermal conductance of snow and Δz_1 the depth range of conduction.

The latent heat of evaporation (LH_{eva}) is parameterized as (*Hartmann*, 1994):

$$LH_{\mathrm{eva}} = \rho_{\mathrm{air}} L_v C_{\mathrm{DE}} U [q_s^*(1-RH) + \frac{RH}{B_e}\frac{c_p}{L_v}(T_s - T_a)]\,, \tag{2.23}$$

where ρ_{air} is the air density, L_v is the latent heat of vaporation, C_{DE} an exchange coefficient, U the wind speed, q_s^* the sea surface humidity, B_e the equilibrium Bowen ratio, c_p the specific heat of dry air and RH the relative humidity.

The latent heat associated with snowfall (LH_{snow}) depends on the accumulation of snow:

$$LH_{\mathrm{snow}} = L_s A\,, \tag{2.24}$$

where L_s is the latent heat of sublimation and A the accumulation. The snow is considered to be evaporated in the low latitude box, accounting for the LH-term in the energy equation (Eq. 2.11). The total accumulation and its latitudinal distribution is tuned to the present-day total Antarctic accumulation and depends on the distance to the South Pole (r), the surface height (h_{sfc}) and the daily surface temperature (T_s) (*Oerlemans*, 2002, 2004). It therefore includes processes such as the 'elevation-desert effect' (*Pollard*, 1983a):

$$A = (c_a + c_b r) e^{\frac{-h_{\mathrm{sfc}}(r)}{c_d}} e^{\kappa T_s} , \tag{2.25}$$

where $c_{a,b}$ are (tuning) constants, c_d is a characteristic length scale and κ a constant describing the precipitation dependence on temperature. Only when the local temperature is below 2°C, snow is accumulated (*Oerlemans*, 2001).

The amount of energy available for melting F_m depends on the incoming energy and the thickness and heat capacity of the top layer (*Fraedrich et al.*, 2005). The affected layer is 20 cm deep (d_{top}) and consists of snow (d_{snow}), soil (d_{soil}) or a mixture of both. The heat capacity C_s used for computation of the surface temperature is therefore computed by:

$$C_s = \frac{C_{\mathrm{snow}} C_{\mathrm{soil}} d_{\mathrm{top}}}{C_{\mathrm{snow}} d_{\mathrm{soil}} + C_{\mathrm{soil}} d_{\mathrm{snow}}} . \tag{2.26}$$

The atmospheric and surface temperature equations are simultaneously solved. Daily computation is necessary, because the orbital cycle as well as processes of snow accumulation and melting have a strong seasonal imprint (*Pollard*, 1983a). The meridional heat transport (ΔF_{eo}) accounts for the coupling between the boxes, and is proportional to the temperature gradient based on the diffusion approximation (*Sellers*, 1970; *North*, 1975). The atmospheric temperatures, and also the surface temperatures, are further extrapolated towards their altitudes (h_{sfc}) according to the prescribed lapse rate, Γ_{lapse}:

$$T_a = T_a + \Gamma_{\mathrm{lapse}} h_{\mathrm{sfc}}(r) . \tag{2.27}$$

2.3.2 Mass balance

The mass balance is solved cumulatively on a daily basis. The specific mass balance, the total amount of accumulation or ablation (per latitude) within one year, possibly reduced by (surface or bottom) melting, evaporation or calving, is annually added to or subtracted from the snow/ice-sheet.

The ice sheet is allowed to grow into the surrounding ocean as long as it is hydrostatically floating. When the total weight of the ice column exceeds the floating criteria, calving occurs (*Pollard*, 1982) and the total mass balance G will be set to a negative value (c_{bal}):

$$G = c_{\mathrm{bal}} \quad \text{if} \quad \rho_{\mathrm{air}} h_{\mathrm{ice}} < \rho_w (h_{\mathrm{sfc}} - h_{\mathrm{ice}}) , \tag{2.28}$$

where ρ_{ice} and ρ_w are the densities of ice and water, respectively, h_{ice} is the ice thickness, and h_{sfc}, the elevation of the surface with respect to the current sea level, which is taken as a constant reference level. This crude calving parameterization also accounts for occurrence of proglacial lakes and/or marine incursions (*Pollard*, 1982).

Bottom melting (S) occurs when the temperature in the basal layer (T_{base}) exceeds the pressure melting point (T_{pmp}):

$$S = \frac{C_{\mathrm{ice}}}{L_m}(T_{\mathrm{base}} - T_{\mathrm{pmp}})\frac{\Delta z_{\mathrm{base}}}{\Delta t}\,, \tag{2.29}$$

where C_{ice} is the specific heat of ice and L_m the specific latent heat of fusion of ice and Δz_{base} the thickness of the basal layer.

2.3.3 Albedo

A separate snow balance is computed to parameterize the surface albedo. The formulas for this cumulative balance resemble the previous surface mass and energy balance equations, except for the fact that the snow depth cannot become negative. The daily derived surface albedo α_s depends on the snow depth d_{snow}, when the snow layer is thicker than 10 cm:

$$\alpha = \frac{\alpha_{\mathrm{snow}} + \alpha_{\mathrm{ice}}}{2} + \frac{\alpha_{\mathrm{snow}} - \alpha_{\mathrm{ice}}}{2}\tanh(A_{\mathrm{snow}}(d_{\mathrm{snow}} - B_{\mathrm{snow}}))\,, \tag{2.30}$$

where the slope (A_{snow}) and shift (A_{snow}) are constant and α_{snow} and α_{ice} are the albedos of snow and ice, respectively. When there is less or no ice/snow, the land, ocean (low and middle latitude boxes) or sea-ice albedos (high latitude box) are used. The latitudinal extent of sea-ice (lat_{si}) is given by (*Jentsch*, 1987):

$$lat_{\mathrm{si}} = \sin^{-1}[\tanh(x_0(\frac{T_{\mathrm{pd}}}{T_a})^{x_1})] - C_{\mathrm{si}}\,, \tag{2.31}$$

where x_0 and x_1 are tuning constants, T_{pd} a measure for the present-day value of sea-water temperature and C_{si} a latitudinal shift.

The planetary (α_p) and atmospheric (α_a) albedos are parameterized as functions of latitude (*Wang and Mysak*, 2000):

$$\alpha_p = 0.6 - 0.4\cos(lat)\,, \tag{2.32}$$

$$\alpha_a = 0.3 - 0.1\sin(lat)\,. \tag{2.33}$$

2.3.4 Greenhouse effect

The longwave radiation constant ε_1 accounts for the greenhouse effect due to $p\mathrm{CO}_2$ and other greenhouse gases:

$$\varepsilon_1 = \varepsilon_{10} + \varepsilon_{11}\sqrt{e'}\,, \tag{2.34}$$

where e' is the atmospheric vapor pressure, related to the saturation specific humidity (q_{sat}) and relative humidity (RH):

$$e' = 1.6 \times 10^3 RH q_{\mathrm{sat}} , \tag{2.35}$$

where:

$$q_{\mathrm{sat}} = \frac{1.57 \times 10^{11}}{\rho_{\mathrm{air}} R_{\mathrm{air}} T_a} e^{\frac{-5421}{T_a}} , \tag{2.36}$$

with R_{air} being the gas constant for dry air.

According to *Staley and Jurica* (1970) and *Jentsch* (1991), the CO_2-emission factor can be parameterized by:

$$\varepsilon_{10}^{\mathrm{CO_2}} = 0.1 + 0.025 \ln(\mathrm{CO_2}) . \tag{2.37}$$

The other main greenhouse gas, water vapor (H_2O), also contributes about half to the (present-day) greenhouse effect. Because of the fact that we do not explicitly compute the hydrological cycle, this feedback can not be parameterized separately. To still include the effect of water vapor, we increased the climate sensitivity to $p\mathrm{CO_2}$ Eq. 2.37 is therefore expanded and retuned to:

$$\varepsilon_{10} = \varepsilon_{10}^{\mathrm{CO_2}} + \varepsilon_{10}^{\mathrm{H_2O}} = 0.1 + 0.025 \ln(\mathrm{CO_2}) . \tag{2.38}$$

A doubling of atmospheric CO_2 now results in a climate sensitivity of 2.8°C and modeled present-day ice-sheet size, accumulation and temperature distribution are similar to estimates (*Huybrechts et al.*, 2000; *Oerlemans*, 2002).

The climate forcing in Pliocene computations is largely taken from the output of the Community Climate System Model CCSM2 (version CCSM2/T31x3a, *Prange*, 2008). The ice-sheet forcing, Antarctic near-surface air temperatures and accumulation, is interpolated from the large-scale three-dimensional CCSM2 to the small-scale axial symmetric ice-sheet model. Ablation, however, is still computed by the ice-sheet model.

2.4 Oxygen-isotopic forcing

The present-day isotopic composition of snow $\delta^{18}\mathrm{O}_{\mathrm{snow}}$ depends on the location (surface elevation and distance from the coast) and climatic parameters (temperature and precipitation). It therefore shows a high correlation to the annual mean surface temperature T_{sfc} ($r > 0.9$ *Giovinetto and Zwally*, 1997; *Masson-Delmotte et al.*, 2008) and is mostly parameterized as only depending on T_{sfc}. For example as in *Masson-Delmotte et al.* (2008):

$$\delta^{18}\mathrm{O}_{\mathrm{snow}}[‰] = 0.80 \times \mathrm{T}_{\mathrm{sfc}}[°\mathrm{C}] - 8.11 . \tag{2.39}$$

Past $\delta^{18}\mathrm{O}_{\mathrm{snow}}$ changes can be derived from the present-day distribution accounting for local changes in surface elevation $\Delta\mathrm{h}_{\mathrm{sfc}}$ and changes in the mean surface temperature of the ice sheet $\Delta\mathrm{T}_s$ (*Cuffey*, 2000; *Lhomme*, 2004; *Lhomme et al.*, 2005):

$$\delta^{18}\mathrm{O}_{\mathrm{snow}}(\lambda,\mathrm{t}) = \delta^{18}\mathrm{O}_{\mathrm{snow}}(\lambda) + \alpha_{\mathrm{c}}\Delta\mathrm{T}_{\mathrm{s}}(\mathrm{t}) + \beta_{\delta}\Delta\mathrm{h}_{\mathrm{sfc}}(\mathrm{t})\,, \tag{2.40}$$

where α_c is the isotopic sensitivity to temperature and β_δ the isotopic lapse rate. According to Lhomme (2004) and references therein β_δ is -11.2 ‰/km, while α_c ranges between 0.6 and 0.8 ‰/°C. This method is shown to introduce large errors when applied to central Greenland (e.g. *Cuffey et al.*, 1995). It is however applicable to Antarctica (e.g. *Delaygue et al.*, 2000; *Cuffey*, 2000; *Lhomme et al.*, 2005).

The simulated bulk $\delta^{18}\mathrm{O}_{\mathrm{ice}}$ is converted into the oxygen-isotopic composition of sea water $\delta^{18}\mathrm{O}_{\mathrm{sw}}$ considering a well-mixed ocean (*Sima et al.*, 2006):

$$\delta^{18}\mathrm{O}_{\mathrm{sw}} = -\frac{\mathrm{S_i}}{\mathrm{d_0}-\mathrm{S_i}}\delta^{18}\mathrm{O}_{\mathrm{ice}}\,, \tag{2.41}$$

where d_0 is the averaged depth and A_0 the (present-day) surface area. Furthermore, S_i is the Antarctic volume-equivalent sea level, using ρ_{ice} and ρ_w as densities of ice and water, respectively:

$$S_i = \frac{\rho_{\mathrm{ice}}V_{\mathrm{ice}}}{\rho_w A_0}\,. \tag{2.42}$$

Here, Antarctica is considered to be the only ice sheet influencing $\delta^{18}\mathrm{O}_{\mathrm{sw}}$ and changes in sea level, which is a reasonable assumption for the Middle Miocene.

2.5 Initial bedrock topography

For the initial bedrock topography the database of the BEDMAP consortium (*Lythe et al.*, 2000) is consulted. This contains high resolution data of the present-day surface and bedrock elevation of the Antarctic ice sheet. Assuming local isostasy, and the absence of large geological deformation processes (volcanic and/or tectonic), the initial ice-free bedrock was reconstructed. For the axially symmetric ice-sheet model, the spatial resolution was reduced to 0.5 ° wide latitude bands. The ice-free bedrock topography used in for the Middle Miocene simulations is a simplified, smoothed version of the zonally-averaged topography that includes a flatter hinterland and bulge close to the coast, accounting for coastal mountain ranges (e.g. the Dronning Maud Land).

The simple initial bedrock profile on which the Pliocene Antarctic ice sheet is grown is proposed by *Pollard* (1983b).

2.6 Other boundary conditions

Besides the climate and $\delta^{18}\mathrm{O}_{\mathrm{snow}}$ forcing and the initial ice-free bedrock topography, there are few additional boundary conditions applied at the ice-sheet surface and base. These depend on the conditions at the surface X_{sfc} or X_{snow}, in the upper ice layer $X_{\mathrm{ice(k=1)}}$ and at the base of the ice sheet X_{base}.

Diffusive heat fluxes Q consider a restoring time scale τ_{damp} and the thickness of the upper ice layer Δz_{sfc} for the surface flux and the geothermal heat for the flux at the base:

$$\begin{aligned} Q^T_{\mathrm{sfc}} &= \rho_{\mathrm{ice}} c_{\mathrm{ice}} \Delta z_{\mathrm{sfc}} \frac{T_{\mathrm{sfc}} - T_{\mathrm{ice(k=1)}}}{\tau_{\mathrm{damp}}} \,, \\ Q^T_{\mathrm{base}} &= -G \,, \end{aligned} \tag{2.43}$$

where ρ_{ice} and c_{ice} are the densitiy and specific heat capacity of ice, respectively, and G the geothermal heat flux. The advective heat fluxes F at the ice surface are described by:

$$F^T_{\mathrm{sfc}} = \begin{cases} \rho_{\mathrm{ice}} c_{\mathrm{ice}} M T_{\mathrm{sfc}} & \text{if } M \geq 0 \,, \\ \rho_{\mathrm{ice}} c_{\mathrm{ice}} M T_{\mathrm{ice(k=1)}} & \text{if } M < 0 \,, \end{cases} \tag{2.44}$$

where M defines the surface mass balance. If melt S occurs, the advective heat flux reaches:

$$F^T_{\mathrm{base}} = -\rho_{\mathrm{ice}} c_{\mathrm{ice}} S T_{\mathrm{base}} \tag{2.45}$$

at the base of the ice sheet.

Also for $\delta^{18}\mathrm{O}$ the advective fluxes depend on the surface mass balance M (surface) or bottom melt S (base):

$$F^{\delta^{18}\mathrm{O}}_{\mathrm{sfc}} = \begin{cases} M \delta^{18}\mathrm{O}_{\mathrm{snow}} & \text{if } M \geq 0 \,, \\ M \delta^{18}\mathrm{O}_{\mathrm{ice(k=1)}} & \text{if } M < 0 \,, \end{cases} \tag{2.46}$$

and

$$F^{\delta^{18}\mathrm{O}}_{\mathrm{base}} = S \delta^{18}\mathrm{O}_{\mathrm{base}} \,. \tag{2.47}$$

No diffusive processes are considered for the passive $\delta^{18}\mathrm{O}$ tracer.

2.7 Model validation and climate sensitivity

The accuracy of the numerical schemes that form the basis of the ice-sheet model are checked by comparing model results to the European Ice Sheet Modeling INiTiative (EISMINT, *Huybrechts et al.*, 1996) benchmarks. A set of simple experiments showed that the model solved the continuity, flow and temperature equations, well in the range of the EISMINT models (*Sima*, 2005). Computing the tracer values in a stretched σ-coordinate grid with 12 vertical layers instead of applying a precise book-keeping method (e.g. *Mix and Ruddiman*, 1984) introduces a small conservation error of less than 2 % (*Sima*, 2005).

The parameters and processes in the entire ice sheet-climate model are tuned to present-day conditions. Under pre-industrial $p\mathrm{CO}_2$ (280 ppm), the ice sheet reaches a volume of 25.1×10^{15} m^3, similar to its estimated modern size ($\sim26\times10^{15}$ m^3; e.g. *Huybrechts et al.*, 2000; *Oerlemans*, 2002; *Huybrechts*, 2004). Also the total Antarctic accumulation and the distribution are based on present-day values (e.g., *Giovinetto and Zwally*, 2000; *Arthern et al.*, 2006), as well as the parameterizations of $\delta^{18}\mathrm{O}_{\mathrm{snow}}$ (see section 2.4 and *Giovinetto and Zwally*, 1997; *Masson-Delmotte et al.*, 2008). All energy balances are tuned by slightly adjusting the diffusivity, heat capacity and planetary emission constants. The resulting mean hemispheric surface temperature is 14.8 °C.

The model sensitivity to a doubling of $p\mathrm{CO}_2$, the climate sensitivity, is tuned to give a reasonable temperature increase. We deliberately enhanced the sensitivity in order to account for the missing water vapour feedback in the model (see Section 2.3.4). While maintaining a fixed ice-sheet height and a present-day insolation distribution, a doubling of $p\mathrm{CO}_2$ resulted in a hemispheric mean temperature increase of 2.8 °C. This is an average value with respect to the climate sensitivity of the more complex models used in the IPCC report (*IPCC*, 2007). Interesting to note is the large polar amplification due to the included ice-abledo feedback, causing Antarctic temperatures to increase by values up to 11.6 °C.

2.8 List of constant parameters

Table 2.1 gives an overview of the parameters used in the ice sheet-climate model.

Table 2.1: *List and description of constant parameters. Some constants differ for the Middle Miocene (MMIO) and mid-Pliocene (PLIO) simulations.*

Symbol	Description	Value	Unit
r_E	Radius of the Earth	6371.0×10^3	kg m^{-3}
A_0	Surface of the ocean	3.605×10^{14}	m^2
d_0	Depth of the ocean	3800	m
g	Gravitational acceleration	910	m s^{-1}
n	Ice rheology exponent	3	-
Ar_0	Multiplier in Arrhenius relation	3.61×10^{-13} if $T^\star < -10°$C	s^{-1}Pa^{-3}
		1.73×10^{-3} if $T^\star \geq -10°$C	s^{-1}Pa^{-3}
Q	Creep activity energy	6.0×10^4 if $T^\star < -10°$C	J mol^{-1}
		13.9×10^4 if $T^\star \geq -10°$C	J mol^{-1}
E	Flow-enhancement factor (MMIO;PLIO)	5; 4	-
T_0	Triple-point water	273.15	K
Φ	Dependence of melting on pressure	9.8×10^{-8}	K Pa^{-1}
B	Multiplier in sliding law	8.0×10^{-3}	m yr^{-1}Pa^{-1}
G	Geothermal heat flux (*Fox Maule et al.*, 2005)	-6.5×10^{-2}	W m^{-2}
τ_{damp}	Time scale for restoring T_{sfc} to $T_{\mathrm{ice(k=1)}}$	1	yr
τ_b	Time scale of bedrock relaxation	5000	yr
ε_p	Planetary emissivity (at 15; 45; 75°S)	0.61; 0.66; 0.69	-
ε_{11}	Emissivity constant (*Sellers*, 1970)	0.05	-
ε_2	Emissivity constant (*Jentsch*, 1987)	0.30	-

Table 2.2: *Continuation of Table 2.1*

Symbol	Description	Value	Unit
σ	Stefan-Boltzmann constant	5.67×10^{-8}	W $m^{-2}K^{-4}$
τ	Atmospheric transmissivity (*Wang and Mysak*, 2000)	0.65	-
λ	Heat exchange coefficient	10.0	W $m^{-2}K^{-1}$
k_1	Thermal conductance of snow	0.31	W $m^{-1}K^{-1}$
Δz_1	Depth range of subsurface conduction	3.0	m
ρ_{air}	Density of air	1.2	kg m^{-3}
ρ_{ice}	Density of ice	910	kg m^{-3}
ρ_w	Density of water	1000	kg m^{-3}
ρ_{bed}	Density of bedrock	3300	kg m^{-3}
C_{DE}	Exchange coefficient for latent heat	1.0×10^{-3}	-
U	Wind speed	5.0	m s^{-1}
q_s^*	Sea surface specific humidity	0.8×10^{-3}	kg kg^{-1}
RH	Relative humidity (*Bintanja*, 1999, p. 122)	0.75	-
B_e	Equilibrium Bowen ratio	2.0	-
R_{air}	Gas constant for dry air	287.04	J $kg^{-1}K^{-1}yr^{-1}$
Γ_{lapse}	Atmospheric temperature lapse rate (MMIO;PLIO)	-0.012; -0.007	°C m^{-1}
L_v	Latent heat of vaporation of ice	2.26×10^6	J kg^{-1}
L_m	Latent heat of melting of ice	0.334×10^6	J kg^{-1}
C_p	Specific heat capacity of dry air	1005	J $kg^{-1}K^{-1}$
C_{ice}	Specific heat capacity of ice	2009	J $kg^{-1}K^{-1}$
λ_{ice}	Latent heat capacity of ice	3.35×10^5	J kg^{-1}
k_{ice}	Thermal conductivity of ice	6.62×10^7	J $m^{-1}K^{-1}yr^{-1}$
d_{top}	Affected snow/soil layer	0.2	m
c_d	Precipitation constant	3000.0	m
κ	Precipitation dependence on temperature	0.0345	K^{-1}
A_{snow}	Tangent hyperbolicus constant	50	-
B_{snow}	Tangent hyperbolicus constant	0.05	-
c_{bal}	Calving constant	-2	m yr^{-1}
α_{snow}	Albedo of snow	0.75	-
α_{ice}	Albedo of ice	0.35	-
α_{seaice}	Albedo of seaice	0.60	-
α_{land}	Albedo of land	0.30	-
α_w	Albedo of ocean water	0.10	-
x_0	Constant for sea-ice extent	2.1	-
x_1	Constant for sea-ice extent	0.6	-
T_{pd}	Temperature constant for sea-ice extent	-41	°C
C_{si}	Latitudinal shift constant for sea-ice extent	19	°
α_c	Isotopic sensitivity to temperature	0.6-0.8	‰/°C
β_δ	Isotopic lapse rate	-11.2	‰/km

Published as: Langebroek, P.M., A. Paul and M. Schulz (2008), Constraining atmospheric CO_2 content during the Middle Miocene Antarctic glaciation using an ice sheet-climate model, *Clim. Past Discuss. 4*, 859-89.

Chapter 3

Constraining atmospheric CO_2 content during the Middle Miocene Antarctic glaciation using an ice sheet-climate model

Abstract

Foraminiferal oxygen isotopes from deep-sea sediment cores suggest that a rapid expansion of the Antarctic ice sheet took place in the Middle Miocene around 13.9 million years ago (Ma). The origin for this transition is still not understood satisfactorily. Among the proposed causes are a drop in the partial pressure of atmospheric carbon dioxide (pCO_2) in combination with orbital forcing. An additional complication is the large uncertainty in the magnitude and age of the reconstructed pCO_2 values and the low temporal resolution of the available record in the Middle Miocene. We used an ice sheet-climate model with an energy and mass balance module to assess variations in ice-sheet volume induced by pCO_2 and insolation forcing and to better constrain atmospheric CO_2 in the Middle Miocene. The ice-sheet sensitivity to atmospheric CO_2 was tested in several scenarios using constant pCO_2 forcing or a regular decrease in pCO_2. Small, ephemeral ice sheets existed under relatively high atmospheric CO_2 conditions (between 400-450 ppm), whereas more stable, large ice sheets occurred when pCO_2 is less than 400 ppm. Transitions between the states were largely CO_2-induced, but were enhanced by extremes in insolation. In order to explain the Antarctic glaciation in the Middle Miocene as documented by the oxygen isotope records from sediment cores, pCO_2 must have decreased by approximately 150 ppm in about 30 ka, crossing the threshold pCO_2 of 400 ppm around 13.9 Ma. Forcing the ice sheet-climate model with cyclic pCO_2 variations at a period of 100 ka and amplitudes of approximately 40 ppm generated late Pleistocene glacial-interglacial like ice-volume variations, where the ice volume lagged pCO_2 by 11-16 ka.

3.1 Introduction

In the Middle Miocene, around 13.9 million years ago (Ma), a large shift towards heavier benthic oxygen isotope values ($\delta^{18}O$) is found in deep-sea sediment records (*Zachos et al.*, 2001; *Holbourn et al.*, 2005). This increase coincided with a global sea-level drop (*Miller et al.*, 1998, 2005) and is interpreted as an expansion of the Antarctic ice cap and a global transition into a colder climate (e.g. *Zachos et al.*, 2001; *Shevenell et al.*, 2004). Several causes for the transition are proposed, ranging from the effect of ocean circulation and gateways (e.g. *Flower and Kennett*, 1995), enhanced chemical weathering and burial of organic matter (e.g. *Raymo*, 1994a), to orbital forcing in combination with variations of partial pressure in the atmosphere (pCO_2) (*Holbourn et al.*, 2005, 2007). A remarkable difference of this glaciation with respect to previous large-scale events (e.g. the Eocene-Oligocene transition (*Coxall et al.*, 2005; *Pollard and DeConto*, 2005)) is the relatively small decline in atmospheric CO_2, varying only in the order of 100-200 ppm (cf. *Pearson and Palmer*, 2000; *Royer et al.*, 2001; *Pagani et al.*, 2005; *Kürschner et al.*, 2008; *Zachos et al.*, 2008). This raises questions about the origin of the Middle Miocene transition. Was orbital forcing by itself sufficient to cause a large-scale continental glaciation? Or was some additional reduction of atmospheric CO_2 needed? And if so, how large and how quick was this pCO_2 drop? Considering the large uncertainties in the most recent pCO_2 reconstructions for the Middle Miocene (*Pearson and Palmer*, 2000; *Royer et al.*, 2001; *Pagani et al.*, 2005; *Kürschner et al.*, 2008; *Zachos et al.*, 2008), this study aims to give constrains on for timing, duration and speed of the pCO_2 transition using a modelling approach. We examine these questions using a geometrically simplified, but physically comprehensive ice sheet-climate model, which is forced by insolation (derived from the orbital parameters) and atmospheric CO_2 only.

3.2 Methods and experimental set-up

3.2.1 Ice sheet-climate model

We used a coupled ice sheet-climate model. The climate component consists of three large-scale boxes covering the entire southern hemisphere: a low (0-30° S), middle (30-60° S) and high (60-90° S) latitude box (Fig. 2.1). Forcing consists of seasonal orbital forcing following the work of *Laskar et al.* (2004) in combination with prescribed atmospheric CO_2 levels. In the large-scale boxes of the climate model, energy is conserved and is redistributed by meridional energy transport, taking into account the latent heat fluxes due to evaporation and snow accumulation. The physical processes within the high latitude box are resolved in 0.5° latitude bands. In these boxes energy balances the for atmosphere and surface are resolved separately, but computed simultaneously. Additionally, the mass balance for the ice-sheet component is modeled. Daily computation is necessary, because the orbital cycle as well as processes of snow accumulation and melting have a strong seasonal imprint (*Pollard*, 1983a).

The atmospheric and surface energy balances include parameterizations for short- and longwave radiation, latent heat of evaporation and snowfall, sensible heat exchange, heat flux into the surface and energy used by melting of ice and snow (*Pollard*, 1982, 1983a; *Jentsch*, 1987, 1991; *Wang and Mysak*, 2000). Total accumulation and its latitudinal distribution is tuned to the present-day (total) Antarctic accumulation and depends on surface temperature, distance from the coast, surface height and daily surface temperature (*Oerlemans*, 2002, 2004). It therefore includes important processes such as the elevation-desert effect (*Pollard*, 1983a). The ice-sheet model is symmetric around the axis of the South Pole. Within the ice sheet velocities and temperatures are computed with a vertical resolution of 12 layers. The altitude and ice thickness of every latitude grid cell are derived by solving the continuity equation using basal melting, local bedrock isostasy and a surface mass balance (*Sima*, 2005; *Sima et al.*, 2006). The initial ice-free bedrock topography is reconstructed using the BEDMAP project database (*Lythe et al.*, 2000) for bedrock elevation and ice thickness, considering local isostasy. For the axially symmetric ice-sheet model, the high spatial resolution of the dataset is reduced, averaging the topography into the 0.5°-wide latitude bands. The initial bedrock used by the model is a simplified version of the zonally-averaged topography that includes a bulge close to the continental shelf and a flatter hinterland. Although no separate ocean component is included in the model, the energy and mass balances within the Antarctic box include the albedo of (seasonally varying) sea-ice. This is parameterized depending on the near-surface temperature of the appropriate grid cells. The surface albedo of the Antarctic continent depends on the ice and snow content of the corresponding grid cell and combines albedos of land (0.3), ice (0.35) and snow (0.75). A more detailed description of the climate forcing as well as a list of all constant parameters used in the model can be found in Chapter 2.

3.2.2 Climate sensitivity of the model

The equilibrium climate sensitivity as estimated from 19 atmospheric general circulation models ranges from 2.1 to 4.4°C, with an average of 3.2°C (*IPCC*, 2007). These models do not include a dynamic ice-sheet component, but do account for changes in snow cover and albedo. The large spread in sensitivity is introduced by differences in feedback parameterizations. To tune the climate sensitivity of our model, we first ran the coupled ice sheet-climate model for the last 100 ka with constant pre-industrial $p\mathrm{CO}_2$ of 280 ppm and varying orbital parameters. The modeled present-day ice sheet is in equilibrium with the radiative forcing and has a volume of 25.1×10^{15} m^3, similar to its estimated present-day size (e.g. *Huybrechts et al.*, 2000; *Oerlemans*, 2002; *Huybrechts*, 2004). The mean hemispheric surface temperature is 14.8°C. The model is tuned such that a doubling of $p\mathrm{CO}_2$ gives a reasonable temperature increase. We deliberately enhanced the sensitivity to changes in $p\mathrm{CO}_2$ in order to account for the missing water vapor feedback (see Appendix). In the tuned model, a doubling of $p\mathrm{CO}_2$ while maintaining fixed ice-sheet height and (seasonal) insolation distribution resulted in a hemispheric mean temperature increase of 2.8 °C. This value falls well within the range of the values reported by the IPCC report (2007). The largest increase is found in atmospheric and surface temperatures in the Antarctic, high latitude box, with values up to 11.6 °C. The large polar amplification is due to the included ice-albedo feedback.

3.2.3 Insolation and $p\mathrm{CO}_2$ forcing

Based on Earths orbital elements as computed by *Laskar et al.* (2004) we compute daily insolation (*Berger*, 1978a,b) at the top of the atmosphere (for every latitude box) and at the surface for the high resolution Antarctic cells (60-90°S). We will use two different averages for comparison to ice-volume variations: annual mean and caloric summer (half-year of highest values) insolation. Since the atmospheric CO_2 level in the Middle Miocene is not very well constrained, the model is forced by prescribed scenarios of constant $p\mathrm{CO}_2$, constant decrease in $p\mathrm{CO}_2$ and a $p\mathrm{CO}_2$ forcing including a 100-ka cycle (eccentricity).

3.2.4 Experimental set-up

First, hysteresis experiments are carried out, in order to find $p\mathrm{CO}_2$-threshold values at which the Antarctic continent (de)glaciates. In addition, different levels of constant atmospheric

CO_2 are applied for model runs of 1 Ma, from 14.2 to 13.2 Ma (preceded by a 100 k spin-up time), in order to investigate the effect of insolation fluctuations on ice-sheet volume under different constant pCO_2 conditions. Between 200 and 450 ppm, every 10 ppm is used for constant model forcing, with an increased resolution of 5 ppm between 390 and 410 ppm. Second, sensitivity experiments involving a reduction in pCO_2 are carried out, focusing on ice-sheet response to the level, speed and timing of pCO_2 decrease. Finally, pCO_2 forcing with a frequency of 100 ka is used to look into the mechanism causing eccentricity cycles within the sedimentary records. In all experiments specific daily insolation for appropriate latitudes is applied.

3.3 Results

3.3.1 Hysteresis experiments

To assess the sensitivity of the simulated ice volume to pCO_2 changes and in order to find the critical range of pCO_2 at which the Antarctic continent (de)glaciates, two types of hysteresis experiments were performed. The first included orbital variations, while the second is only forced by atmospheric CO_2 (Fig. 3.1). In both experiments the (rapid) transition into a large ice-sheet occurred around 400 ppm, preceded by a semi-stable small ice sheet. In case of omitting orbital variations, deglaciation occurred at approximately 550 ppm, accounting for a hysteresis window of $\sim$150 ppm. Orbital forcing acts as noise, therefore the ice sheet melts under much lower pCO_2 when it is included ($\sim$425 ppm). The modeled rate of pCO_2 change was slow at 50 ppm/Ma, comparable to the 280 ppm/5 Ma used by *Pollard and DeConto* (2005).

3.3.2 Constant pCO_2 experiments

The critical pCO_2 for glaciation is approximately 400 ppm. Below this threshold the entire Antarctic continent is glaciated, with mean ice volumes between 23 and 25×10^{15} m^3 (Fig. 3.2). Between $\sim$405 and $\sim$430 ppm (almost) continuous small ice sheets existed for the modeled period. Higher pCO_2 levels resulted in small, ephemeral ice sheets. Under constant pCO_2 forcing and insolation derived from orbital parameters of the Middle Miocene (between 14.2 and 13.2 Ma) either large or small ice sheets occurred (Fig. 3.2 and 3.3). Only constant pCO_2 values close to the threshold of 400 ppm caused a transition between these two states. Using constant 400 ppm forcing, Antarctic glaciated at 13.43 Ma. All small ice sheets showed large variations in ice volume, up to $\sim2.5\times10^{15}$ m^3 for constant pCO_2 of 410 ppm. Volume of large ice sheets varied less under constant pCO_2 conditions, with a maximum variance of $\sim1.1\times10^{15}$ m^3 for pCO_2 values close to the threshold and nearly no variance at lower pCO_2 levels. For further comparison two runs of constant pCO_2 close to the glaciation threshold value and with maximum ice-volume variance are used to represent the large ice sheet (390 ppm) and the small ice sheet (410 ppm).

The correlation between ice-volume variations and annual and summer mean insolation was computed for every 5° of southern latitude (Fig. 3.4). Both ice-sheet variations correlated

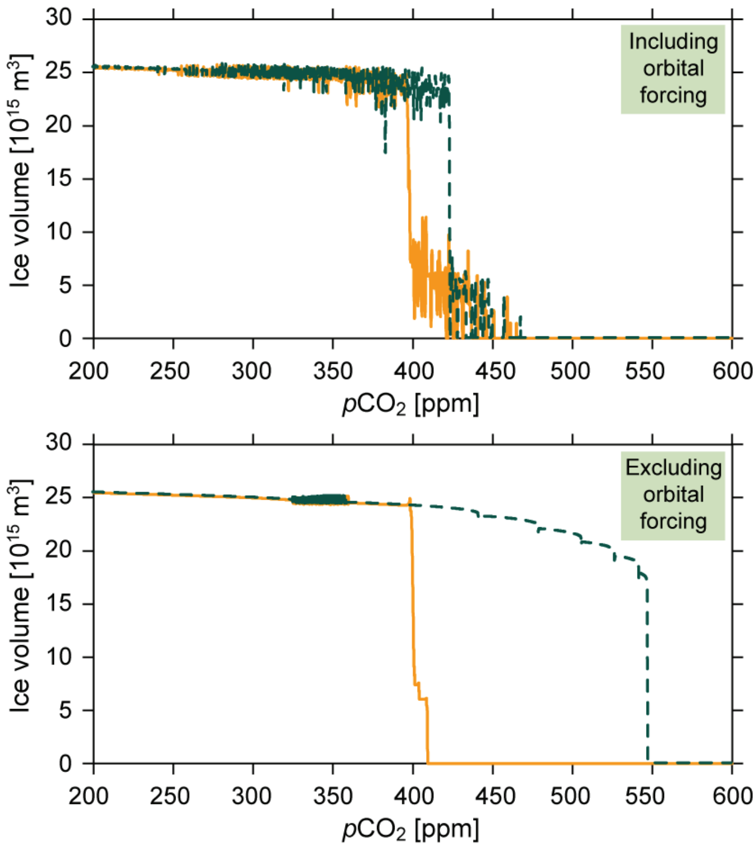

Figure 3.1: *Hysteresis experiment. Starting from no-ice conditions and high $p\mathrm{CO_2}$ (orange solid) or starting from full ice sheet and low $p\mathrm{CO_2}$ (green dashed).* ***Upper*** *panel shows hysteresis including orbital forcing,* ***lower*** *panel without orbital variations. Rate of $p\mathrm{CO_2}$ change is 250 ppm/5 Myr, comparable to 280 ppm/5 Myr used by Pollard and DeConto (2005).*

better to high (around 70 °S), than to low latitudes. In the case of the large ice-sheet, highest correlation coefficients were reached when ice volume lagged insolation by approximately 2 ka. Maximum correlation coefficient values were 0.29 and 0.75 for annual and summer mean, respectively. The small ice-sheet matched insolation averages best for a lag of 5 to 6 ka. Maxima for annual and summer mean insolation were 0.49 and 0.60, respectively.

3.3.3 Sensitivity experiments

In the first sensitivity experiment atmospheric CO_2 decreased linearly at a rate of 50 ppm/ka (Fig. 3.5 - red curves). For every experiment, the timing of the drop was simultaneous, only the extent, and therefore the initial and final levels of $p\mathrm{CO_2}$ were different. The resulting ice volume transitions occurred around the same moment in time, whereby the largest difference in $p\mathrm{CO_2}$ forced the most rapid ice-sheet transition (Fig. 3.5 - blue curves). This experiment focusing on initial and final levels of $p\mathrm{CO_2}$ is repeated for different slopes of the $p\mathrm{CO_2}$ transition, with identical results (not shown). The second test focused on the effect of

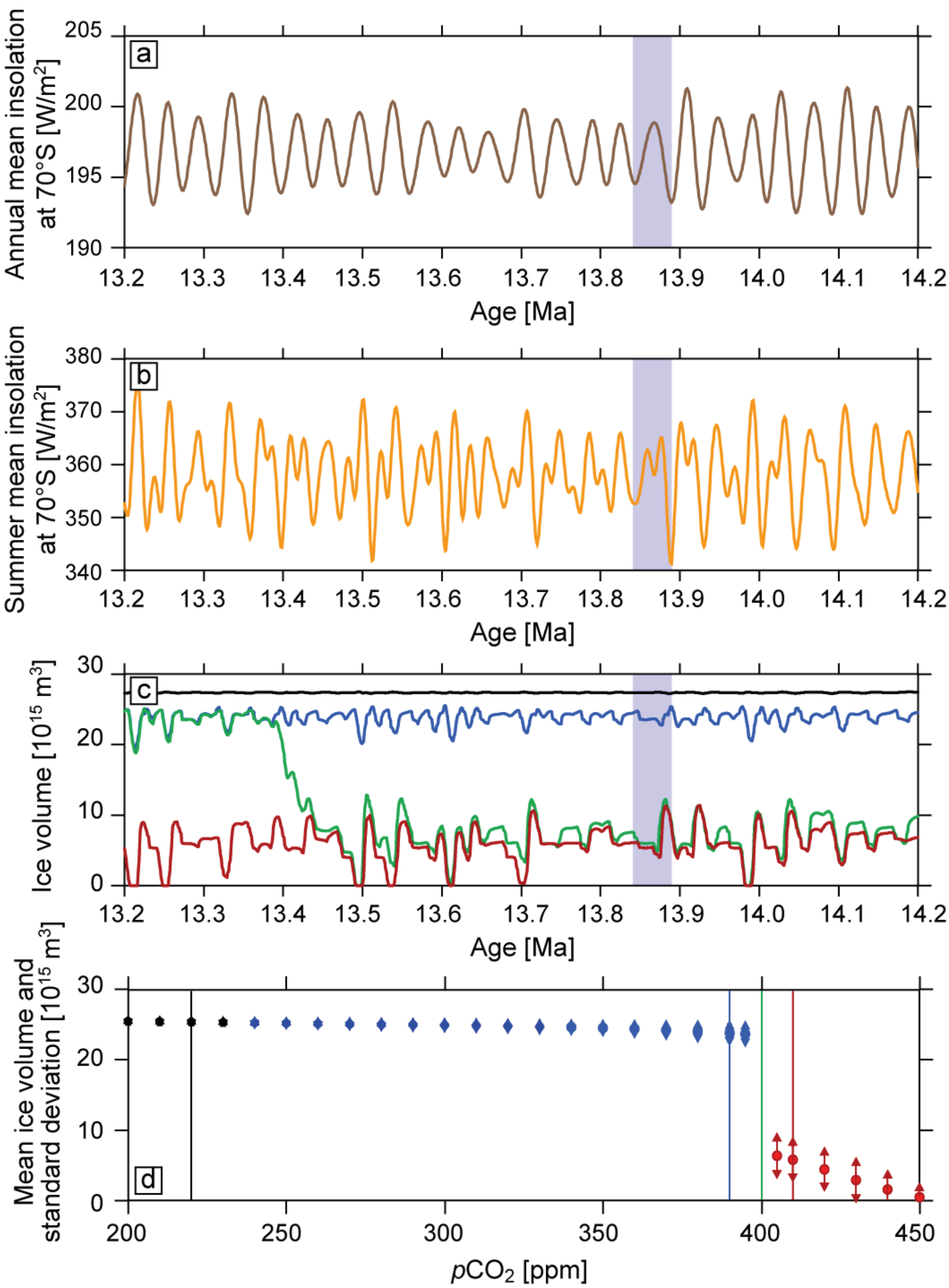

Figure 3.2: *Constant pCO_2 experiments in the Middle Miocene (14.2-13.2 Ma).* ***(a)*** *Annual mean insolation at 70 °S.* ***(b)*** *Summer mean insolation at 70 °S.* ***(c)*** *Resulting ice-volume variations of four typical pCO_2 forcing (220 ppm (black), 390 ppm (blue), 400 ppm (green) and 410 ppm (red).* ***(d)*** *Mean ice volume (dot) and standard deviation (arrows) of large (black/blue) and small (red) ice sheets, defined by their pCO_2 level. The blue rectangle encompasses the Middle Miocene glaciation period as depicted by oxygen isotope records.*

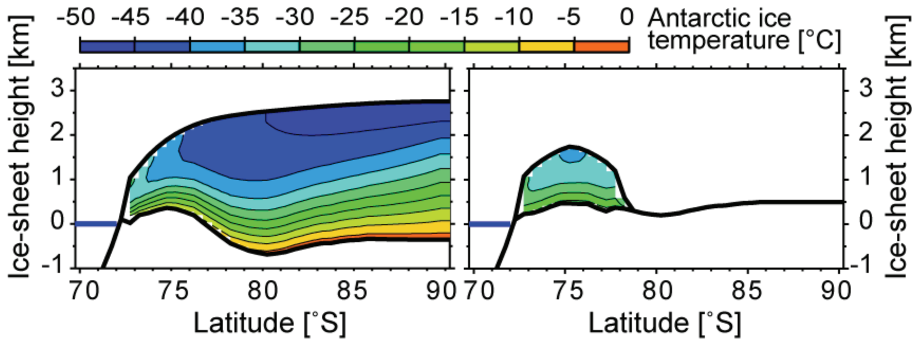

Figure 3.3: *Cross-section of large (**left**) and small (**right**) Antarctic ice sheets. Color scale corresponds to annual mean ice temperatures.*

the pace at which the atmospheric CO_2 is decreasing on the ice-sheet transition (Fig. 3.5). Experiments forced by a slow decrease in pCO$_2$ resulted in a variable duration of ice-sheet transition, between 20-30 ka. In runs with a fast pCO$_2$ drop, the transition length was independent of the speed of pCO$_2$ drawdown. This relation also holds for different timing of the pCO$_2$-transition (not shown). In the last sets of sensitivity experiments the forcing was applied at different moments in time (Fig. 3.6). Antarctica would have glaciated during the appropriate time interval (13.84-13.88 Ma) if a fast pCO$_2$ transition occurred around 13.9 Ma or due to a slower pCO$_2$ drawdown between 14.03 and 13.83 Ma.

3.4 Discussion

3.4.1 Constant pCO$_2$ experiments

In our coupled ice sheet-climate model, which is tuned to present-day conditions and a climate sensitivity of 2.8 °C, relatively stable, large ice sheets occurred under pCO$_2$ below ∼400 ppm (Fig. 3.2). Very stable ice sheets under relatively low pCO$_2$ levels (below 235 ppm) showed extremely small ice-volume variations. Correlations between continental ice volume and benthic oxygen isotopes vary between 1 ‰ (*Zachos et al.*, 2001) and 2.2 ‰ (*Pekar et al.*, 2002) for 100 m sea-level change. Taking the present ocean area (3.6×10^6 km^2) and the densities of water and ice (1000 kg/m^3 and 910 kg/m^3, respectively), an apparent sea level (ASL) drop of 100 m is equivalent to the build-up of ice with a volume of approximetely 33×10^{15} m^3. Using the maximum oxygen-isotope sea-level calibrations (∼2.2 ‰ $\approx 33\times10^{15}$ m^3), the standard deviation in the oxygen-isotope ratio derived from ice volume would be approximately 0.002 ‰ (Tab. 3.2) and resulting global sea-level fluctuations would be impossible to detect in the geological record. Larger variances are found in the modeled ice-volume record for a constant pCO$_2$ of 390 ppm (for a large ice sheet) and 410 ppm (for the small one) (Fig. 3.2)). Ice-volume fluctuations in the small (big) ice sheet accounted for a maximum of 77 % (41 %) of the mean of the standard deviations in the benthic oxygen-isotope records (standard deviations are computed from the orginal oxygen-isotope data and afterwards averaged for comparison to the modeled ice-volume fluctuations; Table 3.1 and 3.2).

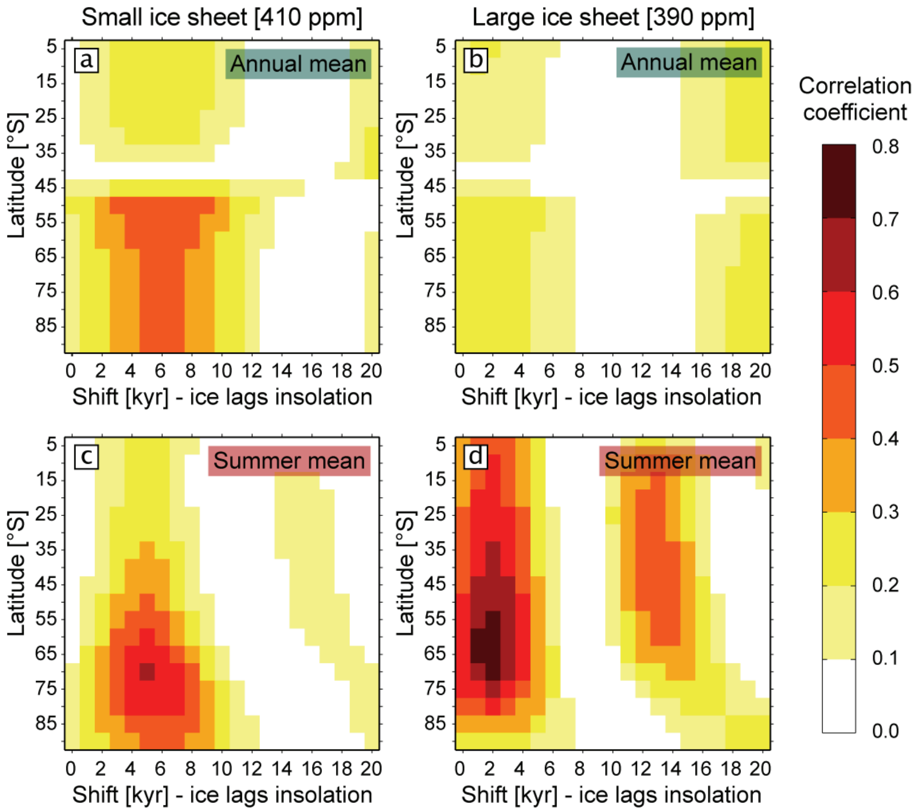

Figure 3.4: *Ice-sheet variations correlated to insolation at latitudes between 0 and 90 °S. Insolation is shifted backwards per 1 ka on horizontal axis (ice volume lags insolation). Correlation coefficients are given for a small (**a** and **c**) and large (**b** and **d**) ice sheet and for annual (**a** and **b**) and summer mean (**c** and **d**) insolation. Best correlation is found for latitudes around 70° S and a shift of 5-6 ka (small ice sheet) or 2 ka (large ice sheet). Highest correlation coefficients for a small ice sheet are 0.49 and 0.60, for annual and summer mean insolation respectively. Maxima for a large ice sheet are 0.29 (annual) and 0.75 (summer mean insolation).*

The modeled result that small ice sheets were more easily perturbed than large ice sheets can partly be traced back to the oxygen-isotope record (Table 3.1). An F-test showed that the variances of the original oxygen-isotope data in the restricted time domains were significantly different (significance level of 95 %). This difference might be explained by the fact that small ice sheets are more easily perturbed by changes in the forcing. Additionally, ablation, which plays a major role in ice-volume variations, occurred on two sides of the small ice sheet, whereas the large ice sheet only had an ablation zone at the outer rim. Considering the very crude calibration used to compute these values, not taking care of any effects caused by changes in (deep sea) temperature, salinity, local runoff, oxygen-isotope ratio of the ice and so on, the correlation between the standard deviations of data- and model derived oxygen-isotope ratios is surprisingly high. Further more, these experiments were performed under constant pCO_2-levels. In the final part of this paper an experiment forced by large pCO_2 fluctuations will be discussed.

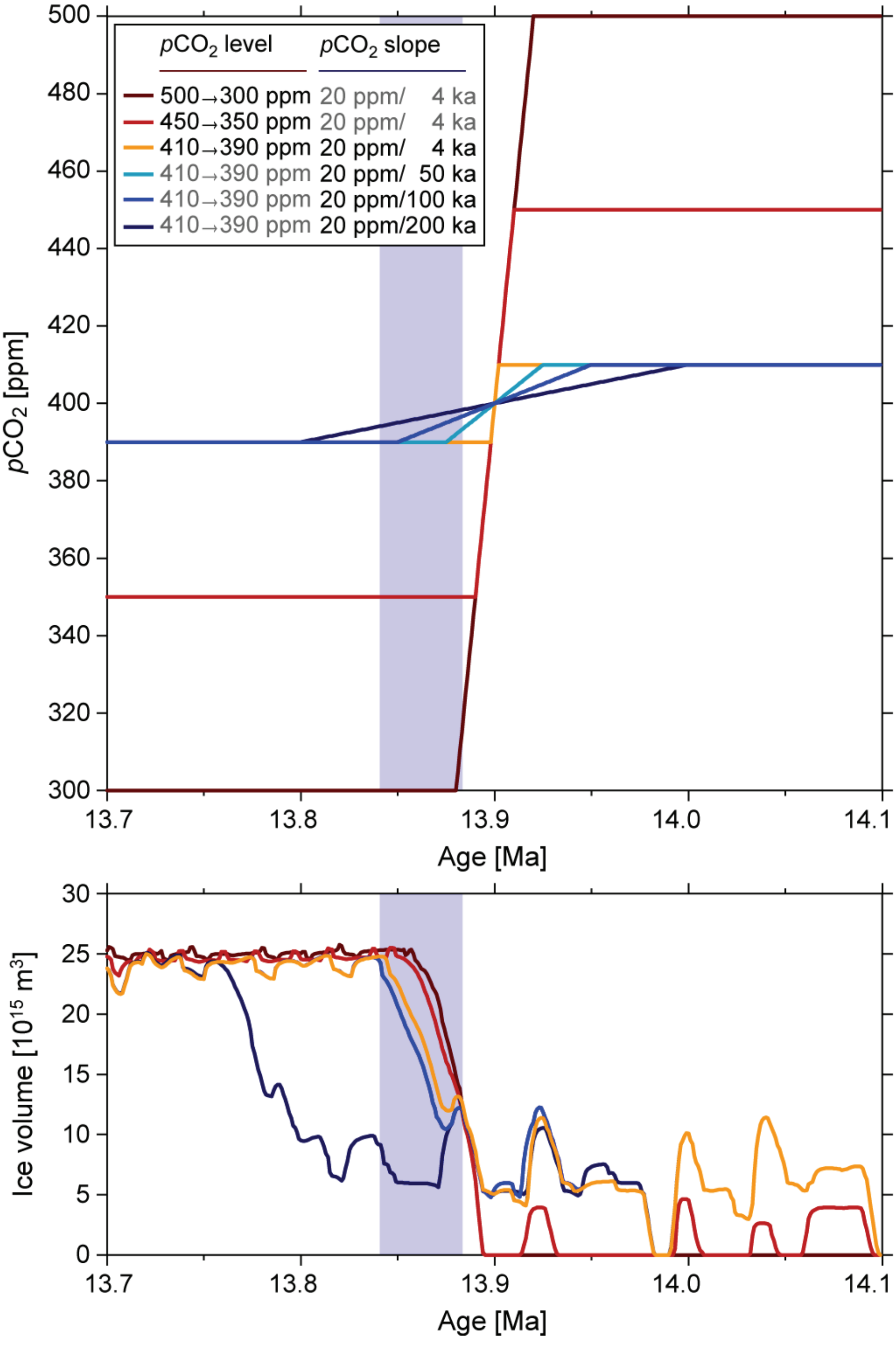

Figure 3.5: *pCO$_2$ sensitivity experiments - level of initial and final pCO$_2$ (red colors) and speed of pCO$_2$ decrease (blue colors). Colors in* ***upper*** *panel show pCO$_2$ forcing and correspond to ice-volume transition in* ***lower*** *panel. Blue box indicates approximate Antarctic glaciation as retrieved from sedimentary records. Glaciation is independent from initial and final pCO$_2$ levels (red to orange). On the contrary, the speed of the pCO$_2$ drawdown is important. Extremely slow drop in pCO$_2$ (dark blue) results in delayed ice-sheet extension, relatively slow decrease (light blue) causes appropriate timing with glaciation. A pCO$_2$ drop of 20 ppm/50 ka or faster (for example 20 ppm/4 ka in orange) give the same ice-sheet transition as 20 ppm/50 ka.*

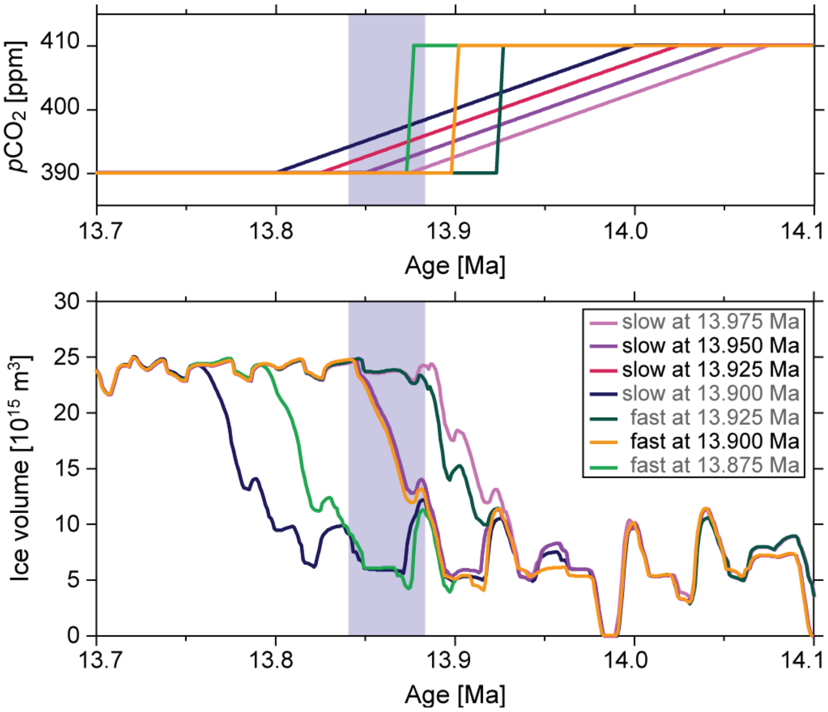

Figure 3.6: *pCO_2 sensitivity experiment - timing of pCO_2 decrease. Colors in* **upper** *panel show pCO_2 forcing and correspond to ice-volume transition in* **lower** *panels. Blue box indicates approximate Antarctic glaciation as found in sedimentary records. Green/orange curves result from fast pCO_2 transition (20 ppm/4 ka); purple/blue ones from a slow drop (20 ppm/200 ka). The center lines (black text in legend) indicate best fitting solutions (see Discussion section). Orange and dark blue curves correspond to their counterparts in Fig. 3.5.*

Table 3.1: *Standard deviation of benthic oxygen-isotope records (‰) of Holbourn et al. (2005).*

Time interval	(Ma)	References and comments
13.2-13.8	13.9-14.5	
0.160	0.207	Site 1146
0.127	0.159	Site 1237
0.144	**0.183**	Mean of above two standard deviations for comparison to modeled ice-volume fluctuations
(Fig. 3.3 **left**)	(Fig. 3.3 **right**)	

The synchronous minima of eccentricity and obliquity at ∼13.84 Ma (*Abels et al.*, 2005) result in a relatively constant and average-to-low insolation, which has been proposed as being partly responsible for the large-scale glaciation in the Middle Miocene (*Holbourn et al.*, 2005). In our ice sheet-climate model, the occurrence of such a special configuration or the natural variability in insolation by itself is not sufficient for an Antarctic glaciation. Only constant atmospheric CO_2 levels at or very close to the threshold of 400 ppm induced a transition

Table 3.2: *Standard deviation of modeled ice-volume variation and equivalent oxygen-isotope ratios using 33×10^{15} m^3 = 1 ‰ [1] (Zachos et al., 2001) and 33×10^{15} m^3 = 2.2 ‰ [2] (Pekar et al., 2002).*

Time interval (Ma)	pCO$_2$ (ppm)	Standard deviation (10^{15} m^3)	ASL (m)	δ^{18}O (‰) [1]	δ^{18}O (‰) [2]	Percentage of data (%)
13.2-13.8	220	0.041	0.104	0.001	0.002	**1 % of 0.144**
13.2-13.8	390	1.059	2.677	0.027	0.059	**41 % of 0.144**
13.9-14.5	410	2.542	6.426	0.064	0.141	**77 % of 0.183**

from small to large ice volume (Fig. 3.2), in a period that does not precisely corresponding to the transition depicted from oxygen isotope records. Therefore, in order to appropriately glaciate the Antarctic continent, some decrease in pCO$_2$ must have occurred.

3.4.2 Sensitivity experiments

In order to constrain the atmospheric CO$_2$ transition in the Middle Miocene, experiments with a constant pCO$_2$ decrease were performed. Three important factors defining the transition (the amount of pCO$_2$ drawdown, the slope and the timing of the event) are highly unknown, and were therefore tested in the following sensitivity experiments. First the ice-sheet model is forced by a decrease in atmospheric CO$_2$ with identical slopes and timing (Fig. 3.5 - red curves). The resulting glaciations occurred around the same time, with some difference in ice-sheet growth efficiency. The larger the difference between initial and final pCO$_2$, the faster the transition was. This can be explained by the different variability of the ice sheet at different pCO$_2$ levels. The larger standard deviations of 1.059×10^{15} m^3 and 2.542×10^{15} m^3 (Tab. 3.1) in the 390- and 410 ppm-runs, respectively, enhance the possibility for insolation variations to act against a rapid ice-volume transition. Because of the fact that sedimentary records do not indicate such a rapid glaciation (e.g. *Holbourn et al.*, 2005) and do show large variance in time, the relatively small difference in pCO$_2$ (410 to 390 ppm) is used for the remaining experiments.

The second sensitivity test dealt with the slope of the atmospheric CO$_2$ drawdown (Fig. 3.5 - blue curves). Six experiments with slopes varying between 20 ppm/2 ka to 20 ppm/200 ka were overlapping in time and had equivalent initial and final pCO$_2$ levels. For most runs, the ice-volume transition took place at the same moment. Exception was the slowest forcing (20 ppm/200 ka), which glaciates much later. The duration of the ice-sheet transition was defined as the period in which ice volume is larger than the maximum volume of the small ice sheet and smaller than the minimum size of the large ice sheet. Additional experiments show that slow forcing does not have a strong correlation to the time necessary for glaciation (not shown). It is also evident that the rate of pCO$_2$ drop has no effect on the length of the ice-sheet transition. The duration merely depends on the timing of the pCO$_2$ drop. This quite constrained timing (see next paragraph) limits the glaciation event to a length of approximately 30 ka. Compared to the duration of glaciation depicted by available data (30-40 ka according to δ^{18}O records by e.g. *Holbourn et al.* (2005)) this is on the fast side, indicating that the ice-sheet model may respond more rapidly than the real Antarctic ice sheet. Most probably the difference in pCO$_2$ before and after the transition is relatively small, in the order of

100-200 ppm (cf. *Pearson and Palmer* (2000); *Royer et al.* (2001); *Pagani et al.* (2005); *Kürschner et al.* (2008); *Zachos et al.* (2008), which make the slowest pCO_2 transitional experiments not very likely.

Nevertheless, the third set of sensitivity experiments investigated the timing of the pCO_2 decrease, for the (too) slow pace of 20 ppm/200 ka and for the faster and more realistic speed of 20 ppm/4 ka (Fig. 3.6). The best fit to data (glaciation time shown by vertical green lines) occurred either with a fast drawdown around 13.9 Ma, or a slow drawdown starting centered around 13.925-13.95 Ma (bold lines). Shifting this by only 2 ka resulted into a much earlier (~13.91 Ma) or later (~13.78 Ma) glaciation. This experiment was based on a 20 ppm difference in pCO_2, but extending this range would give similar results (see first sensitivity test).

The comparison of the three sensitivity experiments to glaciation- and pCO_2-estimates from sedimentary records indicates that the pCO_2 drop should cross the threshold at approximately 400 ppm and should have occurred just before the ice-sheet transition (around 13.9 Ma) with a slope of approximately 20 ppm/4 ka (corresponding to ~150 ppm/30 ka). Because of the fact that the exact values are model dependent, these numbers should only be taken as guidelines, but they do put some constraints on the amount, pace and extent of the pCO_2-decrease.

Our results also contradict the hypothesis that Antarctic glaciation partly originated due to synchronous minima in eccentricity and obliquity around 13.84 Ma (e.g. *Holbourn et al.*, 2005; *Abels et al.*, 2005). The ice sheet-climate model is forced by daily insolation, which were averaged over the whole year (annual mean) and over the caloric summer (half year of largest daily insolation) to promote comparison to the resulting ice-volume variations. The two upper panels in Fig. 3.2 show the annual and summer mean insolation over the Middle Miocene period. The latitude of 70° S is chosen, because the large as well as the small ice-sheet volume variations correlated best to this latitude, although with a different lag time (see Result section). The combined minima in eccentricity and obliquity at ~13.84 Ma resulted in an average to high summer and annual mean insolation at 70° S. From the sensitivity experiments it can be seen that Antarctic glaciation is favored by maxima in ice-volume variations of the small ice sheet. These maxima are correlated to minima in insolation. For an ice-sheet extension in the Middle Miocene to occur, similar as illustrated by benthic oxygen-isotope records, the minima in high-latitude insolation at approximately 13.88 Ma is the most suitable candidate. So, instead of pointing to 13.84 Ma as an important insolation moment for the Antarctic glaciation, 13.88 Ma is more appropriate.

3.4.3 100-ka cycles

Without a carbon cycle implemented in the ice sheet-climate model, it is of course difficult to discuss possible interactions between the carbon cycle, ice volume and global climate. On the other hand the low computation time allowed us to easily test the effect of various pCO_2 scenarios on ice volume. Here we focus on pCO_2-cycles with a frequency of 100 ka, similar to glacial-interglacial cycles of the Quaternary. It has been proposed that these cycles are caused by variability in the carbon cycle (e.g. *Shackleton*, 2000; *Pälike et al.*, 2006) in contrast to

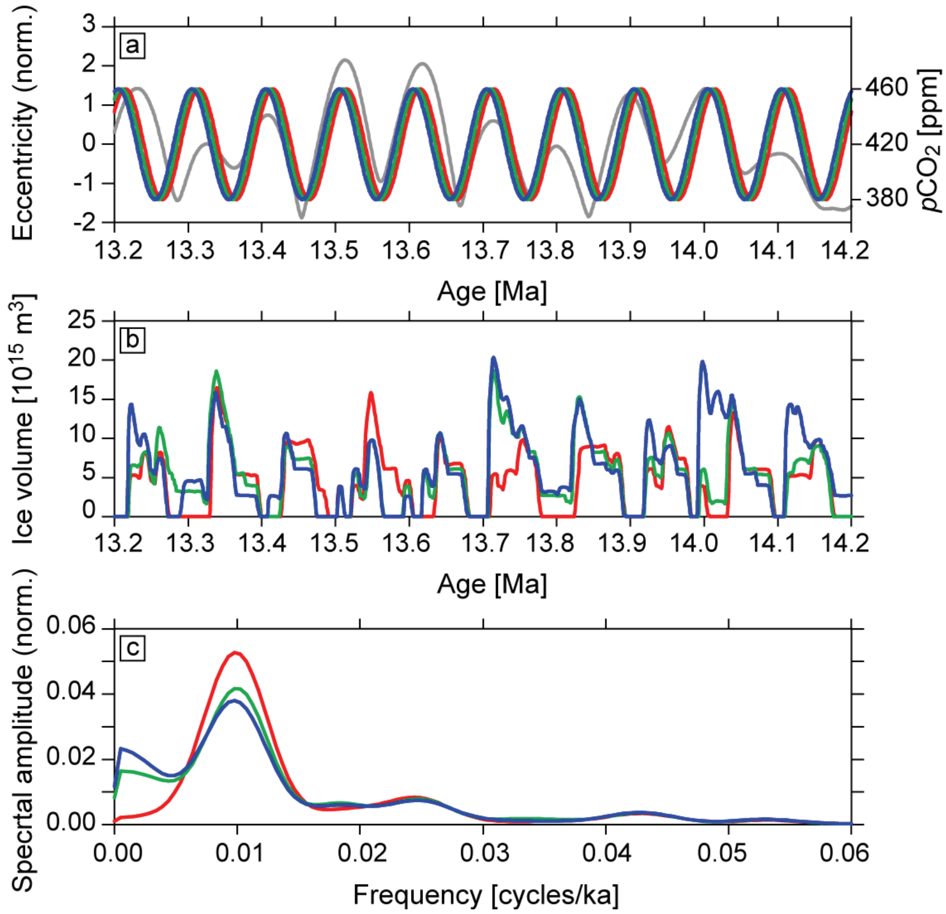

Figure 3.7: *Forced 100-ka pCO_2 cycles.* ***(a)*** *Normalized eccentricity (grey).* ***(b)*** *and* ***(c)*** *pCO_2 scenarios (colors) with mean levels of 420 ppm and amplitude of 40 ppm. Maxima in pCO_2 are tuned to maxima in eccentricity (best fit in green). Resulting glacial-interglacial ice-volume cycles. Normalized power spectral densities, with a strong 100-ka periodicity. Spectral analyses were performed using function pwelch in MATLAB 7.3.0.*

studies showing that internal ice-sheet dynamics could result in the appropriate periodicity (*Pollard*, 1982, 1983a). Following the previous ideas, the model was forced by atmospheric CO_2 changes that included a 100-ka cycle. Glacial-interglacial-like ice-volume cycles are found when the mean pCO_2 is around 420 ppm and the amplitude is about 40 ppm (Fig. 3.7). This is comparable to the ~50 ppm amplitude in pCO_2 found in ice-core records (e.g. *Petit et al.*, 1999). When maxima in pCO_2 are close to maxima in eccentricity, the 100-ka cycle is most apparent. Similar to ice-volume cycles in the late Quaternary recorded in marine sediment records (e.g. *Lisiecki and Raymo*, 2005) the modelled ice volume showed slow ice build-up and rapid terminations. This asynchronous, threshold behaviour originates from internal model feedbacks, as the eccentricity rhythm within the input forcing was purely sinusoidal. Ice volume lagged pCO_2 with approximately 11-16 ka, which is in range with the 14 ka deducted by *Shackleton* (2000).

3.5 Conclusions

Despite the relatively simple geometry of our ice sheet-climate model, the realistically tuned climate sensitivity and hysteresis experiments indicate that the mechanism described in the following conclusions can be considered robust. However, exact numbers are model dependent and should only be taken as a guideline.

1. It is very unlikely that a constant pCO_2 forcing induced the large-scale Antarctic glaciation in the Middle Miocene. Constant levels produced either a large (below ~400 ppm threshold) or a small (above ~400 ppm) ice sheet. Large ice sheets covered the whole Antarctic continent and had a smaller ice-volume variation than expected from sedimentary deep-sea records (~41 %). The variance in the small ice sheet explained the fluctuation in oxygen-isotope ratios in these records for ~78 %. Residual variation in the isotope records can originate from fluctuations in pCO_2 or other changes in climatic conditions. Ice-volume variations correlated best to insolation at relatively high latitudes (~$70°S$). In case of the small ice sheet summer mean insolation was the main forcing, which lead ice volume by ~2 ka. Ice volume lagged insolation by 5-6 ka in the large ice sheet and correlated only to some extent better to summer than annual mean values.

2. The extent of the pCO_2 drawdown was not important for timing or duration of the glaciation event, as long as it crosses the 400 ppm threshold. Moderate or quick pCO_2 reductions resulted in comparable and realistic ice-sheet extension. The ice-sheet response was fast, which limited the pCO_2 drawdown to happen around 13.9 Ma. A relatively slow drop in pCO_2 caused a delayed glaciation and had to occur at 13.925-13.950 Ma. The best guess for the Middle Miocene pCO_2 decline was a scenario crossing the threshold of 400 ppm around 13.9 Ma with a speed of ~150 ppm/30 ka.

3. Forcing the ice sheet-climate model with 100-ka pCO_2 cycles of 40 ppm amplitude resulted in late Pleistocene ice-age-like behavior, with slow ice-volume build-up, and rapid terminations. Ice-volume variations lagged pCO_2 cycles by 11-16 ka, similar to what had been found by *Shackleton* (2000).

Submitted to *Paleoceanography* (October 2008) as: Langebroek, P.M., A. Paul and M. Schulz, Comparison of simulated oxygen isotopes from an ice sheet-climate model to proxy data during the Middle Miocene.

Chapter 4

Comparison of simulated oxygen isotopes from an ice sheet-climate model to proxy data during the Middle Miocene

Abstract

Oxygen-isotopic ratios are implemented in an ice sheet-climate model in order to directly compare the modeled isotopic ratio of the sea water to the high-resolution isotopic records from deep-sea sediment cores in the Middle Miocene. The isotopic depletion resulting from the modeled ice-sheet expansion explains a significant part of the 0.5 ‰ step defined from deep-sea sediment records. Furthermore, we took the opportunity to investigate the relation between sea level (or global ice volume) and the isotopic composition of sea water. Our experiments confirm validity of the relation of approximately 1 ‰ enrichment per 100 m sea-level lowering. We further show that this relationship is restricted by the mean ocean depth and oxygen-isotopic composition of the ice sheet. Large continental ice sheets are more depleted in heavy oxygen isotopes and reach therefore a slightly higher ratio. In contrast, small ice sheets have a less depleted isotopic composition and correspondingly have a smaller effect on the isotopic composition of the ocean.

4.1 Introduction

The ratio of oxygen isotopes measured in the shells of (benthic) foraminifera ($\delta^{18}O_c$, the relative deviation in ‰ from a known external standard) is one of the most commonly used proxies for paleoclimate reconstructions. Interpretation of this ratio is, however, not straight forward, because it is influenced by temperature and the isotopic composition of the water surrounding the foraminifera (*Shackleton*, 1974). The oxygen-isotope ratio of seawater ($\delta^{18}O_{sw}$, deviations with respect to Vienna Standard Mean Ocean Water (*Gonfiantini*, 1978)) itself depends on the global ice volume (V_{ice}), the isotopic composition of the ice ($\delta^{18}O_{ice}$) and local variations (e.g. *Waelbroeck et al.*, 2002). By stacking deep-sea records from different locations (*Zachos et al.*, 2001; *Lisiecki and Raymo*, 2005) the local $\delta^{18}O_{sw}$ and temperature effects are thought to be reduced and $\delta^{18}O_c$ can be used as a proxy for global ocean temperatures and ice volume. Often, the $\delta^{18}O_c$ record is disentangled using independent temperature proxies (e.g. Mg/Ca (e.g. *Lear et al.*, 2000)). After correcting for the temperature effect, in principle global ice volume can be deducted assuming a constant $\delta^{18}O_{ice}$ in time.

During the Middle Miocene (~13.9 Ma), an increase in benthic $\delta^{18}O_c$ (*Zachos et al.*, 2001; *Holbourn et al.*, 2005) in combination with a global sea-level fall (*Miller et al.*, 1998, 2005) strongly indicate a shift towards colder climatic conditions. However, it is still not well defined to what extent the increase in $\delta^{18}O_c$ is caused by the expansion of the Antarctic ice sheet, possibly in combination with a change in $\delta^{18}O_{ice}$, and which part is due to a decrease in deep-sea temperature. Low-resolution studies using the ratio of Mg/Ca in benthic foraminifera to separate the temperature from the ice-volume effect suggested that the major part (70-85 %) of the increase in benthic $\delta^{18}O_c$ during the Middle Miocene can be explained by the expansion of continental ice (e.g. *Lear et al.*, 2000; *Shevenell et al.*, 2008). In this study we used a different approach, focusing on the ice-sheet part of the proxy (following the work of (*Mix and Ruddiman*, 1984; *Lhomme et al.*, 2005; *Sima et al.*, 2006)). In our ice sheet-climate model, fluctuations in Antarctic ice volume as well as variations in $\delta^{18}O_{ice}$ were computed. Resulting $\delta^{18}O_{sw}$ anomalies could then directly be compared to the deep-sea records of benthic oxygen isotopes. We applied this technique to the large-scale cooling event in the Middle Miocene and found that indeed a significant part (if not all) of the deep-sea record can be explained by Antarctic glaciation. Combining ice volume and $\delta^{18}O_{ice}$ (or $\delta^{18}O_{sw}$) in a coupled model also creates a unique opportunity to investigate the relation between these parameters. Previous estimates range from 0.8-2.2 ‰ increase in $\delta^{18}O_c$ per 100 m sea-level fall (*Fairbanks and Matthews*, 1978; *Schrag et al.*, 1996; *Pekar et al.*, 2002). We validated this relationship and concluded that a 1 ‰ increase in the isotopic composition of seawater is bound to be related to a sea-level lowering of approximately 100 m.

4.2 Methods and Experimental Set-up

4.2.1 Ice Sheet-Climate Model

The coupled ice sheet-climate model is an extension of the ice-sheet model used by *Sima et al.* (2006). It has been adapted to Antarctica and is described in detail in Chapter 3. In the version used in this research, the oxygen-isotope ratio of ice ($\delta^{18}O_{ice}$) is implemented as a passive tracer (as for the Laurentide ice sheet in *Sima et al.* (2006)). In short, the coupled ice sheet-climate model consists of three large-scale boxes spanning the entire southern hemisphere and is symmetric around the axis of the South Pole. In the two lower-latitude boxes (0-30 °S and 30-60 °S) climatic parameters (e.g. temperature, T; albedo, α) are described as mean values for the entire box. Parameters in the high-latitude box (60-90 °S) are resolved at a higher resolution of 0.5° latitude. This Antarctic box includes separate atmospheric and surface energy balances that are solved simultaneously. The mass balance of the Antarctic ice sheet within this box depends on the daily accumulated precipitation, evaporation and ablation, possibly reduced by (surface and/or bottom) melting and calving. The entire model is forced by daily insolation (depending on orbital parameters (*Berger*, 1978a,b; *Laskar et al.*, 2004)) combined with prescribed atmospheric CO_2 (pCO_2) levels. Within the ice-sheet, velocities and temperatures are computed in each of the 12 vertical layers. In the current extended version, the same advection scheme transporting ice temperature is also used to trace $\delta^{18}O_{ice}$ within the layers. The spatial and temporal parameterizations of surface $\delta^{18}O_{ice}$, or rather the oxygen-isotope ratio of snow, are described in the next two sections.

4.2.2 Present-day Spatial Distribution Oxygen Isotopes

The present-day isotopic composition of snow ($\delta^{18}\mathrm{O}_{\mathrm{snow}}$) depends on geographical characteristics (latitude, λ; surface elevation, h_{sfc}; distance from the open ocean, d_{sea}) and climatic parameters (annual mean surface temperature, T_{sfc} and precipitation, P). *Giovinetto and Zwally* (1997) compiled a large data set containing mean $\delta^{18}\mathrm{O}_{\mathrm{snow}}$ values combined with corresponding geographical and climatic parameters for over 400 sites on Antarctica. Their linear regression shows an optimum correlation between $\delta^{18}\mathrm{O}_{\mathrm{snow}}$ and T_{sfc} according to:

$$\delta^{18}\mathrm{O}_{\mathrm{snow}}[‰] = 0.852 \times T_{\mathrm{sfc}}[^{\circ}\mathrm{C}] - 6.78\,, \tag{4.1}$$

with a correlation coefficient (r^2) of 0.92. Using several (or all) parameters in multivariate or stepwise regression analysis did not really improve the correlation between parameterized and observed $\delta^{18}\mathrm{O}_{\mathrm{snow}}$. The minor effect of the geographical parameters on the $\delta^{18}\mathrm{O}_{\mathrm{snow}}$ parameterization is mainly due to the fact that T_{sfc} itself already largely depends on these variables. A more recent publication using a database of more than 1000 locations estimated a similar linear relationship between T_{sfc} and $\delta^{18}\mathrm{O}_{\mathrm{snow}}$ (r^2=0.92; *Masson-Delmotte et al.* (2008)):

$$\delta^{18}\mathrm{O}_{\mathrm{snow}}[‰] = 0.80 \times T_{\mathrm{sfc}}[^{\circ}\mathrm{C}] - 8.11\,. \tag{4.2}$$

4.2.3 Past Isotopic Distribution

For reconstructing the past isotopic composition of the Antarctic ice sheet the only available data comes from ice-core records. These cores only extend back to ~800 ka (*EPICA community members*, 2004) and therefore cannot constrain $\delta^{18}\mathrm{O}_{\mathrm{ice}}$ during the Middle Miocene. Bore hole paleothermometry indicates that the spatial relationship between $\delta^{18}\mathrm{O}_{\mathrm{snow}}$ and T_{sfc} can introduce large errors when used for temporal $\delta^{18}\mathrm{O}_{\mathrm{snow}}$ reconstructions between the present-day and the Last Glacial Maximum (LGM) in central Greenland (e.g. *Cuffey et al.*, 1995). On the other hand, atmospheric models for Antarctica suggest that the isotopic-temperature slope remained valid for the LGM (e.g. *Delaygue et al.*, 2000). Past $\delta^{18}\mathrm{O}_{\mathrm{snow}}$ can therefore be derived from the present-day spatial distribution of $\delta^{18}\mathrm{O}_{\mathrm{snow}}$, corrected for local changes in surface elevation (Δh_{sfc}) and changes in mean surface temperature of the ice sheet ($\Delta\ T_s$) (*Cuffey*, 2000; *Lhomme*, 2004; *Lhomme et al.*, 2005):

$$\delta^{18}\mathrm{O}_{\mathrm{snow}}(\lambda,\mathrm{t}) = \delta^{18}\mathrm{O}_{\mathrm{snow}}(\lambda) + \alpha_{\mathrm{c}}\Delta T_{\mathrm{s}}(\mathrm{t}) + \beta_{\delta}\Delta h_{\mathrm{sfc}}(\mathrm{t})\,, \tag{4.3}$$

where α_c is the isotopic sensitivity to temperature and β_δ the isotopic lapse rate. According to *Lhomme* (2004) and references therein the value of β_δ is -11.2 ‰/km, while α_c ranges from 0.6 to 0.8 ‰/°C.

4.2.4 Computation of the Oxygen-Isotopic Composition of Seawater

The modeled bulk $\delta^{18}O_{ice}$ composition of the Antarctic ice sheet was converted into the oxygen-isotopic composition of seawater ($\delta^{18}O_{sw}$) by a simple closed-balance computation, assuming a well-mixed ocean with constant average depth (d_0) and surface area (A_0) similar to present-day and by setting the initial $\delta^{18}O_{sw}$ to zero (*Sima et al.*, 2006):

$$\delta^{18}O_{sw} = -\frac{S_i}{d_0 - S_i}\delta^{18}O_{ice}\,, \tag{4.4}$$

where S_i is the Antarctic volume-equivalent sea level, using ρ_{ice} and ρ_{water} as densities of ice and water, respectively:

$$S_i = \frac{\rho_{ice} V_{ice}}{\rho_{water} A_0}\,. \tag{4.5}$$

Accordingly, Antarctica is considered to be the only ice sheet influencing $\delta^{18}O_{sw}$ and changes in sea level. For the experiments during the Middle Miocene we focused on the transition from a small to a large ice sheet, therefore the initial conditions were not crucial for the final interpretation. Present-day mean values of 3800 m, 3.605×10^{14} m^2, 910 kg/m^3 and 1000 kg/m^3 were used for d_0, A_0, ρ_{ice} and ρ_{water}, respectively. Using the simplified $\delta^{18}O$ rather than tracing the actual mass ratios for all oxygen isotopes in the model introduces a negligible conservation error (*Sima*, 2005).

4.2.5 Experimental Set-up

The ice sheet-climate model was forced by varying orbital parameters (*Laskar et al.*, 2004) and several scenarios of pCO$_2$. The present-day spatial distribution of $\delta^{18}O_{snow}$ was deduced under constant pCO$_2$ conditions of 280 ppm. The model was spin-up for a 1 million years (Ma), before comparing the modeled present-day conditions to measured $\delta^{18}O_{snow}$. For the Middle Miocene four different constant levels of pCO$_2$ were used as model forcing, pre-industrial (280 ppm) and three levels close to the modeled glaciation threshold of $\sim$400 ppm (390, 410 and 420 ppm), resulting in two large and two small, ephemeral ice sheets (see also Chapter 3. The scenarios were computed over a period from 14.1 to 13.6 Ma after a 200 ka spin-up. The $\delta^{18}O_{snow}$ parameterizations were tested for all four resulting ice sheets. Both spatial relations relationship between $\delta^{18}O_{snow}$ and T_{sfc} (*Giovinetto and Zwally*, 1997; *Masson-Delmotte et al.*, 2008) were applied using a set of values for the constants in the temporal parameterization of *Lhomme* (2004). After these sensitivity experiments, the climatic transition in the Middle Miocene was modeled using one of the parameterizations and a pCO$_2$ reduction from 410 to 390 ppm around approximately 13.9 Ma (Chapter 3).

Table 4.1: *Characteristics of benthic foraminiferal oxygen-isotope records during the Middle Miocene before (13.9-14.5 Ma) and after (13.2-13.8 Ma).*

	Number of data		Mean $\delta^{18}O_c$ (‰)		Increase	Reference
	before	*after*	*before*	*after*	(‰)	
Site 1164	167	251	1.20	1.71	0.51	*Holbourn et al.* (2005)
Site 1237	100	158	1.64	2.15	0.51	*Holbourn et al.* (2005)
Site 1171	82	87	1.50	2.03	0.52	*Shevenell and Kennett* (2004)
Leg 154	601	115	1.84	2.33	0.49	*Raffi et al.* (2006)
Compilation	107	250	1.89	2.23	0.34	*Zachos et al.* (2001)

4.3 Results

4.3.1 Oxygen-Isotope Records Spanning the Middle Miocene

Before discussing the $\delta^{18}O$ results computed by our ice sheet-climate model, we would like to give a brief overview of the characteristics of the available records of the oxygen-isotope ratio measured on benthic foraminifera ($\delta^{18}O_c$). To our knowledge only three high-resolution records cover the period between 14.5 and 13.2 Ma (Ocean Drilling Program (ODP) Sites 1146 and 1237 (*Holbourn et al.*, 2005, 2007)) and ODP Site 1171 (*Shevenell et al.*, 2004; *Shevenell and Kennett*, 2004). One additional record covers the Middle Miocene transition, but unfortunately terminates at approximately 13.7 Ma (*Raffi et al.*, 2006). Many other, lower resolution records are combined into the *Zachos et al.* (2001) compilation. Table 4.1 and Figure 4.1 summarize the main features of these records for two particular time periods; before the oxygen-isotope shift (13.9-14.5 Ma) and after the transition (13.2-13.8 Ma). The mean increase in $\delta^{18}O_c$ per individual record is approximately 0.5 ‰.

4.3.2 Present-day Conditions

Figure 4.2a shows the modeled annual-mean present-day $\delta^{18}O_{\mathrm{snow}}$ distribution from our ice sheet-climate model using the parameterizations of *Giovinetto and Zwally* (1997) and *Masson-Delmotte et al.* (2008) (see Section 4.2.2). Results are compared to the database of *Masson-Delmotte et al.* (2008, red dots). Spatial coverage of the data at high latitudes (poleward of 75 °S) remains poor. Therefore the present-day isotopic composition of Antarctic snow from a modeling study using an advanced Rayleigh-type isotope distillation model with 40-yr European Centre for Medium-Range Weather Forecasts (ECMWF) Re-Analysis (ERA-40) data as meteorological input (*Helsen et al.*, 2007) is additionally shown for comparison. This type of modeling also has its deficits and is known to underestimate the depletion of $\delta^{18}O_{\mathrm{snow}}$ values by ~10 % at higher elevations (latitudes) (*Helsen et al.*, 2007). Our ice sheet-climate model computed a latitudinal distribution comparable to the isotope distillation model with a maximum depletion of approximately -45 ‰ near the South Pole as compared to values below -50 ‰ (e.g. *Zwally et al.*, 1998). Interestingly, the annual mean near surface-air temperatures derived from our ice sheet-climate model fell into the range measured temperatures

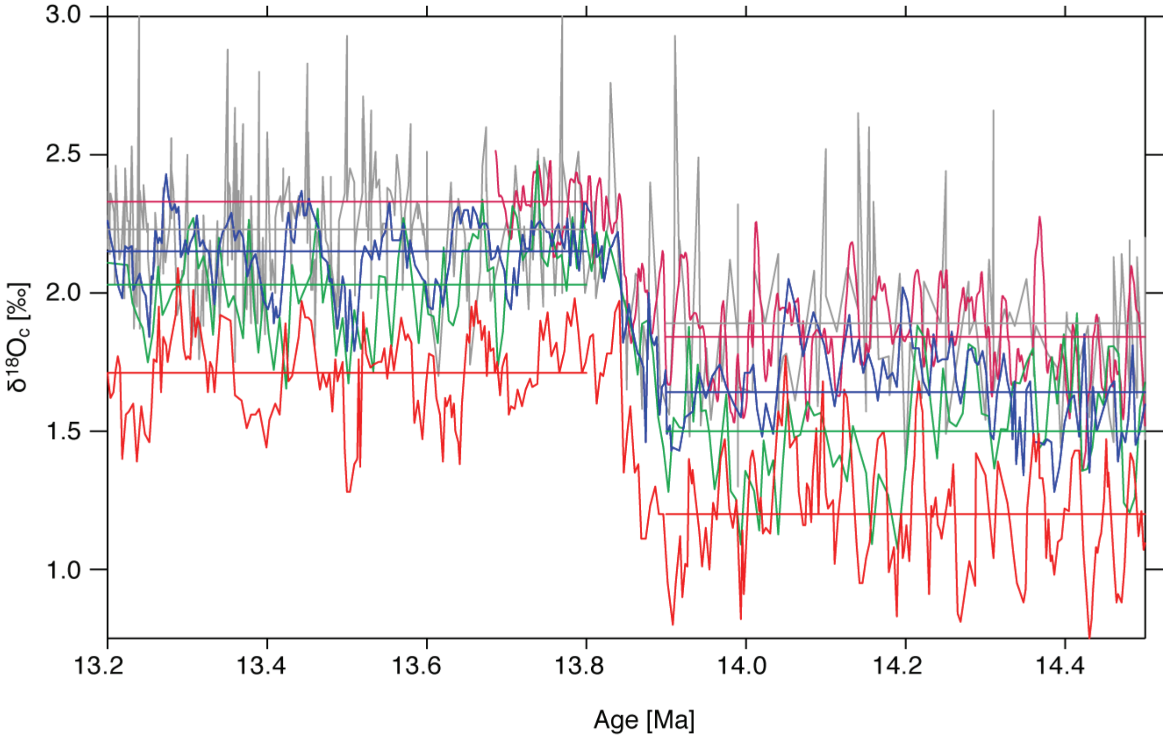

Figure 4.1: *Compilation of high-resolution benthic $^{18}O_c$ records in the Middle Miocene. The two records from Holbourn et al. (2005) are plotted in blue (Site 1237) and red (Site 1146). Another ODP record (Site 1171), at latitudes closer to Antarctica, is indicated in green-blue (Shevenell et al., 2004) on the same age scale. The record with the highest resolution only extends from ∼16.6 Ma to ∼13.7 Ma (purple; Raffi et al. (2006)). The compilation of over 40 records of Zachos et al. (2001) is shown in gray for comparison. The mean values for every records in the period before (13.9-14.5 Ma) and after (13.2-13.8 Ma) the transition are indicated in horizontal straight lines (cf. Tab. 4.1).*

of the database from *Masson-Delmotte et al.* (2008) and are colder than ERA-40 temperatures (Fig. 4.2b). Colder temperatures should result in more depleted $\delta^{18}O_{snow}$. The underestimation of $\delta^{18}O_{snow}$ in the ice-sheet model left its imprint on the mean $\delta^{18}O$ of the entire ice sheet ($\delta^{18}O_{ice}$). The parameterizations of *Giovinetto and Zwally* (1997) and *Masson-Delmotte et al.* (2008) resulted in mean $\delta^{18}O_{ice}$ values of -44.1 and -43.2 ‰, respectively. A different numerical model, combining ice dynamics and tracer transport, indicates more depleted present-day values for the East Antarctic ice sheet of -56.5 ‰ (*Lhomme et al.*, 2005). As this paper focuses on temporal variations in $\delta^{18}O$ of the entire ice sheet and the mean $\delta^{18}O_{ice}$ changes between differently-sized ice sheets, we consider the above described parameterizations between $\delta^{18}O_{snow}$ and T_{sfc} accurate enough.

Figure 4.3 shows annual-mean temperature, velocity and $\delta^{18}O_{ice}$ in the modeled present-day ice sheet. The annual mean temperatures reach maxima just above the pressure-melting point near the bedrock and minima of ∼-50 °C at the inland surface . Meridional velocities of over 150 m/yr are computed at the rim of Antarctica and close to zero between 80 °S and the South Pole. Vertical velocities are very small everywhere, because of the low accumulation of

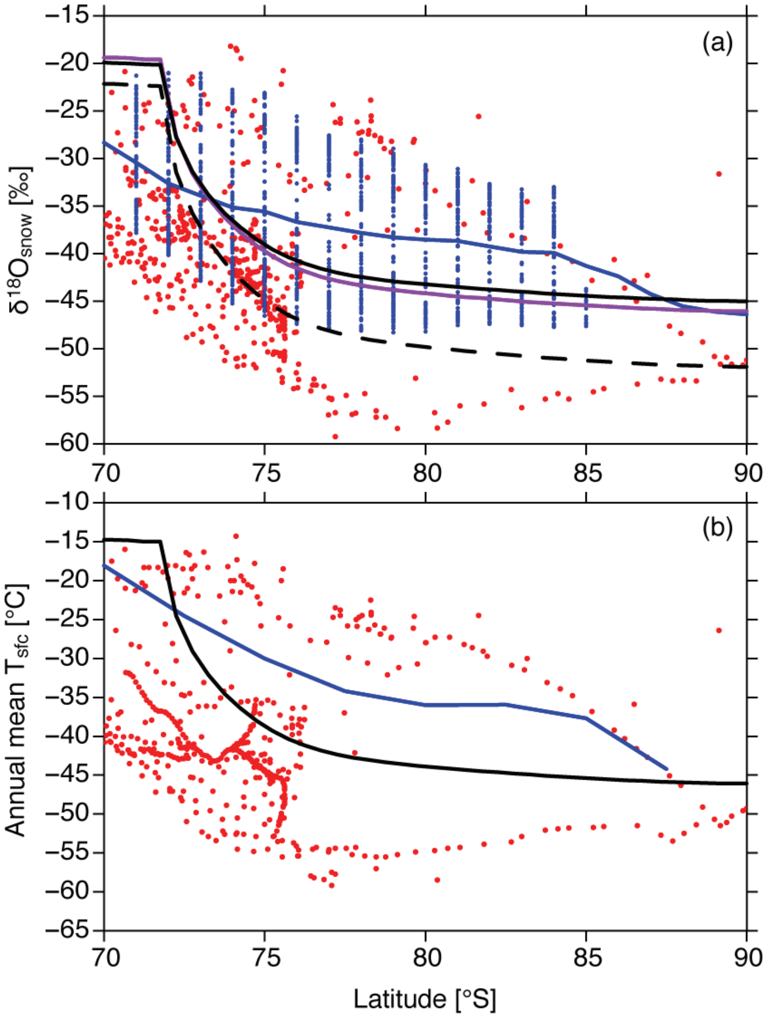

Figure 4.2: *Present-day spatial distribution of **(a)** $\delta^{18}O_{\mathrm{snow}}$ and **(b)** near-surface air temperature. **(a)** Measurements are indicated by red dots (compilation by Masson-Delmotte et al. (2008)). The modeled distribution from a Rayleigh-type isotope distillation model forced by ERA-40 data (Helsen et al., 2007) is shown by blue dots; the mean values are connected by the solid blue line. Our model results using 0.852 $\times T_{\mathrm{sfc}}$ - 6.78 (Giovinetto and Zwally, 1997) are shown in purple and correspond to a present-day bulk $\delta^{18}O_{\mathrm{ice}}$ of -43.1 ‰. Applying the Masson-Delmotte et al. (2008) parameterization (0.80 $\times T_{\mathrm{sfc}}$ - 8.11) resulted in a mean $\delta^{18}O_{\mathrm{ice}}$ values of -42.3 ‰ (black solid line). The effect of increasing the sensitivity to T_{sfc} in the previous equation to 0.95 ‰/°C is indicated by the black dashed line. The bulk $\delta^{18}O_{\mathrm{ice}}$ then reached -48.7 ‰. **(b)** Temperatures from the re-analysis (ERA-40) and Masson-Delmotte et al. (2008) datasets are indicated by blue and red dots, respectively. Results from the ice sheet-climate model from the current study are shown in black.*

snow. $\delta^{18}O_{\mathrm{ice}}$ show a similar pattern as the meridional velocities. Most depleted values are found in the center and at the bottom of the ice sheet, with present-day minima of ∼-46 ‰. The coastal surface contains much higher values, closer to -30 ‰.

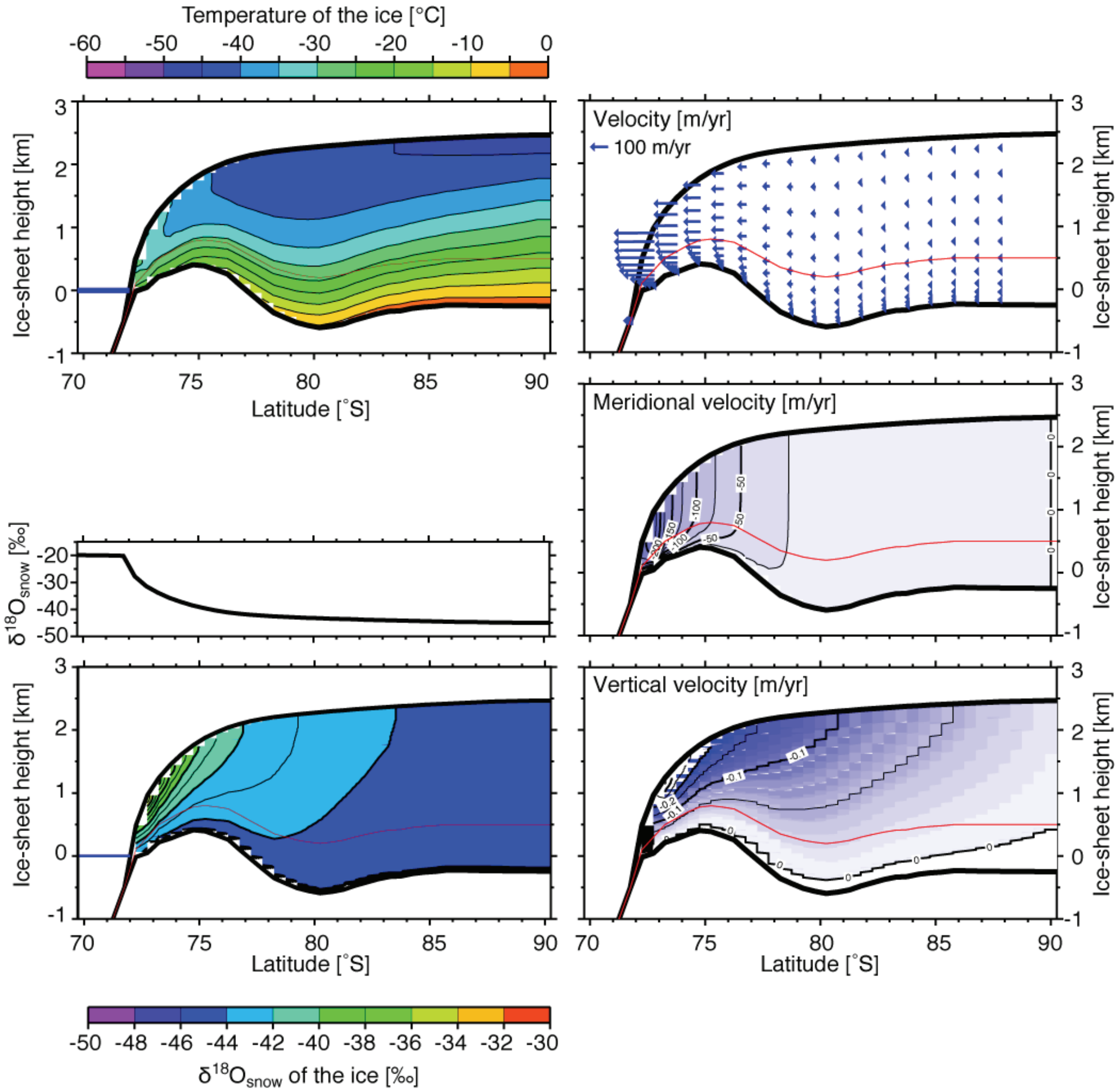

Figure 4.3: *Modeled present-day cross-sections through the Antarctic ice sheet.* ***(Upper left)*** *Temperatures within the ice layers.* ***(Lower left)*** *$\delta^{18}O_{\mathrm{ice}}$ with the corresponding distribution of the $\delta^{18}O_{\mathrm{snow}}$ on top.* ***(Right)*** *Velocity profiles. The thin red line shows the initial bedrock elevation.*

The model is forced by present-day seasonal orbital forcing (*Berger*, 1978a,b; *Laskar et al.*, 2004) combined with prescribed atmospheric CO_2 (pCO_2) levels. Modeled present-day annual mean temperature is 14.8 °C for the southern hemisphere and this value increases by 2.8 °C when pCO_2 is doubled from 280 ppm (the pre-industrial value) to 560 ppm (well within the range of 2.1 to 4.4 °C estimated from atmospheric general circulation models (*IPCC*, 2007), see also Chapter 3).

Table 4.2: *Ice volume, sea level, $\delta^{18}O_{sw}$ and the slope between $\delta^{18}O_{sw}$ and sea level for the four reference experiments. The δ^{18}O-parameterizations of Masson-Delmotte et al. (2008) and Lhomme (2004) (with α_c = 0.6 ‰/°C and β_δ = -11.2 ‰/km) were applied.*

$p\mathrm{CO_2}$ (ppm):	280	390	410	420
Ice volume (10^{15} m^3)	25.07	23.88	6.02	4.49
Mean sea level (m)	63.27	60.28	15.21	11.35
Mean $\delta^{18}O_{sw}$ (‰)	0.73	0.64	0.13	0.09
Slope ($\delta^{18}O_{sw}$/100 m)	1.12	1.08	0.88	0.85

4.3.3 Sea level and oxygen-isotopic composition of sea water

The four different constant $p\mathrm{CO_2}$-levels resulted in four differently-sized ice sheets. Large ice sheets occurred for 280 and 390 ppm, with mean sizes of 25 and 24 × 10^{15} m^3, respectively (Tab. 4.2). The other two forcings (410 and 420 ppm) generated small ice sheets with mean volumes of 6 and 4 × 10^{15} m^3. Converted to sea-level equivalents these mean values resulted in approximately 63, 60, 15 and 11 m. The $\delta^{18}O_{ice}$ computed in these experiments was forced by the present-day distribution parameterization of *Masson-Delmotte et al.* (2008) (Eq. 4.2) together with the temporal equation of *Lhomme* (2004) (Eq. 4.3; α_c=6 ‰/°C, β_δ=-11.2 ‰/km). With decreasing ice volume (increasing $p\mathrm{CO_2}$-forcing), $\delta^{18}O_{sw}$ also decreased (see also Fig. 4.4). Combining all experiments, the relationship between $\delta^{18}O_{sw}$ and sea level and showed a slope of approximately 1 ‰/100 m. Interestingly, this slope reached larger values for large ice sheets and was below this average for small ice sheets. A sea-level drop of 100 m would result in a $\delta^{18}O_{sw}$-increase of (0.86±0.03) ‰ for small ice-sheets and (1.11±0.01) ‰ for large ice sheets.

4.3.4 Sensitivity to $\delta^{18}O_{snow}$ parameterization

To test the robustness of the above described results, we performed a set of sensitivity experiments varying the δ^{18}O-parameterization. In addition to the relationship given by *Masson-Delmotte et al.* (2008) (Eq. 4.2), also the older *Giovinetto and Zwally* (1997) relation (Eq. 4.1) was used as $\delta^{18}O_{snow}$ forcing. For all experiments the parameterization of *Lhomme* (2004) was applied to compute variations in $\delta^{18}O_{snow}$ in the past. Two parameters are used in this approximation: α_c and β_δ. According to *Lhomme* (2004) the former realistically ranges between 0.6 and 0.8 ‰/°C, whereas the latter is set to -11.2 ‰/km. Sensitivity analysis for both extremes in α_c were performed, as well as a larger negative value for β_δ (Tab. 4.3 and Fig. 4.4). The resulting variations in $\delta^{18}O_{sw}$ are quite small. Smaller negative values for β_δ induced similar small deviations (not shown). The uncertainty introduced by the $\delta^{18}O_{snow}$ parameterization is less than 4 % for $\delta^{18}O_{snow}$ as well as for the estimated $\delta^{18}O_{sw}$-sea level slope.

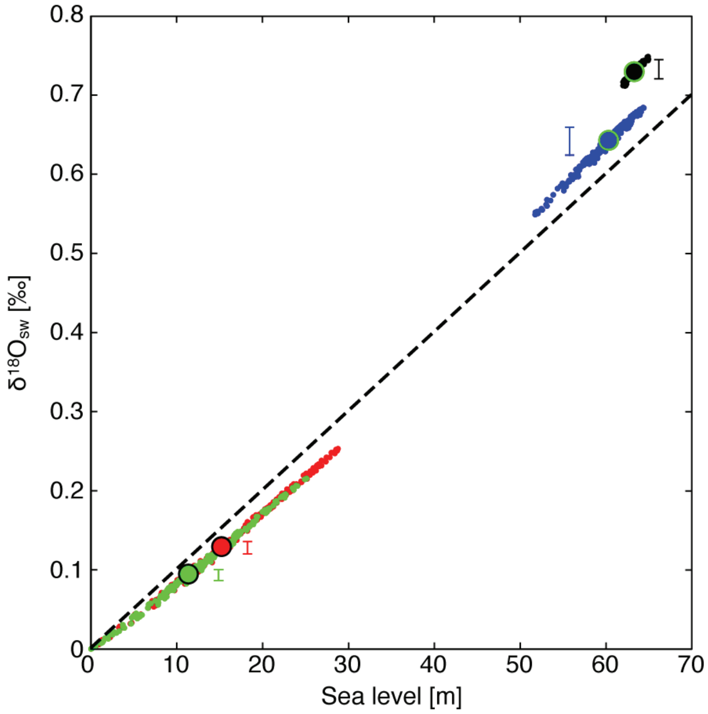

Figure 4.4: *Modeled sea level-$\delta^{18}O_{\mathrm{sw}}$ relationship. Shown are reference experiments forced by 280, 390, 410 and 420 ppm (black, blue, red and green). Here the parameterizations of Masson-Delmotte et al. (2008); Lhomme (2004), with α_c = 0.6 ‰/°C and β_δ = -11.2 ‰/km, were used. Larger dots indicate the mean of each experiment. The error in $\delta^{18}O_{\mathrm{snow}}$ induced by the parameterizations is indicated by the error bars. Dashed line represents the 1 ‰/100 m solution.*

Table 4.3: *Mean $\delta^{18}O_{\mathrm{sw}}$ and $\delta^{18}O_{\mathrm{sw}}$-sea level results from the sensitivity computations. Spatial $\delta^{18}O_{\mathrm{snow}}$-$T_{\mathrm{sfc}}$ equations from Masson-Delmotte et al. (2008) (Eq. 4.2) and Giovinetto and Zwally (1997) (Eq. 4.1) were used. The temporal relation was taken from Lhomme (2004) (Eq. 4.3), in which α_c and β_δ were varied.*

	Temporal (Eq. 4.3)		mean $\delta^{18}O_{\mathrm{sw}}$ (‰)				Slope (‰/100 m)			
Spatial	α_c	β_δ	280	390	410	420	280	390	410	420
Eq. 4.2	0.6	-11.2	0.730	0.643	0.129	0.095	1.122	1.081	0.882	0.853
Eq. 4.2	0.8	-11.2	0.730	0.626	0.124	0.090	1.118	1.063	0.848	0.815
Eq. 4.2	0.8	-12.0	0.729	0.642	0.128	0.094	1.125	1.083	0.876	0.847
Eq. 4.1	0.6	-11.2	0.746	0.658	0.132	0.097	1.143	1.103	0.902	0.872
Eq. 4.1	0.8	-11.2	0.747	0.642	0.127	0.092	1.139	1.084	0.870	0.834
Mean (‰)			0.736	0.642	0.128	0.094	1.129	1.083	0.876	0.844
Error (‰)			0.009	0.016	0.004	0.003	0.012	0.020	0.026	0.028
Error (%)			1.180	2.506	3.297	3.508	1.070	1.849	3.007	3.324

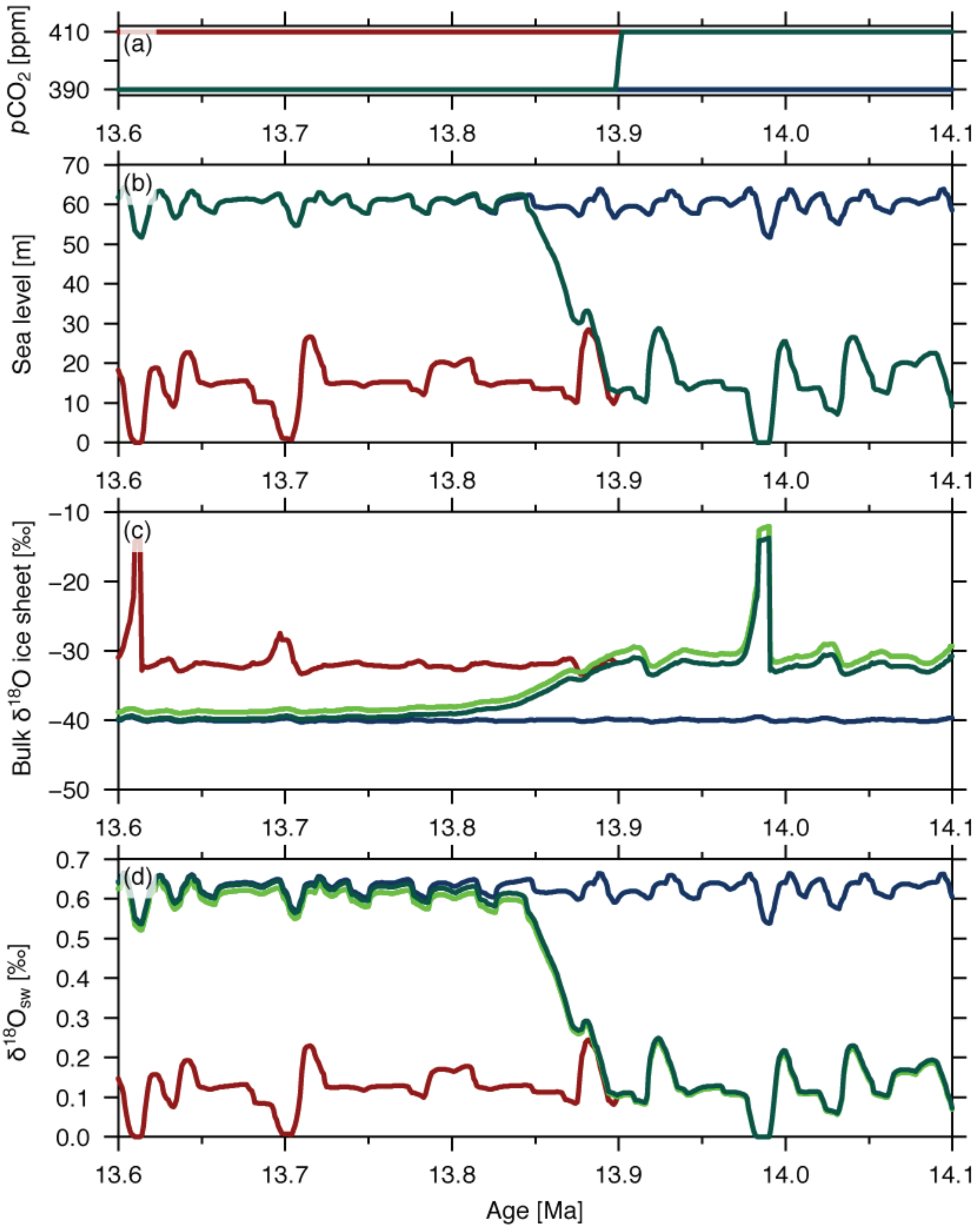

Figure 4.5: *Modeled Middle Miocene transition.* ***(a)*** *pCO_2 (ppm),* ***(b)*** *ice volume in sea-level equivalents (m),* ***(c)*** *bulk $\delta^{18}O_{\mathrm{ice}}$ (‰) and* ***(d)*** *$\delta^{18}O_{\mathrm{sw}}$ (‰). Constant pCO_2-forcing of 410 (390) ppm in red (blue). Transient pCO_2-forcing in dark green for α_c = 0.6 ‰/°C and in light green for α_c = 0.8 ‰/°C.*

4.3.5 Middle Miocene Transition

In Chapter 3 the ice sheet-climate model was used to constrain the atmospheric CO_2 during the Middle Miocene. One of the experiments that showed a good fit to the timing of the glaciation event was forced by a $p\mathrm{CO}_2$ decrease of 410 to 390 ppm, between 13.902 and 13.898 Ma. The same forcing was used in this study in order to create an appropriate transition from a small to a large ice sheet. Before $\sim$13.9 Ma a small ice sheet existed, with a mean ice volume of about 6×10^{15} m^3 or 15 m sea-level equivalent (Fig. 4.5). After $\sim$13.9 Ma, when the $p\mathrm{CO}_2$ level dropped to 390 ppm, the Antarctic continent became entirely glaciated and the mean ice volume reached 24×10^{15} m^3 (60 m sea-level equivalent). With the waxing of the ice sheet, the bulk $\delta^{18}\mathrm{O}_{\mathrm{ice}}$ decreased from $\sim$-32 ‰ to the more depleted values of a large ice sheet ($\sim$-41 ‰). If the Antarctic ice was the only large continental ice volume, the development of the small ice sheet would account for an enrichment of the $\delta^{18}\mathrm{O}_{\mathrm{sw}}$ of mean ocean water by (0.13$\pm$0.01) ‰ relative to an ice-free world. The full grown ice sheet corresponded to a rise of (0.64$\pm$0.02) ‰, implying a difference of (0.51$\pm$0.02) ‰ between a small and a large ice sheet. Figure 4.6 compares the modeled $\delta^{18}\mathrm{O}_{\mathrm{sw}}$ curve with two of the high resolution $\delta^{18}\mathrm{O}_c$ records (*Holbourn et al.*, 2005). The modeled record was shifted such that its mean before the transition corresponds to the mean of the $\delta^{18}\mathrm{O}_c$ data prior to large scale glaciation (13.9-14.5 Ma). The timing as well as the increase in $\delta^{18}\mathrm{O}$ in both, the proxy and the modeled, records is very similar. However, the variance in the $\delta^{18}\mathrm{O}_{\mathrm{sw}}$ data is much smaller than in the measured $\delta^{18}\mathrm{O}_c$.

4.4 Discussion

4.4.1 Oxygen-isotope Parameterizations

The spatial parameterizations used to describe $\delta^{18}\mathrm{O}_{\mathrm{snow}}$ depends entirely on T_{sfc} and resulted in an underestimation of the present-day distribution of $\delta^{18}\mathrm{O}$ within the ice sheet (Fig. 4.3). Time-dependent simulations, based on the present-day values of $\delta^{18}\mathrm{O}_{\mathrm{snow}}$ (corrected for changes in ice-sheet elevation and mean temperatures), therefore had too high $\delta^{18}\mathrm{O}_{\mathrm{ice}}$ values. This could cause problems when the model would be used for specific (ice-core) locations or for any comparison to events depicted by a specific ice-core record. However, the focus of is this study is the relative changes in mean $\delta^{18}\mathrm{O}_{\mathrm{ice}}$ during the Middle Miocene, and the present-day underestimation of $\delta^{18}\mathrm{O}_{\mathrm{snow}}$ is therefore not crucial. The temporal parameterization of $\delta^{18}\mathrm{O}_{\mathrm{snow}}$ derived from observations is valid for a range of values for the constant α_c. We examined the effect of changes in this parameter on the bulk $\delta^{18}\mathrm{O}_{\mathrm{ice}}$ and computed $\delta^{18}\mathrm{O}_{\mathrm{sw}}$ by taking the extremes (0.6 and 0.8 ‰/°C). Higher values resulted in slightly less depleted bulk isotopic compositions of the ice sheet, but the difference in $\delta^{18}\mathrm{O}_{\mathrm{sw}}$ profiles was vanishingly small (Fig. 4.5). The sensitivity study implies that the different $\delta^{18}\mathrm{O}_{\mathrm{snow}}$ parameterizations have only a minor effect (less than 4 %) on the computed $\delta^{18}\mathrm{O}_{\mathrm{ice}}$ (and $\delta^{18}\mathrm{O}_{\mathrm{sw}}$). Therefore, we applied Eq. 4.2 (*Masson-Delmotte et al.*, 2008) and Eq. 4.3 (*Lhomme*, 2004), with α_c = 0.6 ‰/°C and β_δ = -11.2 ‰/km for the remaining part of this study.

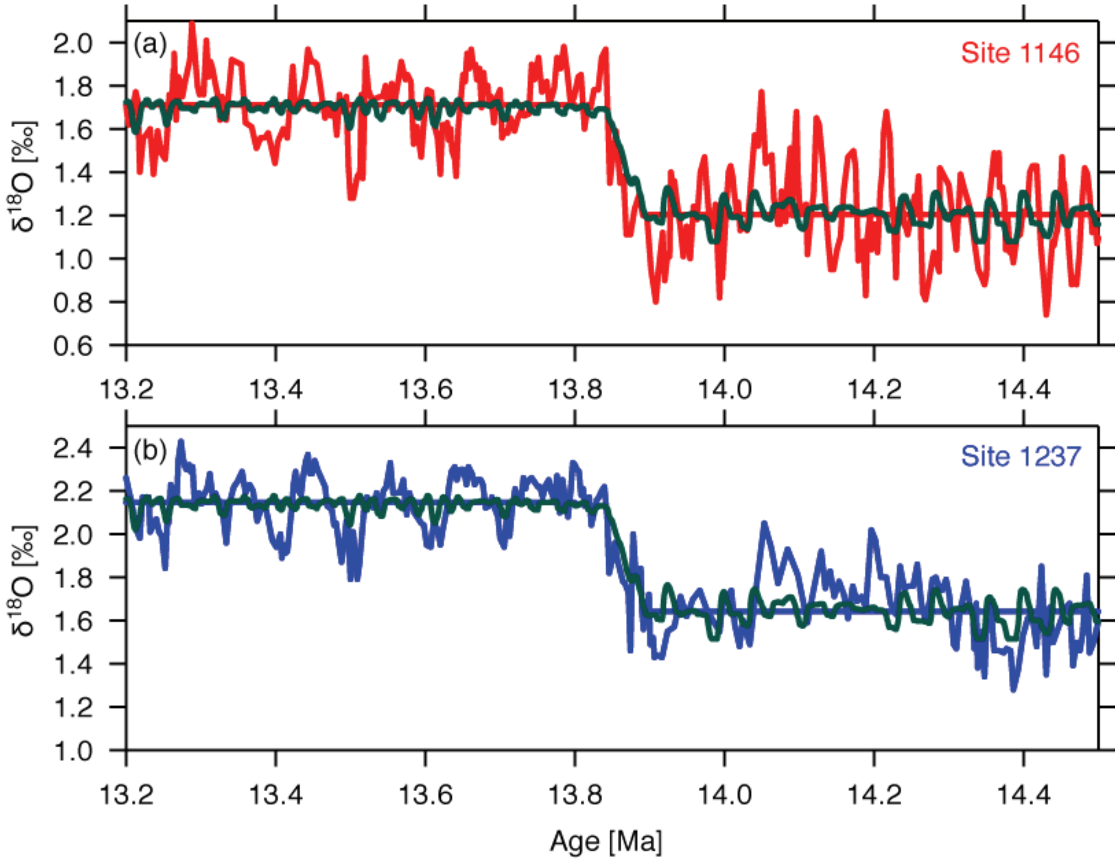

Figure 4.6: *Comparison of modeled $\delta^{18}O_{sw}$ (α_c = 0.6 ‰/°C in dark green and α_c = 0.8 ‰/°C in dashed light green) to $\delta^{18}O_c$ from sediment cores.* ***(a)*** *Site 1146 (red) and* ***(b)*** *Site 1237 (blue). For clarity, the model results are shifted to the mean of each proxy record over the period before the transition (13.9-14.5 Ma).*

4.4.2 Sea level vs. $\delta^{18}O_{sw}$

When no independent information on sea level is available, the part of the measured $\delta^{18}O_c$ which is caused by fluctuations in continental ice volume ($\delta^{18}O_{sw}$) is computed by assuming a linear relation between ice and sea level. From investigating corals, *Fairbanks and Matthews* (1978) derived a value of 1.1 ‰ $\delta^{18}O_{sw}$ increase for a sea level fall of 100 m. Later studies, using pore fluid to constrain the $\delta^{18}O_{sw}$ of the LGM ocean, resulted in values closer to ~0.8 ‰/100 m (c.f. *Schrag et al.*, 1996; *Adkins and Schrag*, 2001). Other assessments, combining sea-level estimates from backstripping of Oligocene sections with benthic $\delta^{18}O_c$ showed a much higher ratio, up to 2.2 ‰/100 m (*Pekar et al.*, 2002; *Pekar and DeConto*, 2006).

By implementing the $\delta^{18}O$ as a tracer in a coupled ice sheet-climate model, we had the opportunity to directly compare sea level (from the ice volume) to $\delta^{18}O_{sw}$ (from $\delta^{18}O_{ice}$) in one model. These experiments were performed under four different levels of pCO_2. The two lower forcings (280 and 390 ppm) resulted in large ice sheets covering the whole of continental Antarctica, whereas the higher pCO_2 levels (410 and 420 ppm) created small, ephemeral ice sheets. Combining all results and converting them to sea levels and $\delta^{18}O_{sw}$-ratios revealed a mean relation of $\sim$1 ‰/100 m, thereby confirming the early studies (e.g. *Fairbanks and Matthews*, 1978; *Schrag et al.*, 1996; *Adkins and Schrag*, 2001). Interestingly, there is a different behavior for the small and the large ice sheets. The $\delta^{18}O_{sw}$ is relatively stronger affected by large ice volumes ($\sim$1.11 ‰/100 m) than by small ice sheets ($\sim$0.86 ‰/100 m).

Both phenomena, the relatively constant relationship between $\delta^{18}O_{sw}$ and S_i and the fact that this ratio slightly varies for differently-sized ice sheets, can be explained by Equation 4.4. Taking the derivative of this equation and neglecting a term that is in the order of 10^{-5} yields:

$$\frac{\partial \delta^{18}O_{sw}}{\partial S_i} = -\frac{\delta^{18}O_{ice}}{d_0 - S_i} \,. \tag{4.6}$$

Typical values for a small ($\delta^{18}O_{ice}$ $\sim$-30 ‰) and a large ($\delta^{18}O_{ice}$ $\sim$-40 ‰) ice sheet result in an $\sim$0.8 and 1.1 ‰ increase of $\delta^{18}O_{sw}$ for a sea-level lowering of 100 m. The mean isotopic ice-volume value of -35 ‰ used in many studies leads to the relation of approximately 1 ‰/100 m. In order to explain much higher ratios, as proposed by *Pekar et al.* (2002), the isotopic composition of the ice sheet should have been $<$ -80 ‰, which is unrealistically depleted. Part of the 2.2 ‰ increase must have been due to an decrease in deep-sea temperature (*Pekar et al.* (2002) suggest about 50 %), which recently has been confirmed by a $\sim$2.5 °C cooling for the same site (*Lear et al.*, 2008).

4.4.3 Oxygen-isotope Transition in the Middle Miocene

We applied the ice sheet-climate model, with $\delta^{18}O$ parameterization included, to the Middle Miocene Antarctic glaciation event. Although Equation 4.4 is based on an initial ice-free world, it is thought that small ice sheets already existed on Antarctica (*Zachos et al.*, 2008; *DeConto et al.*, 2008). We therefore simulated a volume expansion from a small to a large ice sheet. The resulting increase in $\delta^{18}O_{sw}$ is a difference between two states and therefore independent of the assumed initially ice-free conditions of Equation 4.4. *DeConto et al.* (2008) also suggest episodic ice in the Northern Hemisphere. As long as there are no solid constraints on the volume of this ice, it is impossible to consider its effect on global $\delta^{18}O_{sw}$ and we therefore assume that the increase in isotopic composition of sea water is only due to ice expansion on Antarctica.

The available high-resolution records of $\delta^{18}O_c$ measured in benthic foraminifera all show a similar trend in the Middle Miocene. Between $\sim$13.9 and $\sim$13.8 Ma the mean value increased by approximately (0.52$\pm$0.02) ‰ (Tab. 4.1 and Fig. 4.1). Our model experiments show an increase of (0.51$\pm$0.02) ‰ in $\delta^{18}O_{sw}$, indicating that the rise of $\delta^{18}O$ found in the foraminifera could entirely be explained by an increase in ice volume. The overall much larger variations in the reconstructed $\delta^{18}O_c$ records could reflect the effect of fluctuations in (deep) ocean temperature and salinity. The small temperature variations computed in the lower and middle latitude boxes of the ice sheet-climate model are probably too small to explain the large deviations. These temperatures are atmospheric annual mean values for a region of

30° latitude and should show much less variation than local temperature fluctuations of seawater surrounding the foraminifera of a specific deep-sea sediment core. Furthermore, the model forcing was kept (unrealistically) constant at two levels of $p\mathrm{CO}_2$ (390 and 410 ppm). Variations in $p\mathrm{CO}_2$ would also enhance deviations in the modeled $\delta^{18}\mathrm{O}_{\mathrm{sw}}$ record. In Chapter 3 we showed that $p\mathrm{CO}_2$-fluctuations of 80 ppm resulted in Pleistocene ice-age behavior. These glacial-interglacial cycles corresponded to modeled global sea-level variations of approximately 50 m, which leads to a maximum $p\mathrm{CO}_2$-induced variability of ∼0.5 ‰ in the $\delta^{18}\mathrm{O}_c$ record.

4.5 Conclusions

1. This study suggests that the commonly used relation between sea level and $\delta^{18}\mathrm{O}_{\mathrm{sw}}$ (∼1‰/100 m) is also valid for the Middle Miocene and is determined by the mean depth of the ocean and the mean isotopic composition of the ice sheets.

2. Large ice sheets are more depleted in heavy oxygen isotopes (∼-40 ‰) and therefore have a relatively large contribution to the isotopic composition of the ocean (∼1.11 ‰ per 100 m). On the other hand, small ice sheets have a relatively small effect with ∼0.86 ‰ per 100 m, due to their less depleted mean isotopic composition (∼-30 ‰).

3. An ice-volume increase of approximately 18×10^{15} m^3 (or ∼48 m sea-level equivalent) can explain the entire Middle Miocene $\delta^{18}\mathrm{O}_c$ shift found in the benthic foraminifera from high-resolution sediment records.

Submitted to *Paleoceanography* (October 2008) as: Prange, M., P.M. Langebroek, A. Paul and M. Schulz, A possible role of the Panamanian gateway closure in Pliocene Antarctic ice-sheet development.

Chapter 5

A possible role of the Panamanian gateway closure in Pliocene Antarctic ice-sheet development

Abstract

Simulations with the Community Climate System Model CCSM2 in combination with an off-line axially symmetric Antarctic ice-sheet model are performed in order to study the effect of the Panamanian gateway closure on Antarctic ice volume. The gateway closure induces an intensification of the meridional overturning circulation which, in turn, causes a cooling of Antarctica and an expansion of the Antarctic cryosphere. The model results suggest that the corresponding Antarctic ice-volume increase may explain a substantial portion (maybe up to 60%) of the 40–50 m long-term (3.6–2.4 Ma) mid-Pliocene global sea-level lowering that has been calculated by Mudelsee and Raymo (2005). The remaining part of the long-term sea-level change is attributable to the growth of ice sheets in the northern hemisphere. We propose that the first phase (3.6–3.0 Ma) of the mid-Pliocene sea-level decrease was largely caused by Antarctic ice-sheet growth (induced by the Panamanian gateway closure) rather than northern hemisphere glaciation. It is further speculated that the mid-Pliocene Antarctic ice-sheet growth might have had an impact on the global climate system through a possible influence on sea-ice formation, ocean circulation and the carbon cycle.

5.1 Introduction

Deep-sea sediment records reveal a long-term trend towards heavier benthic oxygen isotope values (δ^{18}O) in the course of the last ~50 million years (*Zachos et al.*, 2001). This δ^{18}O increase reflects a long-term global cooling of the ocean as well as the appearance and/or expansion of continental ice-sheets. The gradual Cenozoic cooling trend was punctuated by several 'climate crashes' (i.e. intervals of major global cooling and ice build-up), most notably at or near the Eocene-Oligocene boundary ('Oi-1 Glaciation'), the Oligocene-Miocene boundary ('Mi-1 Event'), in the mid-Miocene and in the mid-Pliocene. The mid-Pliocene 'climate crash' is associated with the Northern Hemisphere Glaciation (NHG), i.e. the significant increase of continental ice volume at high northern latitudes.

Various hypotheses – invoking both terrestrial and extraterrestrial mechanisms – have been proposed to explain the Pliocene NHG (*Raymo*, 1994b; *Mudelsee and Raymo*, 2005, and references therein). Several authors blamed the northern cryosphere expansion on the closing of the Panamanian gateway (e.g. *Weyl*, 1968; *Berggren and Hollister*, 1974; *Keigwin*, 1982; *Haug and Tiedemann*, 1998; *Bartoli et al.*, 2005). However, recent climate modelling studies do not support the 'Panama hypothesis' (*Klocker et al.*, 2005; *Lunt et al.*, 2008a,b). Instead, the models suggest that the closure of the Panamanian gateway had no significant impact on the build-up of northern hemisphere ice-sheets.

These results seem to suggest that the closing of the Panamanian isthmus was "no more than a bit player in global climate change" (*Molnar*, 2008). The closure of the gateway, however, might have affected the climate system in another way than assumed by the 'traditional' Panama hypothesis. Here, we study the possible effect of the Panamanian seaway closure on Pliocene Antarctic ice-sheet development. Indeed, the conventional view of a stable Antarctic ice volume since the mid-Miocene (e.g. *Sugden*, 1996) has been challenged by new data and models that support a more dynamic view of Antarctic ice-sheets (for an overview see, e.g., *Raymo et al.*, 2006; *Hill et al.*, 2007). Recently, *Rebesco and Camerlenghi* (2008) compiled and reviewed the evidence of the latest major step in the evolution of Antarctica as recorded by late Neogene glaciomarine sediments. The authors suggest that the final transition to the modern Antarctic ice-sheet took place during the mid-Pliocene, roughly 3 Ma ago, concurrent with the final closure of the Panamanian seaway.

5.2 Model description and experimental design

In order to study the effect of Panama gateway closure on global climate, we use an adjusted version of the low-resolution NCAR (National Center for Atmospheric Research) Community Climate System Model CCSM2.0.1. This version is referred to as CCSM2/T31x3a and described in detail by *Prange* (2008). The global climate model is composed of four coupled components representing atmosphere, ocean, land, and sea ice. The resolution of the atmospheric component is given by T31 (3.75° by 3.75° transform grid) spectral truncation for 26 layers, while the ocean has a nominal resolution of 3° with 25 levels (the latitudinal resolution of the oceanic model grid is finer near the equator, $\sim$0.9°).

Two climate equilibrium integrations are performed as described in *Steph et al.* (2006), one with closed Panamanian isthmus (present-day control run) and one with open gateway (with all other boundary conditions identical to the control run). In the latter experiment, the seaway has a depth of 800 m and a width of two tracer grid points (ca. 200 km). In both experiments, we adopt the atmospheric composition of 1990 AD along with modern orbital forcing and topography (including present-day ice-sheet configuration). We note that the atmospheric CO_2 concentration of 353 ppmv used here lies well within the broad range of mid-Pliocene estimates (cf. *Kürschner et al.*, 1996; *Raymo et al.*, 1996; *Pearson and Palmer*, 2000). The CCSM2/T31x3a integrations are initialized with modern observational data. After reaching climatic equilibrium (using an asynchronous integration technique, see *Steph et al.* (2006) and *Prange* (2008), both model runs were extended by centennial synchronous integration phases. The last 90 years of each synchronous integration phase serve for the evaluation of the modelled climate states as well as for the forcing of a dynamic Antarctic ice-sheet model.

The Antarctic ice-sheet model is described in detail by Chapter 2 and 3. The model is zonally averaged and symmetric around the axis of the South Pole. Within the ice sheet, velocities and temperatures are computed with a vertical resolution of 12 layers and a latitudinal resolution of 0.5°. The altitude and ice thickness of every latitude grid cell are derived by solving the continuity equation using basal melting and local bedrock isostasy (*Sima*, 2005; *Sima et al.*, 2006). In contrast to the atmospheric energy/mass-balance approach (Chapter 3), the mass balance in the present version of the ice-sheet model is forced by zonally averaged surface air temperature T_a and precipitation (see below). Surface ablation (melting and evaporation) depends on the daily mean surface energy flux ψ_d (*Oerlemans*, 2001). A simple parameterization is used where longwave radiation and turbulent heat exchange are linearized around the melting point according to

$$\psi_d = \tau(1-\alpha)Q - c_0 + c_1 T_a\,, \tag{5.1}$$

where τ is the total transmissivity (0.65), α is the surface albedo, and Q denotes (present-day daily mean) insolation. The surface albedo α depends on the amount of snow and ice covering the bedrock (Section **??**). The constant parameters c_0 and c_1 are typically around 10 W m^{-2} and 10 W m^{-2} °C^{-1}, respectively, but are also considered tuning parameters (*Oerlemans*, 2001). We shall therefore vary these numbers by ±10% in the framework of a sensitivity study.

Since Antarctic temperatures are notoriously difficult to simulate by general circulation models (cf. *Prange*, 2008), we opted for anomaly coupling to force the ice-sheet model, similar to the approach used by *Lunt et al.* (2008a). For the present-day (i.e. Panama closed) simulations, we use a monthly NCEP/NCAR-reanalysis-derived temperature climatology (*Kalnay et al.*, 1996). For the open-Panama experiments, the difference between the two CCSM2/T31x3a simulations (Panama open vs. Panama closed) is added to the NCEP/NCAR climatology. Since the anomaly approach has only a minor effect on ice volume when applied to precipitation, it is used only for the temperature forcing here.

In all experiments the ice-sheet model starts from bare-rock conditions (initial bedrock topography from *Pollard* (1983b)) and reaches equilibrium within 10^5 years. Since the ice-sheet model is run off-line, any climate/ice-sheet feedbacks are ignored. However, the local effect of ice elevation on surface air temperature is taken into account by using a vertical lapse-rate temperature-correction of -0.007°C m^{-1}. We also note that a local surface albedo feedback is included through the surface energy flux (Eq. 5.1).

5.3 Results

In the CCSM2/T31x3a experiment with open Panamanian gateway, the flow through the strait is eastward at all depths except for a thin (<12 m) Ekman-dominated surface layer, in which the flow follows the direction of the trade winds. Driven by the steric sea-level difference between the Pacific and Atlantic oceans, the net volume transport through the gateway into the Atlantic Ocean amounts to 12 Sv (1 Sv=10^6 m^{3}s^{-1}), which is comparable to results from other model studies (e.g. *Nisancioglu et al.*, 2003; *Prange and Schulz*, 2004). The flow of relatively fresh Pacific water through the Panamanian gateway reduces sea surface salinities in the southwestern Caribbean by $\sim$1 psu compared to the control run with closed isthmus (*Steph et al.*, 2006). This salinity anomaly is advected into the northern North Atlantic,

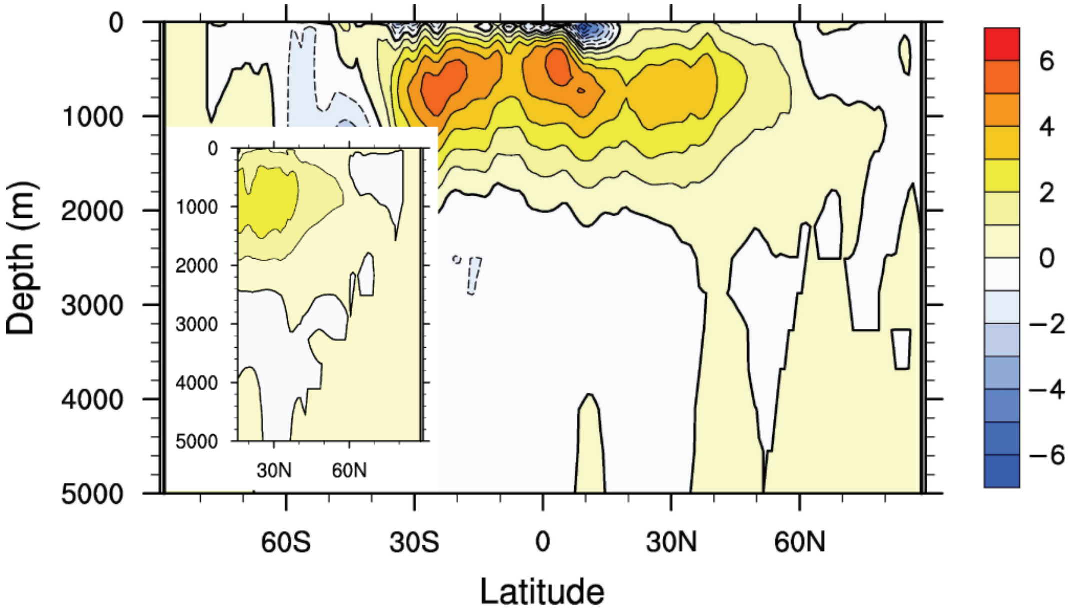

Figure 5.1: *Difference between climate model runs with closed and open Panamanian gateway (i.e. the response to gateway closure) in mean global Eulerian meridional overturning circulation (Sv). The inset shows the meridional streamfunction for the North Atlantic (north of the Panamanian seaway). Positive values indicate clockwise circulation anomalies.*

affecting deepwater formation there. With a closed isthmus, maximum meridional overturning in the North Atlantic is ∼2.5 Sv greater than in the CCSM2/T31x3a run with open gateway (Fig. 5.1). The stronger overturning circulation enhances the northward oceanic heat transport (a 20% increase is found in the peak North Atlantic heat transport, i.e. from 0.5 PW to 0.6 PW), resulting in a sea-surface temperature seesaw-pattern (cf. *Crowley*, 1992) with general warming in the northern hemisphere and cooling in the southern hemisphere (Fig. 5.2). The southern hemisphere cooling also affects the climate of Antarctica, resulting in a year-round surface air temperature reduction that is particularly pronounced along the rim of the Antarctic continent (Fig. 5.3). The cooling of the Southern Ocean and Antarctica comes along with a weakening of the hydrologic cycle and hence less precipitation over the Antarctic continent (Fig. 5.4).

Basically, the 'Panama-induced' climate change results in two opposing effects on the volume of the Antarctic ice-sheet: cooling (i.e. reduced surface ablation) versus reduced precipitation. In order to study the net effect on the Antarctic ice-sheet, CCSM2/T31x3a's model output is taken to force an ice-sheet model as described above. Figure 5.5 displays modelled equilibrium ice-sheet heights for two different parameters c_0 (c_0 = 10 W m^{-2} and c_0 = 11 W m^{-2}), while c_1 is set to 11 W m^{-2} °C^{-1}. For c_0 = 10 W m^{-2}, the Antarctic ice volume increases from $14 \cdot 10^{15}$ m^3 (Panama open) to $24 \cdot 10^{15}$ m^3 (Panama closed), corresponding to a sea-level lowering of about 25 m in response to the closure of the Panamanian isthmus. For c_0 = 11 W m^{-2}, the Antarctic ice volume increases from $21 \cdot 10^{15}$ m^3 to $24 \cdot 10^{15}$ m^3, corresponding to a sea-level lowering of about 8 m. In both open-Panama

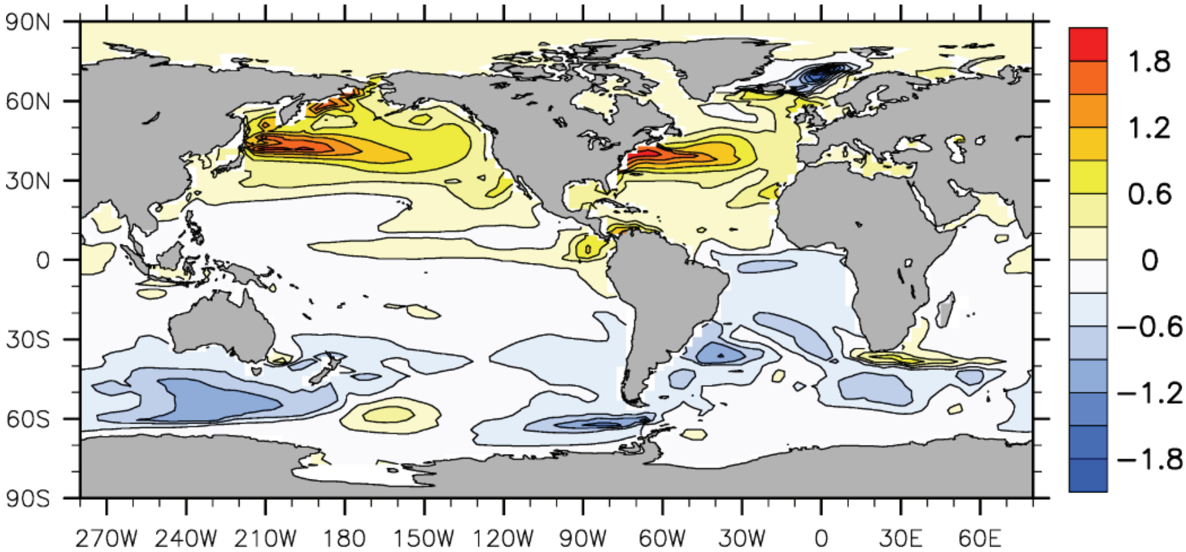

Figure 5.2: *Difference between climate model runs with closed and open Panamanian gateway (i.e. the response to gateway closure) in annual-mean sea surface temperature (°C).*

scenarios ablation occurs only at the rim of the ice sheet, where the positive surface energy flux ψ_d exceeds the accumulation of snow. Within the ice, a flow from the surface and center of the ice sheet towards the bottom and rim maintains the equilibrium. Independent of c_0, the present-day (i.e. Panama closed) simulated ice sheets are very similar to the real modern Antarctic ice-sheet.

A parameter sensitivity study further reveals that the ice-sheet volume is very sensitive to changes in c_0 and c_1 (Eq. 5.1). For a fixed value of c_0 (10 W m^{-2}) and a range of c_1 between 9 and 11 W m^{-2} °C^{-1}, Pliocene (i.e. Panama open) ice volume is relatively small (Figure 5, inset, left). The most realistic option results from c_1=11 W m^{-2} °C^{-1} (as discussed below, the other two simulated ice sheets are unrealistically small). Therefore, we use this value of c_1 in a second suite of sensitivity experiments, where c_0 varies between 9 and 11 W m^{-2} (Fig. 5.5, inset, right). Here, the upper two values result in the Pliocene ice-sheets described above. In contrast to the open-Panama ice-sheet simulations, the present-day simulations are virtually insensitive to the energy flux parameters c_0 and c_1 (Fig. 5.5, inset).

We emphasize that the real Antarctic ice volume prior to the mid-Pliocene transition is poorly constrained from geological data. Estimates of the early-to-middle Pliocene Antarctic ice-sheet volume range from minor changes to ~40% reduction compared to the present (cf. *Dowsett et al.*, 1996). If we accept this number, we can reject those parameter settings (c_0, c_1) that yield extensively small ice volumes (say, significantly smaller than ~40% compared to modern) in the open-Panama experiments (Fig. 5.5, inset, grey dots). By contrast, we consider the ice-sheet changes shown in Figure 5.5 and marked by red and blue dots in the inset as possible.

In summary, the climate/ice-sheet model suggests an increase in Antarctic ice volume in response to the Panamanian seaway closure. This is a robust result that is qualitatively

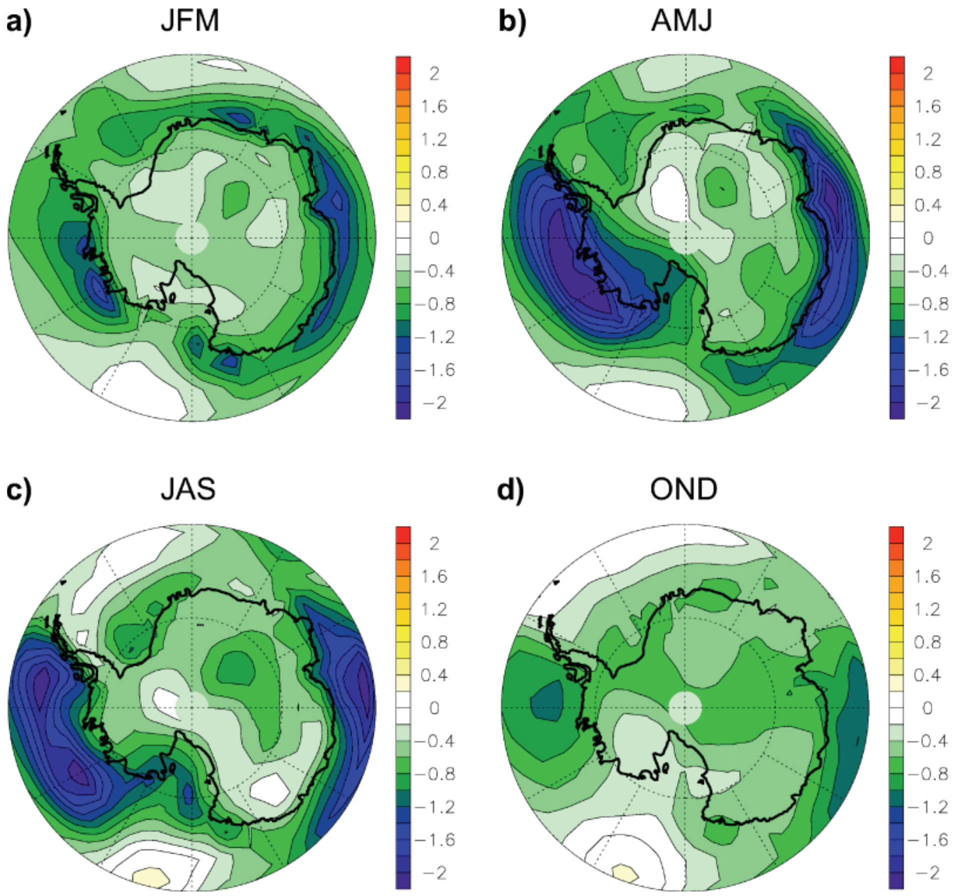

Figure 5.3: *Difference between climate model runs with closed and open Panamanian gateway in mean Antarctic surface air temperature (°C) for (a) January–March, (b) April–June, (c) July–September, and (d) October–December.*

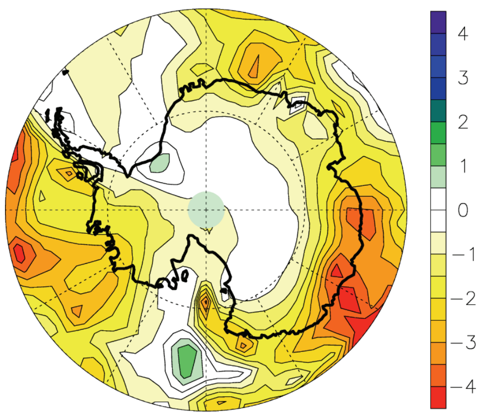

Figure 5.4: *Difference between climate model runs with closed and open Panamanian gateway in annual-mean precipitation over Antarctica (cm/a).*

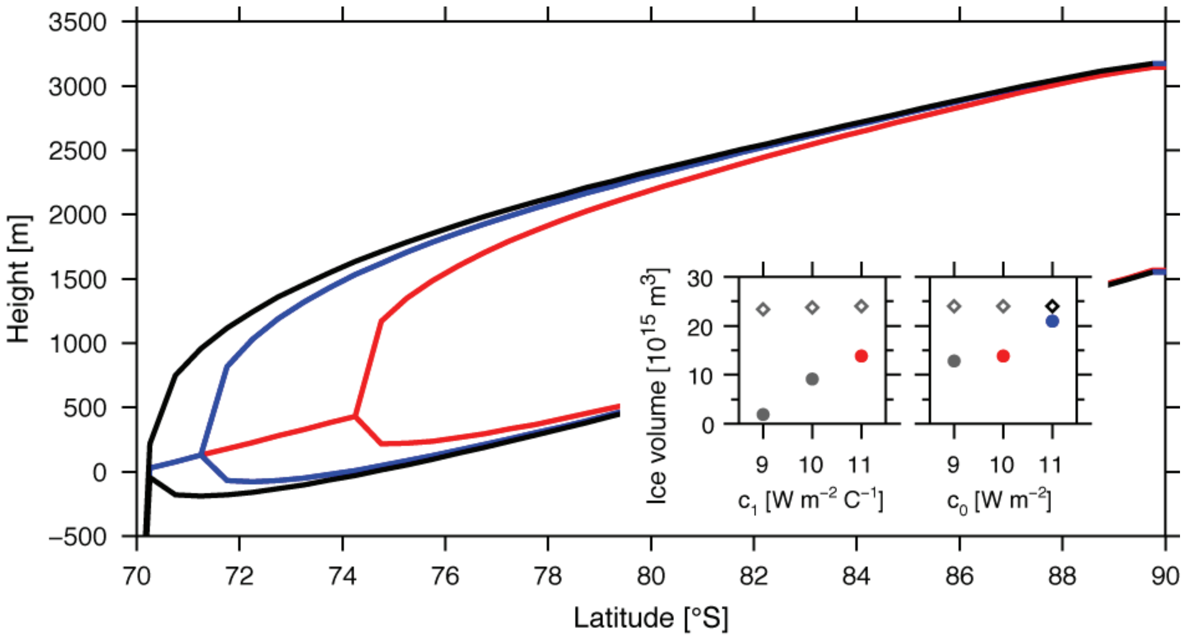

Figure 5.5: *Ice-sheet elevation cross-sections and sensitivity experiments (inset). The modelled present-day (i.e. Panama closed) shape is shown in black. Pliocene (i.e. Panama open) ice-sheets are drawn in red and blue for c_0 values of 10 and 11 W m^{-2}, respectively (c_1 is constant at 11 W m^{-2} °C^{-1}). The inset shows sensitivity with respect to c_1 (left) and c_0 (right). Diamonds indicate present-day and dots Pliocene ice volume. Colors correspond to ice-sheet cross-sections.*

reproduced in every sensitivity experiment (the exact amount of ice growth, however, depends on the tuning of the surface energy flux parameterization). Obviously, the effect of reduced surface ablation due to air temperature cooling overwhelms the effect of reduced precipitation in our simulations. Indeed, CCSM2/T31x3a produces only a small reduction in annual Antarctic precipitation. This annual reduction is generally well below 3 cm (Fig. 5.4) or 6%.

5.4 Discussion

The mid-Pliocene 'climate crash' has been dated to ~2.7 Ma (Marine Isotope Stage 110) in numerous studies (*Pillans and Naish*, 2004, and references therein). It marks the final transition of the Earth's climate into the present 'icehouse' state, which is characterized by NHG, Milankovitch-type glacial-interglacial cycles and the large-scale waxing and waning of northern hemisphere continental ice-sheets. Sub-Arctic marine records of ice-rafted debris show a clear onset of these major glacial episodes beginning around 2.7 Ma (*Maslin et al.*, 1996, and references therein)]. Other studies have documented an abrupt cooling of climate, dramatic paleoceanographic changes and profound reorganizations of floral and faunal provinces accompanying Marine Isotope Stage 110 on a global scale. The geological evidence for the global 'climate crash' is recorded in deep ocean sediments, shallow-marine continental-margin sequences and continental records including loess, lacustrine and glacio-fluvial sediments (*Pillans and Naish*, 2004, and references therein).

However, a recent analysis by *Mudelsee and Raymo* (2005) of 45 globally distributed δ^{18}O records challenges the notion of an abrupt onset of significant NHG around 2.7 Ma and suggests a more gradual trajectory of the mid-Pliocene climate transition. Their analysis indicates the onset of a long-term mid-Pliocene sea-level lowering already at 3.6 Ma, i.e. almost 1 million years earlier than the previously assumed onset of NHG. This mid-Pliocene transition, which took place between 3.6 and 2.4 Ma, witnessed a long-term sea-level lowering of $\sim$40–50 m (*Mudelsee and Raymo*, 2005).

Given these contradictory findings, we suggest the following sequence of events on the basis of our climate/ice-sheet model results. The Pliocene closure of the Panamanian gateway led to a gradual intensification of North Atlantic deepwater formation and, hence, meridional overturning circulation between $\sim$4.5 and 3 Ma as evidenced by paleoceanographic records (*Haug and Tiedemann*, 1998; *Haug et al.*, 2001). As a consequence of the enhanced oceanic northward heat transport, the Southern Ocean and Antarctica progressively became colder until temperatures were low enough to promote Antarctic ice-sheet growth after 3.6 Ma. This conjecture is corroborated by Southern Ocean sea-surface temperature reconstructions from silicoflagellates (*Whitehead and Bohaty*, 2003) which indicate a general cooling after $\sim$4.3 Ma, supporting the hypothesis of enhanced northern hemisphere heat piracy. We therefore suggest that the first phase of long-term mid-Pliocene sea-level lowering, which started at 3.6 Ma (*Mudelsee and Raymo*, 2005), is largely attributable to Antarctic ice growth rather than NHG. Indeed, sub-Arctic records of ice-rafted debris indicate that major ice-sheet build-up in Eurasia and North America did not start before $\sim$2.7 Ma (*Maslin et al.*, 1996, and references therein). Even though a distinct expansion of the Greenland ice-sheet occured several hundred thousand years earlier ($\sim$3.3 Ma) (*Kleiven et al.*, 2002; *Bartoli et al.*, 2005), the effect on the global sea level was small ($\ll$7 m; note that a smaller ice sheet on Greenland had existed at least since the Miocene (e.g. *Larsen et al.*, 1994). We further note that major glaciation of Patagonia has also been dated to $\sim$3.6 Ma (*Mercer*, 1976a,b).

One might further speculate whether the mid-Pliocene Antarctic ice-sheet growth had a global impact apart from its influence on sea level. For instance, the ice-sheet expansion might have promoted Southern Ocean sea-ice formation through intensified katabatic winds. This, in turn, could have had an effect on Antarctic Bottom Water formation and/or on the release of deeply sequestered CO_2 from the ocean to the atmosphere (e.g. *Stephens and Keeling*, 2000). Indeed, a progressive expansion of Antarctic sea-ice coverage after $\sim$3.4 Ma has been inferred by *Hillenbrand and Cortese* (2006) from a decrease of biogenic silica deposition in the Southern Ocean. Moreover, a widespread hiatus in the Southern Ocean between $\sim$3.8 and $\sim$3 Ma has been interpreted to reflect large-scale changes in ocean circulation due to increased bottom water production (*Hodell and Warnke*, 2006, and references therein). Similar effects of Antarctic ice-sheet growth on the global climate system might have been involved in previous Cenozoic 'climate crashes' (*DeConto et al.*, 2007).

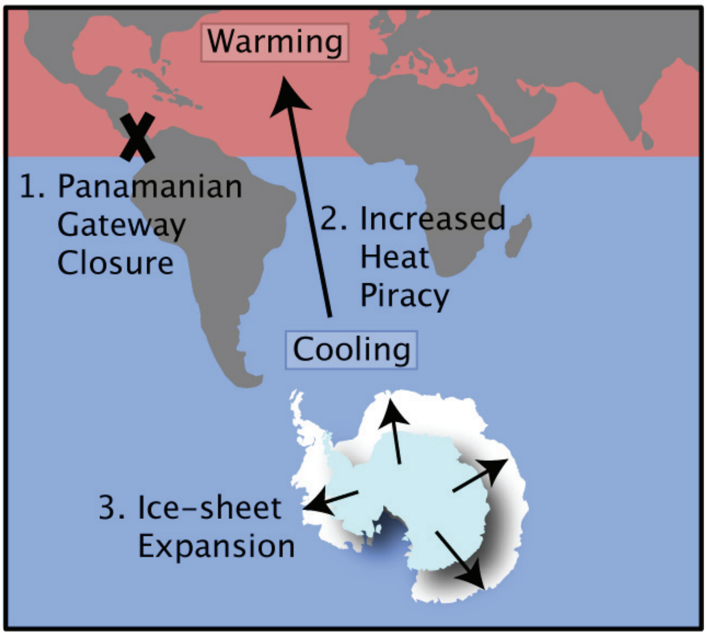

Figure 5.6: *Schematic of the possible role of the Panamanian gateway closure in Pliocene Antarctic ice-sheet development. The gateway closure (1) leads to a stronger meridional overturning circulation which, in turn, increases the northern hemisphere 'heat piracy' (2). The resulting cooling in the south polar region favors the growth of Antarctic ice-sheets (3).*

5.5 Conclusions

On the basis of climate/ice-sheet model results, we suggest that the Pliocene closure of the Panamanian gateway induced an intensification of the meridional overturning circulation which, in turn, caused a cooling of Antarctica and an expansion of the Antarctic cryosphere (Fig. 5.6). The Antarctic ice-volume increase may explain a substantial portion of the mid-Pliocene global sea-level lowering that started around 3.6 Ma (*Mudelsee and Raymo*, 2005). We suggest that the first phase of this long-term sea-level decrease is largely attributable to Antarctic ice growth rather than NHG. After ∼2.7 Ma, the significant growth of northern hemisphere ice-sheets (as evidenced by records of ice-rafted debris) contributed to the mid-Pliocene sea-level reduction.

Our interpretation of the model results may help to reconcile the early onset of mid-Pliocene sea-level lowering with the (almost 1 million years) later onset of significant NHG. While we suggest that the closure of the Panamanian seaway induced a mid-Pliocene expansion of the Antarctic ice-sheet, there is no support from climate models that the gateway closure played a significant role in the build-up of northern hemisphere ice-sheets (*Klocker et al.*, 2005; *Lunt et al.*, 2008a,b). It has been hypothesized in many studies that a decrease in atmospheric CO_2 triggered the mid-Pliocene 'climate crash' (e.g. *Lunt et al.*, 2008a). However, there is no unequivocal evidence for a CO_2 drop during the mid-Pliocene. Our suggestion that the 'Panama-induced' Antarctic ice-sheet expansion might have progressively induced an atmospheric CO_2 drawdown via enhanced Southern Ocean sea-ice formation and hence reduced air-sea gas exchange is admittedly highly speculative (cf. *Archer et al.*, 2003).

According to our model results, the 'Panama-induced' Antarctic ice-volume increase may explain up to 60% of the 40–50 m long-term (3.6–2.4 Ma) mid-Pliocene global sea-level decrease. For the time being, this number cannot be better constrained due to uncertainties in boundary conditions and model parameters. Climate model simulations with interactively coupled three-dimensional ice-sheet modules should be employed in future studies to scrutinize the results presented here. We finally conclude that the role of the Panamanian gateway in late Neogene climate change is still far from understood, and it is too early to claim that it is "no more than a bit player" (*Molnar*, 2008).

Acknowledgements The CCSM2 runs were performed on the IBM pSeries 690 Supercomputer of the 'Norddeutscher Verbund fuer Hoch- und Hoechstleistungsrechnen' (HLRN). This work was funded through the DFG Research Center/Excellence Cluster 'The Ocean in the Earth System' and the European Graduate College 'Proxies in Earth History'.

Chapter 6

General discussion

With the strong likelihood of increasing atmospheric pCO_2 levels in the near future and consequently rising global temperatures and sea level, understanding the interaction between climate and ice sheets becomes very important. Our current knowledge of ice-related climate feedbacks needs to be largely improved in order to better constrain future changes, especially the inevitable sea-level rise. Although this study focuses on the opposite effect, the expansion of continental ice and associated decrease in ocean elevation, it does intent to shed light on the role of pCO_2 in the ice sheet-climate system.

The ice sheet-climate model developed and used in this work has a simplified geometry, but realistic climate forcing. The relatively simple axial symmetric configuration provides a high computation speed, even after implementing the extended energy and mass balances simulating the climate and including the oxygen isotopes as a passive tracer. Therefore, transient experiments spanning a million years (with time steps of 1 ka for ice dynamics and daily computation of all energy and mass fluxes) can easily be conducted and repeated under different forcing and/or boundary conditions. This creates an ideal opportunity to perform sensitivity experiments on the effect of pCO_2 changes in the Middle Miocene, as well as for testing the implemented parameterizations.

The reconstructed pCO_2 values in the Middle Miocene have a large uncertainty in magnitude as well as in age (Fig. 1.2), making it impossible to directly use as a forcing for the ice sheet-climate model. The approach in Chapter 3 is therefore more conceptual. By slowly decreasing and increasing pCO_2 in a reasonable range when compared to the reconstructed pCO_2 compilation, the critical values for modelled ice-sheet expansion and rapid melting where found. Constant pCO_2 forcing below approximately 400 ppm resulted in a largely glaciated Antarctica, whereas pCO_2 levels above this threshold induced small, ephemeral ice sheets. Above $\sim$470 ppm Antarctic temperatures are too high for snow and ice to survive an austral summer. These constant pCO_2 experiments showed that variations in orbital parameters alone are insufficient to induce an ice-sheet expansion. By comparing the resulting increase in ice volume and oxygen-isotopic composition of sea water to foraminiferal oxygen-isotope records, it was possible to put some constrains on the pCO_2 drawdown needed to explain the ice-sheet expansion in the Middle Miocene. A pCO_2 decline crossing the modelled 400 ppm threshold must have occurred around 13.9 Ma. The resulting ice-volume expansion and sea-level lowering of $\sim$48 m covers the entire $\delta^{18}O_c$ step found in the sediment records. These exact numbers are model dependent and should be taken as a guideline. However, the following discussion on the applied parameterizations and tuning of the ice sheet-climate model underlines the robustness of the results.

The modelled distribution of the oxygen-isotopic composition of snow $\delta^{18}O_{snow}$ falling on Antarctica solely depends on the near-surface air temperature T_{sfc}. Both, accumulation and temperature, are mainly affected by latitude, surface elevation and the distance from the open ocean. The overall present-day correlation between measured temperatures and $\delta^{18}O_{snow}$ is therefore high ($r > 0.9$; *Giovinetto and Zwally*, 1997; *Masson-Delmotte et al.*, 2008). Along the coast, where the accumulation is relatively high, the modelled $\delta^{18}O_{snow}$ closely resembles the observed values. More inland, in the dry continental interior, the modelled isotopic composition of snow is less depleted than the measured values. This is a common problem in isotopic modelling of Antarctic snowfall (*Helsen et al.*, 2007; *DeConto et al.*, 2008) and can be induced by the translation of the sparse local measurements to the large modelled areas or by minor deficits in the parameterizations due to applied condensation thresholds, different types of accumulation and/or transport mechanisms (for a detailed discussion see *Helsen*, 2006; *Helsen et al.*, 2007). Although direct use of the present-day spatial relation between $\delta^{18}O_{snow}$ and T_{sfc} for past reconstructions is not ideal, it is shown that the isotopic-temperature slope remained valid for Antarctica during the Last Glacial Maximum (LGM) (*Delaygue et al.*, 2000). However, there is no other option than to define a parameterization (e.g. *Lhomme*, 2004) or use a isotope model (e.g. *Hoffmann et al.*, 2001), since ice cores do not extent further back in time than $\sim$ 800 ka (*EPICA community members*, 2004). Past $\delta^{18}O_{snow}$ in our ice sheet-climate model depends not only on the present-day spatial distribution, but also on changes in temperature and elevation (following the work of *Lhomme*, 2004). Testing the sensitivity of $\delta^{18}O_{snow}$ showed only a minor effect on this parameterization, less than 4 %. *Lhomme et al.* (2005) computed $\delta^{18}O_{sw}$ for the last $\sim$ 150 ka for the three main ice sheets, Greenland, East- and West Antarctica, using a similar approach and parameterization. In order to directly compare their modelled $\delta^{18}O_{ice}$ to values recorded in ice cores, they used temperatures retrieved from the same ice-core records. The strong resemblance of the modelled and measured $\delta^{18}O_{snow}$ records confirms the applicability of the temporal parameterization. The temperatures used in the present ice sheet-climate model represent a much larger region. Therefore, it is impossible to compare modelled $\delta^{18}O_{snow}$ from this model directly to single ice-core records.

Although the climate component of the model may not be perfectly able to capture short-term processes relevant for the local climate as recorded in ice cores, the general sensitivity of the model to changes in $p\mathrm{CO_2}$ is comparable to the atmospheric general circulation models (AGCM) of the Intergovernmental Panel on Climate Change (IPCC) assessments (*IPCC*, 2007). With a tuned hemispheric temperature increase of 2.8 ° for a doubling of $p\mathrm{CO_2}$ it falls in the range of 2.1 to 4.4 ° estimated by the AGCMs. Admittedly, the sensitivity to $p\mathrm{CO_2}$ is slightly enhanced in order to account for the missing water vapor feedback.

It is however interesting to note the abrupt response of the ice sheet to changes in $p\mathrm{CO_2}$ with a glaciation threshold around 400 and a deglaciation threshold around 425 ppm (see Fig. 3.1). To my knowledge, the only other work conducting these type of hysteresis simulations is by *DeConto and Pollard* (2003), *Pollard and DeConto* (2005) and *DeConto et al.* (2008). Their modelled thresholds for Antarctic glaciation and deglaciation reach much higher $p\mathrm{CO_2}$ levels, $\sim$780 and 910 ppm, respectively. The higher values and larger hysteresis window imply a less sensitive model behaviour to changes in $p\mathrm{CO_2}$. Indeed the climate sensitivity of their GCM is somewhat lower than the model discussed in this work (2.5 versus 2.8 ° for a doubling of pCO_2), but this is not likely to explain the entire offset between the hysteresis experiments.

There are other factors that could result in the different hysteresis behaviour. First, the model set-up is very different. *DeConto and Pollard* (2003) use a thermomechanical ice-sheet model which is very similar to the ice-sheet component in this work. It is however fully three-dimensional, based on a polar-stereographic grid of 40×40 km, more realistic than our axially symmetric geometry with $\sim$ 100 km resolution. On the other hand, it is forced by monthly mean meteorological fields from the GCM (with only ablation and refreezing calculated in a diurnal cycle), a coupling which is accounted for every 200 ka. While the climate part of our ice sheet-climate model is less advanced than a GCM, we have the advantage of a direct, even daily coupling of all mass and energy balances. The different resolution and coupling of the climate forcing to the ice sheet models could result in a different sensitivity to pCO_2 changes.

Another major difference, which could account for the different model behaviour, is the initial bedrock topography used. *DeConto and Pollard* (2003) initiate their Antarctic ice sheet on a three dimensional ice-free topography. This creates many more possibilities for ice to start growing and to survive warmer climate conditions than the initial bedrock in our axial-symmetric ice-sheet model. Ice inception is found at elevated regions. In order to account for mountain ranges close to the coast representing, for example, the present-day Dronning Maud Land, we chose an initial bedrock profile with a bulge near the continental margin (see Section 2.5). This promotes ice growth, but probably reduces the possibility of variations within the ice volume. The retreat of a large ice sheet is hampered and might induce more abrupt behaviour. This bedrock-effect might also explain the small (orbital-induced) variability in the ice volume of large ice sheets under constant pCO_2 forcing (pCO_2 below $\sim$300 ppm).

A last important remark concerns the orbital parameters. In the model of *DeConto and Pollard* (2003), these are computed synthetically with periods in multiples of 20 ka. The resulting well ordered, non-interfering frequencies have a slightly smaller energy range than the orbital parameters computed in our ice sheet-climate model (following *Laskar et al.*, 2004) could induce a less abrupt sensitivity to pCO_2 forcing.

Nevertheless, the above described processes are not likely to explain the entire offset in glaciation thresholds and following their simulations it sounds acceptable to define thresholds of around 780 and 910 ppm for the glaciation and deglaciation of the Antarctic ice sheet, respectively (*DeConto et al.*, 2008). However, their research is strongly focussed on the early to mid-Cenozoic, where data does indicate high levels of pCO_2 and large variations. From the early Miocene onwards, the level of pCO_2 in the atmosphere did not exceed 500 ppm (see Fig. 1.1 and 1.2), even after considering maximum errors on the pCO_2 proxies. According to the threshold derived from *Pollard and DeConto* (2005) and *DeConto et al.* (2008) Antarctic (at least the eastern part) must have been largely glaciated ever since the early Miocene.

Yet, the Earth experienced several periods of relatively warm climatic conditions in the last 20 Ma. Transitions from these climate optima into the cold world are marked by an increase in the ratio of oxygen isotopes recorded in deep-sea sediments as well as by sea-level lowering derived from independent sea-level reconstructions. It is very unlikely that all these transitions are only induced by Northern Hemisphere and West Antarctic glaciations.

For example, the Middle Miocene climate transition must have undergone large changes in Antarctic ice volume. Backstripping of seismic profiles indicate a sea-level lowering in the Middle Miocene in the order of 25-50 m (*Miller et al.*, 1998). The error on these estimates is large, but they do confirm an ice volume variation that is hard to explain without the East Antarctic ice sheet. A low resolution study combining deep-sea temperature from Mg/Ca with $\delta^{18}O_c$ records suggests a large increase in ice volume around 14 Ma (*Lear et al.*, 2000). All high-resolution oxygen-isotope records spanning the Middle Miocene futher indicate a step towards higher $\delta^{18}O_c$ (*Shevenell et al.*, 2004; *Holbourn et al.*, 2005; *Raffi et al.*, 2006) and are interpreted as large-scale Antarctic glaciation. The amplitude, timing and increase in $\delta^{18}O_{sw}$ of the Middle Miocene ice-sheet expansion simulated in this thesis is in line with the above described evidence.

Even the stability of the much more recent, Pliocene Antarctic ice sheet is under continuous discussion (see *Raymo et al.* (1996) and *Hill et al.* (2007) for an overview). Two main scenarios have been proposed for ice sheet covering East Antarctica: a permanent large ice sheet since the Middle Miocene or a dynamic ice sheet throughout the late Miocene and Pliocene. A recent study compiled and reviewed architectural changes of margin sediments on Antarctica (*Rebesco and Camerlenghi*, 2008). They concluded that a transition in the Antarctic ice sheet took place around 3 Ma, whereby the bedrock conditions changed from polythermal to cold, wet-based, indicating an ice-volume expansion. Also recent model studies (e.g. *Hill et al.*, 2007) reconstructed an increase in Pliocene Antarctic ice volume. These changes are maybe not as large in scale as proposed by in the latter scenario, but do indicate a dynamic East Antarctic ice sheet during the Pliocene. Chapter 5 of this work also suggests ice-sheet growth on Antarctica in the mid-Pliocene. Instead of the $p\mathrm{CO}_2$ forcing of the Middle Miocene simulations, here we investigated the effect of the closure of the Panamanian gateway, which induces an intensification of the meridional overturning circulation and a consequent cooling of Antarctica. Unfortunately, the huge computation time necessary to execute GCM simulation makes it virtually impossible to perform transient $p\mathrm{CO}_2$ simulations. Recently *Lunt et al.* (2008a) did asses the impact of $p\mathrm{CO}_2$ on the Greenland ice sheet by computing the ice volume under 280 ppm (pre-industrial) and under 400 ppm (Pliocene) in a coupled GCM-ice sheet environment. This experiment lead to the conclusion that a decline in $p\mathrm{CO}_2$ also controlled the glaciation of Greenland in the Pliocene.

Both, the Middle Miocene and mid-Pliocene examples, show a reduced Antarctic ice sheet under, compared to the work of *DeConto et al.* (2008), relatively low $p\mathrm{CO}_2$ levels. The ice sheet-climate model even indicates a large-scale deglaciation threshold of around 425 ppm. $p\mathrm{CO}_2$ concentrations above $\sim$470 ppm force the ice sheet to melt away entirely. These modeled values are in the range of reconstructed $p\mathrm{CO}_2$ for the last 20 Ma (e.g. *Pearson and Palmer*, 2000; *Pagani et al.*, 2005; *Kürschner et al.*, 2008; *Zachos et al.*, 2008; *Royer*, 2008) and have large implications for the future existence of ice sheets. The present-day $p\mathrm{CO}_2$ level is approximately 385 ppm (e.g. *Hansen et al.*, 2008). Even when considering moderate annual pCO_2 growth rates of 1 ppm per year (average over 1960-2005 is 1.4 ppm per year, even larger annual-mean rates are measured for the last 10 years; cf. *IPCC*, 2007), according to the threshold values of our model, the Antarctic ice sheet will start to deglaciate by the year 2050. Indeed, a recent study combining (paleo)climate data and models state that a persistent amount of pCO_2 of $\sim$450 ppm or larger will push the Earth toward an ice-free state (*Hansen et al.*, 2008). They suggest that the present-day level of 385 ppm is already dangerous, with a resulting equilibrium sea-level rise of at least several meters. Luckily ice-sheet response to rising pCO_2 and temperature levels is not immediate. However, if pCO_2 is not stabilized of reduced soon, a large-scale reduction of the Earth's cryosphere is likely to occur within the next centuries.

Chapter 7

Conclusions

This study presents a new ice sheet-climate model as a valuable tool for transient long-term computations simulating the (paleo) Antarctic ice sheet. After applying this model to the Middle Miocene and Pliocene climatic transitions, the following conclusions can be drawn:

1. The decline of atmospheric CO_2 (pCO_2) is an important mechanism forcing the Antarctic ice-sheet expansion in the Middle Miocene. The modelled large-scale glaciation threshold is approximately 400 ppm, which is in line with pCO_2 reconstructions for the same period. The drawdown must have occurred around 13.9 Ma, whereafter a minimum in (summer) insolation induced the cold conditions triggering the transition. Orbital forcing by itself was not sufficient to cause a large-scale ice-sheet expansion.

2. The modelled volume expansion of $\sim 18 \times 10^{15}$ m^3 or $\sim$48 m of sea-level lowering can explain the entire $\delta^{18}O_c$ step found in the benthic foraminifera records of deep-sea sediment cores. The larger variations in the remainder of the measured oxygen-isotope records with respect to the modelled $\delta^{18}O_{sw}$ reconstruction is probably induced by local fluctuations in temperature and salinity and/or global fluctuations in pCO_2 (which is kept at constant levels in the model simulations).

3. The model simulations support the often applied relationship of a 1 ‰ rise in $\delta^{18}O_c$ to a global sea-level drop of 100 m to be valid. However, small ice sheets contain a slightly less depleted bulk isotopic composition and have a smaller relative effect on $\delta^{18}O_{sw}$. In contrast, large ice volumes have a more depleted mean $\delta^{18}O_{ice}$ value and cause a relatively large increase in the isotopic composition of the ocean.

4. The closure of the Panamanian gateway in Pliocene could have induced intensification of meridional overturning circulation. The consequent cooling of Antarctica and resulting ice-sheet expansion may explain up to 60 % of the proposed 40-50 m long-term mid-Pliocene global sea-level lowering.

Chapter 8

Outlook

From this study it can be concluded that the described ice sheet-climate model proofs to be a useful tool for reconstructing past ice volume and isotopic composition of sea water. Its relatively short computation time makes it possible to conduct many experiments testing the sensitivity of the included processes.

There are, however, some features in the model that could be improved in future work. First of all, it is highly recommended to investigate the initial ice-free bedrock. In this study two different initial topographies are used. For the Middle Miocene experiments an ice-free bedrock including some elevation near the coast was necessary to represent the mountain ranges on which ice incepted. In contrast, for the Pliocene simulations, a simple bedrock profile with linearly increasing elevation towards the pole, was chosen in order to simulate the Pliocene ice-sheet expansion in a conceptual approach, without the influence of coastal elevation. It would be very interesting to conduct experiments investigating the direct response of ice-sheet growth and volume under different initial bedrock scenarios.

Furthermore, it would be useful to expand the ice sheet-climate model into a three dimensional model. This will substantially increase the computation time, but could improve our knowledge of interactions between ice volume and $p\mathrm{CO_2}$. Moreover, the extended model could be used to test the abrupt ice-sheet response to the $p\mathrm{CO_2}$ decline put forward in this study.

A topic only touched briefly in Chapter 3, the orbital-induced frequencies, also needs further investigation. Variations in the sediment records as well as in the modelled ice volume are dominated by Milankovitch frequencies. The occurrence of shifts between these frequencies, for example the transition from obliquity to eccentricity pacing in the Middle Miocene (e.g. *Holbourn et al.*, 2005), are still not well understood.

Another interesting remaining frequency dilemma is the 100 ka variability that is found in ice-core and deep-see sediment cores. This orbital period has a significantly smaller impact of solar forcing than precession or obliquity, but somehow converts to the strongest climate signal in the last million years. Over the last decades scientists proposed several hypotheses assessing this problem (e.g. *Imbrie et al.*, 1993; *Shackleton*, 2000; *Toggweiler*, 2008), but none of them are satisfactorily proven.

With the help of the ice sheet-climate model described in this study, these frequency phenomena can be addressed, especially by focussing on the interactions between solar and $p\mathrm{CO_2}$ forcing and global temperature and ice volume. The computed $\delta^{18}\mathrm{O_{sw}}$ can further on serve as a direct method to compare the modelled results to proxy data.

Appendix A

Manual

Ice Sheet-Climate Model

Version: Antarctica

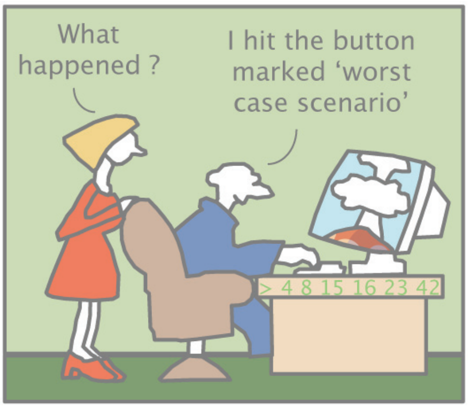

Petra Langebroek and André Paul

Department of Geosciences and
MARUM, Center For Marine Environmental Sciences
University of Bremen

October 2008

A.1 Introduction

The coupled ice sheet-climate model (ISCM) is a tool to compute ice-volume and oxygen-isotope variations in time. The current version represents the Antarctic ice sheet and has a simple axial symmetric geometry, but an advanced climate forcing mechanism. It is developed using the same design and ice-flow equations as *Sima* (2005) and *Sima et al.* (2006) for the Laurentide ice sheet, but is extended such that it suits Antarctic geometry and climate conditions. The model can be used to compute present-day conditions or transient experiments spanning different time periods within the last 50 million years (Ma).

The purpose of this manual is not to state or discuss the parameterizations or numerical implementations of the model, but rather to give an overview of its possibilities and improve its accessibility for users. After a brief model description and some comments about the computational speed and environment, a short overview of the model is given. Every directory, subroutine and switch is dicussed briefly in the Chapters A.2 (Input) and A.3 (Source). After some short comments about the numerical implementions (Chapter A.4), a cook-book with a example recipes is given (Chapter A.5). The scripts for these examples can be found in the `work` directory and the results are saved in the `output` directory. A general index can be found at the last pages of this manual.

A.1.1 Brief model description

The ISCM consists of three large-scale boxes ranging from the equator to the South Pole. In the two lower-latitude boxes (0-30 °S and 30-60 °S) climatic parameters are described as means of the entire box (Fig. 2.1). Parameters in the high-latitude box (60-90 °S) are resolved at a higher resolution of 0.5 ° latitude. The entire ISCM is forced by insolation (from orbital parameters) and atmospheric CO_2. Ice-sheet growth in this Antarctic box is constrained by coupled mass and energy balances. The ice sheet contains 12 stretched horizontal layers, with thicknesses decreasing towards the basis of the ice sheet. Within the layers, horizontal (meridional) and vertical velocities, temperatures and $\delta^{18}O_{ice}$ can be computed. An extended model description can be found in Chapter 2.

A.1.2 Computational speed and environment

The ISCM can be used to compute present-day conditions or transient experiments spanning different time schales within the last 50 Ma. Run time depends on the computational level and length of the experiment and on the operating system you execute it on. As an example: an experiment using thermomechanical coupling (and therefore also computation within the horizontal layers), varying orbital parameters (insolation) computing $\delta^{18}O_{ice}$ over 1 Ma takes approximately 7 hours on an Intel Core 2 Duo (3.0 GHz) processor. The model runs under UNIX and is written in FORTRAN95. For all experiments the Lahey `lf95` compiler is used, but this can be changed to the prefered compiler of the user in the `work` directory (files `cmp_ice.lnx` and `cmp_proc.lnx`). In the `output` directory post-processing scripts for MATLAB® (2006) and GMT (1988) can be found.

A.1.3 Model flow chart

Systematically, the ice sheet-climate model is divided in five directories: input, output, src, tmp and work (Fig. A.1). The real FORTRAN model code can be found in src (source), but is compiled by the cmp_ice.lnx and cmp_proc.lnx-scripts in work. input contains the namelist file, defining most important model controls, as the initial and final model time, the $p\mathrm{CO}_2$ input file and the root-name for the output files. Other boundary conditions (e.g. initial bedrock topography) are also stored in the input directory. tmp (short for temporary) is the location for temporarily saved files, during model compilation. output contains the results of the different model experiments, and also includes the MATLAB and GMT scripts used for post-processing.

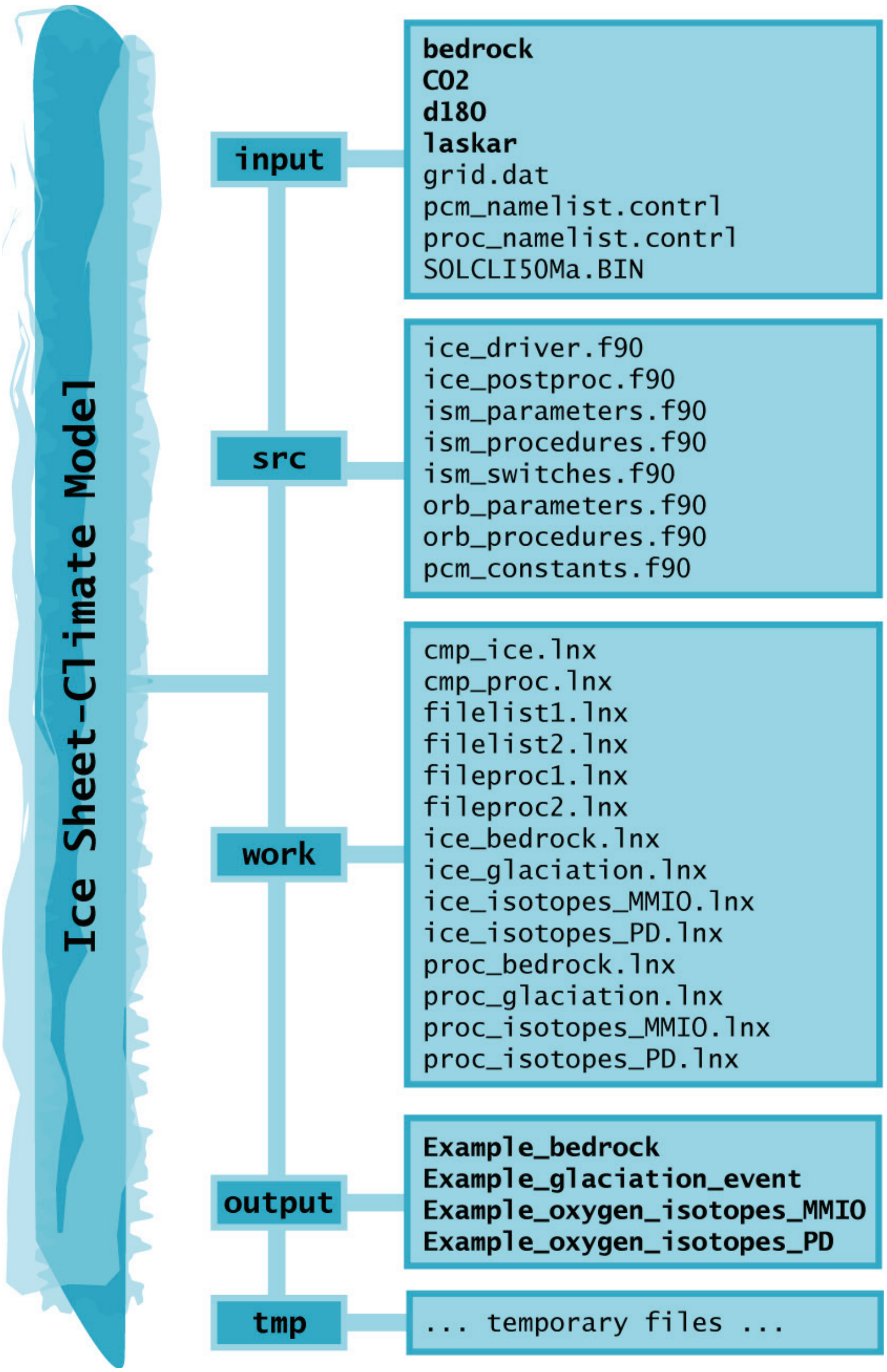

Figure A.1: *Model flow chart. The ISCM is build up in five directories:* `input`*,* `output`*,* `src`*,* `tmp` *and* `work`*. All files needed for forcing or initializing the model can be found in* `input`*. The model code is written in* `src` *and can be compiled by executing the* `cmp_ice.lnx` *or* `cmp_proc.lnx` *files in* `work`*. During computations files are temporarily saved in* `tmp`*. Modelled result are written in* `output`*.*

A.2 Input

The most important input and boundary conditions are defined in the control file (`pcm_namelist.contrl`). Here the paths to the orbital element and pCO_2 input files can be modified, as well as the paths for the output files. This is also the file where the initial and final model dates (times) are set (Table A.1). Other input and boundary conditions are set in `ice_driver.f90` and `ism_procedures.f90`. The following sections give a more extended description of the most relevant input and boundary conditions.

Initial and boundary conditions	File name	Directory
orbital elements	`pcm_namelist.contrl`	`input`
pCO_2 scenarios	`pcm_namelist.contrl`	`input`
paths for output files	`pcm_namelist.contrl`	`input`
initial and final model dates	`pcm_namelist.contrl`	`input`
history file name	`ice_driver.f90`	`src`
initial bedrock topography	`ice_driver.f90`	`src`
present-day spatial $\delta^{18}O_{snow}$	`ice_driver.f90`	`src`
temporal $\delta^{18}O_{snow}$ parameterization	`ism_proceduces.f90`	`src`

Table A.1: *List of most relevant initial and boundary conditions, plus the file name in which they can be set differently and the location of this file.*

A.2.1 Orbital parameters

The ISCM is forced by orbital parameters and atmospheric CO_2. The orbital elements can be computed from *Berger* (1978a,b), *Laskar et al.* (2004) or synthetically defined (following *DeConto and Pollard*, 2003). The options for the type of orbital elements are regulated by switch 4 (`isw4`) in `ism_switches.f90` (Fig. A.2). The direct access (DA) file used for the Laskar-based orbital parameters is located in the input directory (`SOLCLI50Ma.BIN`), which is valid for computations between present-day and 50 Ma. For more information see `input/laskar` or *Laskar et al.* (2004). When the orbital elements are calculated by the Berger-option, the subroutine `calc_elements` in `orb_procedures.f90` is executed. The constants used in this computation can be found in `orb_parameters.f90`. The synthetic orbital parameters are based on the ones used by *DeConto and Pollard* (2003), but can be enhanced in `orb_procedures.f90`. The FORTRAN code used for retrieving the appropriate orbital elements can be found in `orb_procedures.f90`, which uses also `orb_parameters.f90`.

The ISCM is using daily insolation . It is however possible to compute caloric summer and/or winter insolation in the off-line program `make_caloric_inso.f90` (`input`).

```
INTEGER :: isw4 = 0 ! isw4 = 0 => read orbital elements by
                    !             Laskar (2004) from
                    !             direct access (DA) file
                    ! isw4 = 1 => use orbital elements by
                    !             Berger (1978)
                    ! isw4 = 2 => present-day orbital elements by
                    !             Laskar (2004) from DA file
                    ! isw4 = 3 => Middle-Miocene orbital elements by
                    !             Laskar (2004) from DA file: -13840 ka
                    ! isw4 = 4 => min seasonality orbital elements by
                    !             Laskar (2004) from DA file: -13890 ka
                    ! isw4 = 5 => use synthetic orbital parameters
                    !             as in DeConto&Pollard (2003)
                    ! isw4 = 6 => Max annual mean 75S inso (14.2-13.2 Ma) used by
                    !             Laskar (2004) from DA file (-14111 ka)
                    ! isw4 = 7 => Min annual mean 75S inso (14.2-13.2 Ma) used by
                    !             Laskar (2004) from DA file (-14091 ka)
```

Figure A.2: *Overview of the switches concerning the orbital elements (part of `src/switches.f90`).*

A.2.2 Atmospheric CO_2

The other main model forcing is the atmospheric CO_2 (pCO_2). Its values are defined by the pCO_2-scenario file. These files can be found under `input/CO2` and can be chosen to be constant or varying in time. The path and name of the preferred scenario should be stated in `pcm_namelist.contrl`.

A.2.3 Oxygen isotopes

If there is computation in the vertical (`isw2 = 1`) it is possible to compute oxygen isotopes ($\delta^{18}O$) within the 12 layers of the ice sheet. The three main options are a constant $\delta^{18}O_{snow}$ forcing, $\delta^{18}O_{snow}$ from EPICA Dronning Maud Land (EDML) data or $\delta^{18}O_{snow}$ based on parameterizations from *Giovinetto and Zwally* (1997); *Lhomme* (2004); *Masson-Delmotte et al.* (2008) (`isw11`). The value of the constant $\delta^{18}O_{snow}$ can be changed in the subroutine `ism_tracer` in `ism_procedures.f90`. It is also possible to force a shift at a specific time, in order to test the response time of the ice sheet (see `ism_tracer`). The input file for the EDML-option (`d18o_EDML_2006. asc`) is set in `ice_driver.f90` and can be accessed in `input/d18o`. The last option, using the parameterizations, is the most advanced. It is based on a present-day spatial distribution of $\delta^{18}O_{snow}$, surface elevation and mean Antarctic surface temperature. The former two are read from an input file (`input/d18o`) in `ice_driver.f90`, the present-day temperature is set in `ism_tracer` (*tant_s*0). This present-day starting file can also be generated using the spatial-parameterizations currently commented out in the `ism_tracer` subroutine. Please check the Cook-book examples A.5.2 and A.5.3 for more information.

A.2.4 Initial bedrock topography

The bare bedrock topography on which the ice sheet grows is set as an input file in the `ice_driver.f90`. Different types of bedrock can be found in the directory `input/bedrock`

(Table A.2). Simple initial bedrock used in *Pollard* (1983b) and *Van Tuyll et al.* (2007) are stated in `topog_pollard_1983.asc` and `topo_ van Tuyll_ 2007. asc`, respectively. The BEDMAP project (*Lythe et al.*, 2000) compiled present-day bedrock and ice-sheet elevation. From this a zonally averaged, isostatically adjusted ice-free bedrock is derived. Means over eastern (`east`) and the whole of Antarctica (`total`), as well as averages over certain regions (Dronning Maud Land (`dml`) and Gamburtsev Mountains (`gm`)) are produced. All of these initial ice-free topographies can be used as basis for the ice-sheet model by choosing the corresponding file described in Table A.2.

File name	Reference
`topog_pollard_1983.asc`	*Pollard* (1983b)
`topog_vanTuyll_2007.asc`	*Van Tuyll et al.* (2007)
`topog_bedmap_total.asc`	BEDMAP project - all data
`topog_bedmap_east.asc`	BEDMAP project - Eastern Antarctica
`topog_bedmap_dml.asc`	BEDMAP project - Dronning Maud Land
`topog_bedmap_gm.asc`	BEDMAP project - Gamburtsev Mountains
`topog_bedmap_outside_bulge100.asc`	BEDMAP project - bulge near coast

Table A.2: *Overview of different types of initial bedrock topography. The upper two ice-free initial bedrock topographies are published in Pollard (1983b) and Van Tuyll et al. (2007). The present-day bedrock and ice-sheet elevation of the BEDMAP project are compiled by Lythe et al. (2000).*

A.3 Source

The files in source (`src`) can be separated in files connected to the orbital forcing (`orb_parameters.f90` and `orb_procedures.f90`) and files concerning the ice sheet-climate model (`ism_parameters.f90`, `ism_proceduces. f90` and `ism_switches.f90`). The model is run by executing the driver (`ice_driver.f90`), which in turn uses the parameters, procedures and switches of the ice-sheet and orbital scripts. All general constants, as unit numbers for files, the definition of the computation precision and unit conversions, are set in `pcm_constants.f90`. For some post-processing, namely the making of cross-sections showing the internal structure of temperature, velocity and $\delta^{18}O_{ice}$ in the model at a defined moment in time (snapshot), the script `ice_postproc.f90` can be used. The following subsections shortly describe the subroutines and switches.

A.3.1 Subroutines and functions in `orb_procedures.f90`

`orb_elements`

This subroutine reads the orbital elements from the direct access file `SOLCLI50Ma.BIN` from *Laskar et al.* (2004). With some small adjustments the older direct access file (*Laskar et al.*, 1993) can also be read. Input variables are initial year of the orbital element data and the actual year for which orbital elements should be computed. The *Laskar et al.* (2004) solution produces eccentricity, obliquity and longitude of the perihelion with respect to the moving vernal equinox. The older *Laskar et al.* (1993) direct access file also outputs the orbital inclination of the Earth and the phase angle of this inclination derived from *Quinn et al.* (1991).

`orb_elements_syn`

For a specific year synthetically manufactured orbital elements (eccentricity, obliquity and longitude of the perihelion with respect to the moving vernal equinox) can be computed. The default frequencies and amplitudes are taken from *DeConto and Pollard* (2003), but alterations are proposed in the subroutine.

`ism_daily` (`time2longitude` and `longitude2time`)

This subroutine computes the daily insolation which is equal to the instantaneous insolation integrated over 24 hours of true solar time. Furthermore it provides the annual mean values for 45 and 75 °S. The time loop start at the 1st of January, but computation is with respect to vernal equinox. To shift between true longitudes and calendar days the functions `time2longitude` and `longitude2time` are used.

`set_fourier` and `calc_elements`

These two subroutines are used to compute the Earth's orbital elements using *Berger* (1978a,b). The mean rates and phase of sine and cosine expansions needed in these subroutines are listed in `orb_parameters.f90`.

A.3.2 Subroutines in `ism_procedures.f90`

`ism_grids0`

This subroutine sets up the grids in the latitudinal direction and is only used when there is no computation in the vertical direction.

`ism_grids1`

Here the grid is defined for the latitudinal as well as the vertical direction. Default is an axial symmetry. The model therefore has a variable flowband width. The radii and areas are computed for half a circle. It is possible to change back to a fixed flowband width which is more appropriate for a Cartesian geometry (for example the Laurentide Ice Sheet). Additionally, the horizontal ice layers are set up in this subroutine. The number of latitudinal and vertical grid-cells is defined in `ice_driver.f90` and `pcm_constants.f90`. As default, latitudinal a resolution of 0.5 ° is used. The main ice-sheet computations are executed between `js = 120` and `je = 240` (can be changed in `ice_driver.f90`), which correspond to latitudes of approximately 60 °S. Calculations extent from 60 to 90 to 60 °S, following a hypothetical cross-section through the cone-shaped (axial-symmetric) ice sheet. In the vertical direction, the default value is 12 layers.

`ism_grids_atm`

This subroutine sets up the large-scale grid-boxes in the atmosphere. They have a resolution of 30 ° latitude and reach from the equator to the South Pole. The basal areas are computed using the radius and a spherical representation of the Earth.

`ism_topog`

Here, the initial ice-free bedrock topography is constructed and interpolated for every grid. The input-file is located in `input/bedrock`.

`ism_EBM_MB`

In this subroutine the daily energy (EBM) and mass (MB) balance parameterizations for the ice sheet are solved. Main input factors are the daily insolation and $p\mathrm{CO}_2$. It also uses several geometrical parameters like areas and heights of the grid cells. Many energy and mass variables (e.g. temperature and albedo) are computed using the outcome of the previous time step. Main output arguments are (net) accumulation and temperatures necessary for the build-up or retreat of the ice sheet. The parameterizations in this subroutine are largely described in Section 2.3.

ism_ablation

This ablation subroutine returns the amount of ablation (melting) at the bottom of the ice sheet (which is actually computed in the subroutine `ism_tracer`). It also determines ice calving by proglacial lakes and/or marine incursions (*Pollard*, 1983a).

ism_uvelocity0

When there are no vertical layers, this subroutine is used for computation of the horizontal (meridional) velocity distribution.

ism_uvelocity1

Similar to `ism_uvelocity0`, but the velocities are also derived for every vertical grid cell. When thermomechanical coupling is turned on (`isw7 = 1`) and the temperature of the bottom layer exceeds the melting temperature of ice, sliding velocity is computed.

ism_continuity

In this subroutine the fundamental equation for the entire ice-sheet model is solved, the ice continuity equation. With the use of meridional velocities, the new ice thickness is determined.

ism_geometry

This subroutine computes geometrical elements and time derivatives needed in computing mass and tracer transports.

ism_wvelocity

Here, the vertical velocities are derived from meridional velocities and the volume of ice, using the incompressibility condition of ice. As boundary conditions (net) surface accumulation and bottom ablation (melting) are applied.

ism_sediment

This subroutine computes the sediment thickness and velocity. In the current model version, no sediment is considered, and this subroutine is commented out in the `ice_driver.f90`.

ism_bedrock

This subroutine derives the isostatic adjustment of the lithosphere and asthenosphere. For the lithosphere there are 2 options: local (LL) or elastic (EL) lithosphere. The local adjustment is much quicker, but too localized in signal (*Le Meur and Huybrechts*, 1996; *Oerlemans and van der Veen*, 1984). The elastic computation takes more computing time, but is considered to be the best. For the asthenosphere, a relaxed configuration is assumed, because this option is much more realistic than a diffusive asthenosphere.

`ism_tracer`

In this subroutine the advection and diffusion equations for the tracers in the ice sheet are solved. For temperature the (surface) boundary is the annual mean surface temperature computed in the subroutine `ism_EBM_MB`. The forcing of the second tracer, the ratio of oxygen isotopes in ice, is parameterized in this subroutine and depends on annual mean Antarctic temperature and ice-sheet height. The oxygen-isotope ratio is altered using the same advection scheme as for ice temperature, but discarding diffusion. If the computed temperature is above the pressure-melting point, melting is calculated and the temperature is set to the pressure-melting point. The subroutine is concluded with averaging the tracer values for the entire ice sheet and a check for unrealistic temperatures and ice elevations.

`ism_average`

The list of subroutines is terminated with the computation of mean values for the surface and atmospheric temperature and the precipitation in the Antarctic large-scale box.

A.3.3 Switches

A list of the different switches can be found in Figure A.3.
`isw1` decides whether to use a locally or elastically adjusted lithosphere. Local isostasy makes the computation much quicker, but results in a too localized bedrock signal (*Le Meur and Huybrechts*, 1996; *Oerlemans and van der Veen*, 1984). Elastic isostatic adjustment considers not only the primary grid cell, but deflection is calculated using also the neighbouring grids.
`isw2` sets the computation in the vertical direction. Only if decided for computation in the vertical, temperatures and $\delta^{18}\mathrm{O}_{\mathrm{ice}}$ within the ice layers can be derived, which is also needed for thermomechanical coupling (`isw7`).
In the set-up of the horizontal grid (`ism_grids0` and `ism_grids1`) it is possible to choose between a Cartesian or axially symmetric spherical geometry (`isw3`). Because of the fact that this model version represents an axially symmetric ice sheet, it is strongly advised to keep this switch at 1.
`isw4` defines the type of orbital elements and insolation used. For more information about the options, see Section A.2.1.
`isw7` decides whether the ice temperatures influence the ice velocities (thermomechanical coupling) or not. This option can only be applied if computation in the vertical direction is considered.
`isw9` is another switch affecting the velocity computation. The flow-law parameter in the meridional velocity parameterization depends on the shape of the ice sheet in the latitudinal direction. Please read *Sima* (2005) for more information on this parameterization.
`isw11` sets the type of $\delta^{18}\mathrm{O}_{\mathrm{snow}}$ forcing. It is possible to choose a constant value (`isw11 = 0`),

```
MODULE ism_switches
   IMPLICIT NONE
   INTEGER :: isw1 = 1 ! isw1 = 0 => local lithosphere (LL)
                       ! isw1 = 1 => elastic lithosphere (EL)
   INTEGER :: isw2 = 1 ! isw2 = 0 => no computation in the vertical
                       ! isw2 = 1 => computation in the vertical
   INTEGER :: isw3 = 1 ! isw3 = 0 => cartesian geometry
                       ! isw3 = 1 => axially symmetric
                       !            spherical geometry
   INTEGER :: isw4 = 0 ! isw4 = 0 => read orbital elements by
                       !            Laskar (2004) from
                       !            direct access (DA) file
                       ! isw4 = 1 => use orbital elements by
                       !            Berger (1978)
                       ! isw4 = 2 => present-day orbital elements by
                       !            Laskar (2004) from DA file
                       ! isw4 = 3 => Middle-Miocene orbital elements by
                       !            Laskar (2004) from DA file: -13840 ka
                       ! isw4 = 4 => min seasonality orbital elements by
                       !            Laskar (2004) from DA file: -13890 ka
                       ! isw4 = 5 => use synthetic orbital parameters
                       !            as in DeConto&Pollard (2003)
                       ! isw4 = 6 => Max annual mean 75S inso (14.2-13.2 Ma) used by
                       !            Laskar (2004) from DA file (-14111 ka)
                       ! isw4 = 7 => Min annual mean 75S inso (14.2-13.2 Ma) used by
                       !            Laskar (2004) from DA file (-14091 ka)
   INTEGER :: isw7 = 1 ! isw7 = 0 => no thermomechanical coupling
                       ! isw7 = 1 => thermomechanical coupling
   INTEGER :: isw9 = 0 ! isw9 = 0 => slab profile in latitudinal direction
                       ! isw9 = 1 => parabolic profile
   INTEGER :: isw10 = 1! isw10 = 0 => compute only temp in ice layers
                       ! isw10 = 1 => compute temp and d18o in ice layers
   INTEGER :: isw11 = 2! isw11 = 0 => constant snow-d18o-computation
                       !             also for testing response time
                       ! isw11 = 1 => snow-d18o from EDML data
                       ! isw11 = 2 => snow-d18o from parameterization
END MODULE ism_switches
```

Figure A.3: *Overview of all model switches (`src/switches.f90`).*

read the $\delta^{18}O_{snow}$ from EPICA Dronning Maud Land data (`isw11 = 1`) or use the parameterization based on *Giovinetto and Zwally* (1997), *Lhomme* (2004) and *Masson-Delmotte et al.* (2008) (`isw11 = 2`). See Section A.2.3 for further information.

A.4 Numerical implementation

The ice-sheet model is solved with a finite-difference approach on a staggered grid in both, vertical and horizontal, directions. Tracers (T_{ice} and $\delta^{18}\mathrm{O}_{\mathrm{ice}}$) are solved on the T-grid, whereas fluxes and velocities are computed exactly in between, on the U-grid. The horizontal resolution is 0.5 ° latitude. In the current, Antarctic version of the model, the grid is computed between `js = 120` and `je = 240` (see section A.3.2). In the vertical σ-coordinates are used (e.g. *Payne and Dongelmans*, 1997) and the grid is stretched in 12 layers with uneven thicknesses decreasing towards the base of the ice sheet (Fig. A.4). A first-order upwind scheme is used for advection and a second-order scheme for heat diffusion. For the vertical upwinding, the relative vertical velocity of ice with respect to the down- or uplift of the grid point is used, with the surface mass balance and bottom melting as boundary conditions. The integration in time is computed by an Eulerian-forward scheme. Most equations (continuity, velocities and tracers) are solved in a one year time step, occasionally reduced to a minimum of 0.05 year in periods of extreme melting or ablation. The energy and mass balance equations, however, are solved at a daily time step.

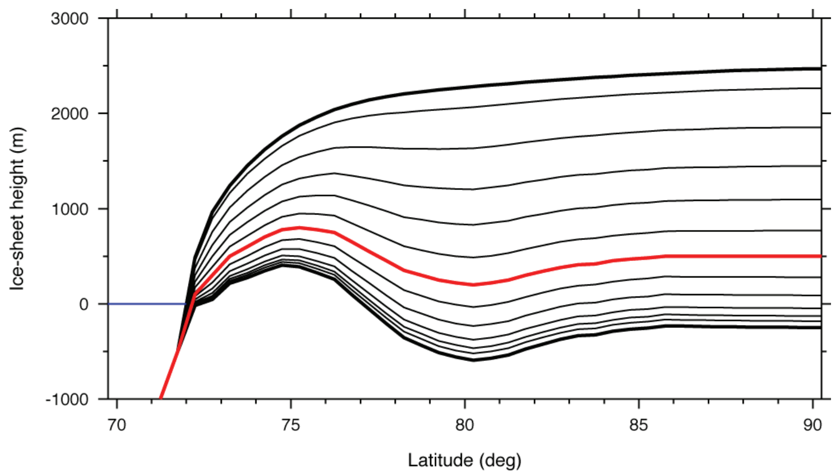

Figure A.4: *Example of the vertical σ-spacing in a large ice sheet. The red line indicates the initial ice-free bedrock topography.*

A.5 Cook-book

A.5.1 Glaciation event

Target: computation of ice-volume increase in the Middle Miocene

Forcing: step-wise decrease in $p\mathrm{CO_2}$ and varying orbital parameters

Time period: 14.1-13.6 Ma

In this example the goal is to simulate the large-scale Antarctic glaciation event in the Middle Miocene. This is possible for different $p\mathrm{CO_2}$ scenarios (see Chapter 3). We chose one scenario in order to illustrate the transition from a small into a large ice sheet (`co2scenario-410_390ppm_13.902-13.898Ma.asc`). Here the $p\mathrm{CO_2}$ is defined to be at a constant level of 410 ppm until 13.902 Ma. It linearly decreases to 390 ppm at 13.898 Ma, where after it stays constant again. The other forcing, the varying orbital elements (and therefore insolation), is taken from *Laskar et al.* (2004). Flow of the ice on Antarctica is influenced by temperature, therefore it is more realistic to switch the thermomechanical coupling on and allow for computation in the vertical direction. In this example we are not interested in the oxygen-isotope ratio of the ice, consequently δ^{18}O is not computed.

Set-up and execute

There are four files in which settings should be adjusted in order to execute this example run properly: `ice_driver.f90`, `cmp_ice.lnx`, `pcm_namelist.contrl` and `ism_switches.f90`. In `ice_driver.f90` the filename of the history (output) file should be set to, for example, `history_glaciation_event.dat`. The executable in `cmp_ice.lnx` takes the name `ice_glaciation_event.lnx` in this example. All proper switches should be set in `ism_switches.f90` (see Fig. A.5). The input files for the orbital parameters and $p\mathrm{CO_2}$, as well as the path for the output files and the initial and final modelling dates should be properly stated in `pcm_namelist.contrl` (see Fig. A.6). After setting all options correctly, the example experiment can be run by the commands `cmp_ice.lnx` and `ice_glaciation_event.lnx` in the `work` directory.

Output

During the experiment, every 1000 years a list of variables (default includes surface, ice and bedrock elevation, different temperature and mass variables, and meridional velocity) depending on the latitudinal grid cell are written to the screen. Changes in the amount and the choice of these parameters can be adjusted in the final part of `ice_driver.f90`. For every 10 ka (changes into 1 ka close to present-day; can also be altered in `ice_driver.f90`) a snapshot of the ice-sheet profile, velocities, temperature and $\delta^{18}\mathrm{O}_{ice}$ are printed in a history file. These results can conveniently be plotted using the post-processing script. Annual-mean model parameters are written to a general history file (`history_glaciation_event.`

```
MODULE ism_switches
   IMPLICIT NONE
   INTEGER :: isw1 = 1 ! isw1 = 0 => local lithosphere (LL)
                       ! isw1 = 1 => elastic lithosphere (EL)
   INTEGER :: isw2 = 1 ! isw2 = 0 => no computation in the vertical
                       ! isw2 = 1 => computation in the vertical
   INTEGER :: isw3 = 1 ! isw3 = 0 => cartesian geometry
                       ! isw3 = 1 => axially symmetric
                       !             spherical geometry
   INTEGER :: isw4 = 0 ! isw4 = 0 => read orbital elements by
                       !             Laskar (2004) from
                       !             direct access (DA) file
                       ! isw4 = 1 => use orbital elements by
                       !             Berger (1978)
                       ! isw4 = 2 => present-day orbital elements by
                       !             Laskar (2004) from DA file
                       ! isw4 = 3 => Middle-Miocene orbital elements by
                       !             Laskar (2004) from DA file: -13840 ka
                       ! isw4 = 4 => min seasonality orbital elements by
                       !             Laskar (2004) from DA file: -13890 ka
                       ! isw4 = 5 => use synthetic orbital parameters
                       !             as in DeConto&Pollard (2003)
                       ! isw4 = 6 => Max annual mean 75S inso (14.2-13.2 Ma) used by
                       !             Laskar (2004) from DA file (-14111 ka)
                       ! isw4 = 7 => Min annual mean 75S inso (14.2-13.2 Ma) used by
                       !             Laskar (2004) from DA file (-14091 ka)
   INTEGER :: isw7 = 1 ! isw7 = 0 => no thermomechanical coupling
                       ! isw7 = 1 => thermomechanical coupling
   INTEGER :: isw9 = 0 ! isw9 = 0 => slab profile in latitudinal direction
                       ! isw9 = 1 => parabolic profile
   INTEGER :: isw10 = 0! isw10 = 0 => compute only temp in ice layers
                       ! isw10 = 1 => compute temp and d18o in ice layers
   INTEGER :: isw11 = 2! isw11 = 0 => constant snow-d18o-computation
                       !              also for testing response time
                       ! isw11 = 1 => snow-d18o from EDML data
                       ! isw11 = 2 => snow-d18o from parameterization
END MODULE ism_switches
```

Figure A.5: *The `switches.f90`-file for Example 'Glaciation event'. Important for this example experiment are computation in the vertical direction (`isw2 = 1`), thermomechanical coupling (`isw7 = 1`) and computation of temperature in the ice layers (`isw10 = 0`). Furtheron, the insolation should be varying and therefore the orbital parameters should be read from the Laskar direct access file (`isw4 = 0`).*

`dat`) and can be analyzed and plotted using the MATLAB or GMT scripts `plot_glaciation_event.m` or `plot_glaciation_event.script`, respectively (see Fig. A.7).

Note that if $\delta^{18}O_{ice}$ is still considered in the output files, the values are some mean of the surface $\delta^{18}O_{snow}$ and do not represent realistic $\delta^{18}O_{ice}$ values. The following two recipes (Sections A.5.2 and A.5.3) show an example including also $\delta^{18}O_{ice}$ variations.

Post-processing

For every time-snapshot the outputted parameters can be post-processed in cross-sections. For this the `proc_namelist.contrl`-file (in the `input` directory) should use the appropri-

```
&contrl
orb_fname          = '../input/SOLCLI50Ma.BIN',
co2_fname          = '../input/CO2/co2scenario410_390ppm_13.902-13.898Ma.asc',
hst_fpath          = '../output/Example_glaciation_event'
hst_froot          = 'h0001'
orb_origin         = 0.D0,
orb_dt             = 1000.D0,
date_initial       = -1.41D1,
date_final         = -1.36D1,
/
```

Figure A.6: *The `pcm_namelist.contrl`-file for Example 'Glaciation event'. The direct access file for the orbital elements and the pCO_2 file are located in the `input`-directory. All results are written in `output/Example_glaciation_event`. Initial and final dates are set to 14.1 and 13.6 Ma, respectively.*

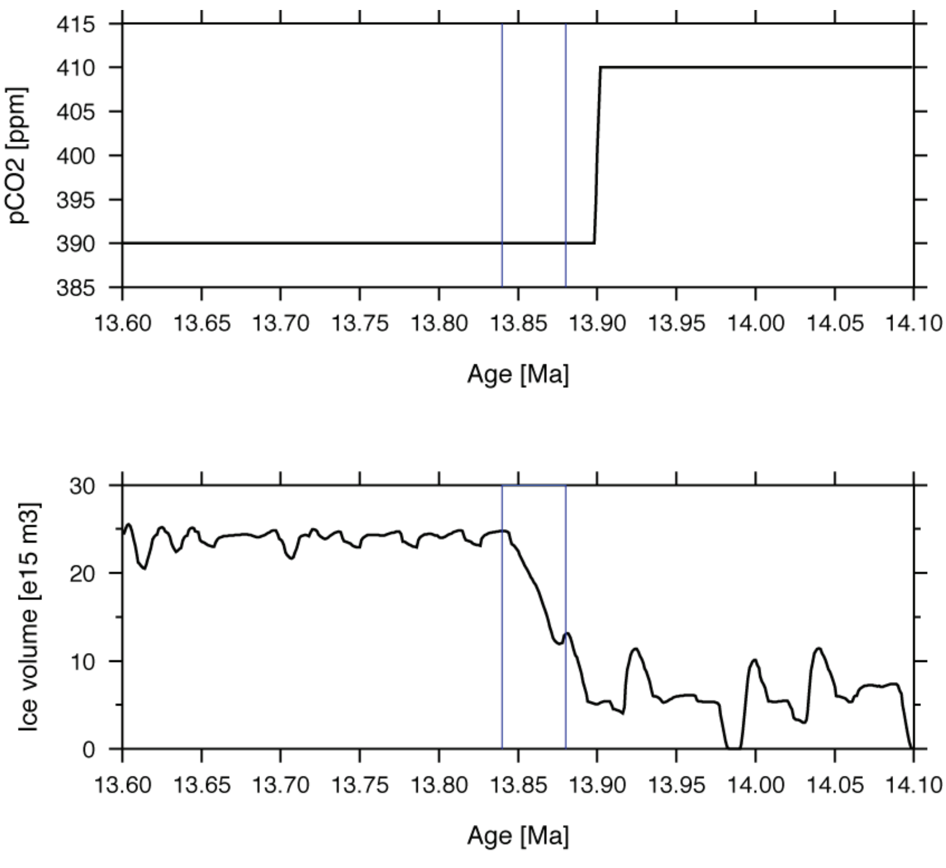

Figure A.7: *Figure showing the resulting total ice volume as function of time. The pCO_2 -forcing is drawn in the panel above. Vertical bars indicate the extention of the Antarctic ice sheet in the Middle Miocene. Figure results from `plot_glaciation_event.m` in MATLAB or `plot_glaciation_event.script` in GMT. Both scripts can be modified according to the user's needs.*

ate settings (see Fig. A.8a). The executable for post-processing `proc_glaciation_event.lnx` can be set in `work/cmp_proc.lnx`. Running `cmp_proc.lnx`, followed by `proc_glaciation_event.lnx`, will ask you for the date of the snapshot to be processed. This date should be typed in ka, whereby the future is in positive and the past in negative values. For example, -14000 should be typed in order to process the results of the snapshot at 14 Ma. GMT scripts to plot the temperature and the velocities should be adapted to the relevant, post-processed files. An example for a temperature cross-section at 14 Ma can be found in `temp_colour.script` and resulting `plot_14000_tem_colour.ps` (Fig. A.8b). Velocity profiles can be generated by `vel.script` and should look like Fig. A.8c-e, where 13.8 Ma is plotted. The colour palette tables needed to draw the cross-sections are located in the `output` directory (and have the suffix $*$.cpt).

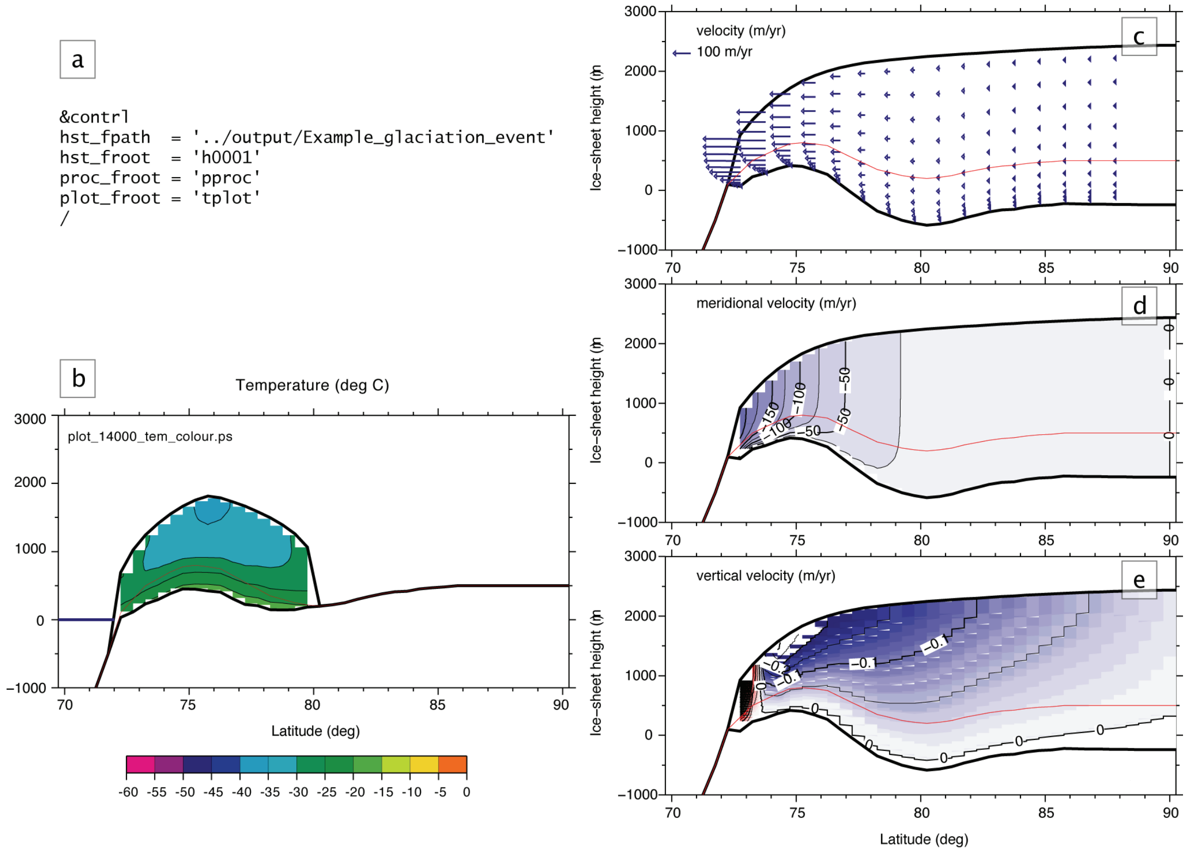

Figure A.8: *The* `proc_namelist.contrl`*-file, temperature and velocity cross-sections for Example 'Glaciation event'.* ***(a)*** `proc_namelist.contrl` *states the paths and roots for post-processing. The model results to be processed are read from* `hst_fpath` *and will be written to the same directory with the specificed roots.* ***(b)*** *Cross-section through the ice-sheet model, showing the temperature distribution at 14 Ma. To generate this figure, first the output from the ice sheet-climate model needs to be post-processes. Then the GMT script* `temp_colour.script` *should produce this figure.* ***(c-e)*** *Velocity profiles at 13.8 Ma. Again post-processing needs to be accomplished succesfully before producing this figure with* `vel.script` *in GMT.*

A.5.2 Present-day oxygen-isotope distribution

Target: present-day distribution of $\delta^{18}O_{ice}$

Forcing: constant pre-industrial pCO$_2$ and varying orbital parameters

Present-day $\delta^{18}O_{snow}$ forcing: *Masson-Delmotte et al.* (2008)

Temporal $\delta^{18}O_{snow}$ forcing: *Lhomme* (2004) (α_c=0.6 ‰/°C; β_δ=-11.2 ‰/km)

Time period: last 1 Ma

Here we compute the oxygen-isotopic composition of the present-day Antarctic ice sheet. The distributions within the ice as well as the $\delta^{18}O_{snow}$ at the surface are generated. The pCO$_2$ forcing can be kept at the constant pre-industrial level of 280 ppm. Varying orbital parameters are used here, but they could be kept constant. The lengthy computation time is applied in order to not only account for ice-volume spin-up, but also to make sure the $\delta^{18}O_{ice}$ distribution within the ice is close to equilibrium. During the ice waxing process $\delta^{18}O_{snow}$ changes from less depleted (lower elevations) to more depleted (high elevation) values. It takes a long time before the depleted values reach the bottom layers of the ice sheet. The parameterizations used for the δ^{18}O forcing are described and tested in Section 2.4 and Chapter 4.

Set-up and execute

The main files that need to be modified are again: `ice_driver.f90`, `cmp_ice.lnx`, `pcm_namelist.contrl` and `ism_switches.f90`. Examples of the latter two are shown in Figures A.10a and A.9. In `cmp_ice.lnx` the relevant lines should be commented out. Important is the type of δ^{18}O forcing applied. This can partly be adjusted by switch 11. Forcing the ice sheet-climate model with data from EPICA Dronning Maud Land (`isw11 = 1`) is only possible for the last 800 ka. This example deals with a longer period and needs a more general approach. The different $\delta^{18}O_{snow}$ parameterizations are described and explained in Section 2.4 and Chapter 4. The spatial present-day files can be found in the input directory and were generated by applying the spatial relationships between $\delta^{18}O_{snow}$ and T_{sfc} from *Giovinetto and Zwally* (1997) and *Masson-Delmotte et al.* (2008) to a previous 1 Ma model experiment. These results can now be used in order to compute past changes in $\delta^{18}O_{snow}$. For this, one of the parameterizations needs to be chosen and set as input-file in `ice_driver.f90`. Modifications to the parameterizations and its constants can be done in the subroutine `ism_tracer` in the final part of the `src`-file `ism_procedures.f90`. In this example the relation between $\delta^{18}O_{snow}$ and T_{sfc} of *Masson-Delmotte et al.* (2008) is used for the present-day distribution of $\delta^{18}O_{snow}$. This parameterization resulted in a basis present-day file, which is refered to in `ice_driver.f90` (`PD_1Ma_280ppm_sp_MD2008_hsfc_d18o_tsat.dat`). For the translation into the past, the relation defined by *Lhomme* (2004) is used (with its constants set to α_c=0.6 ‰/°C and β_δ=-11.2 ‰/km). To output not only the $\delta^{18}O_{ice}$ distribution in the ice, but also the present-day surface $\delta^{18}O_{snow}$ forcing, another file can be written in the `ice_driver.f90` (under section `Open history and other output files`).

```
MODULE ism_switches
   IMPLICIT NONE
   INTEGER :: isw1 = 1 ! isw1 = 0 => local lithosphere (LL)
                       ! isw1 = 1 => elastic lithosphere (EL)
   INTEGER :: isw2 = 1 ! isw2 = 0 => no computation in the vertical
                       ! isw2 = 1 => computation in the vertical
   INTEGER :: isw3 = 1 ! isw3 = 0 => cartesian geometry
                       ! isw3 = 1 => axially symmetric
                       !            spherical geometry
   INTEGER :: isw4 = 0 ! isw4 = 0 => read orbital elements by
                       !            Laskar (2004) from
                       !            direct access (DA) file
                       ! isw4 = 1 => use orbital elements by
                       !            Berger (1978)
                       ! isw4 = 2 => present-day orbital elements by
                       !            Laskar (2004) from DA file
                       ! isw4 = 3 => Middle-Miocene orbital elements by
                       !            Laskar (2004) from DA file: -13840 ka
                       ! isw4 = 4 => min seasonality orbital elements by
                       !            Laskar (2004) from DA file: -13890 ka
                       ! isw4 = 5 => use synthetic orbital parameters
                       !            as in DeConto&Pollard (2003)
                       ! isw4 = 6 => Max annual mean 75S inso (14.2-13.2 Ma) used by
                       !            Laskar (2004) from DA file (-14111 ka)
                       ! isw4 = 7 => Min annual mean 75S inso (14.2-13.2 Ma) used by
                       !            Laskar (2004) from DA file (-14091 ka)
   INTEGER :: isw7 = 1 ! isw7 = 0 => no thermomechanical coupling
                       ! isw7 = 1 => thermomechanical coupling
   INTEGER :: isw9 = 0 ! isw9 = 0 => slab profile in latitudinal direction
                       ! isw9 = 1 => parabolic profile
   INTEGER :: isw10 = 1! isw10 = 0 => compute only temp in ice layers
                       ! isw10 = 1 => compute temp and d18o in ice layers
   INTEGER :: isw11 = 2! isw11 = 0 => constant snow-d18o-computation
                       !             also for testing response time
                       ! isw11 = 1 => snow-d18o from EDML data
                       ! isw11 = 2 => snow-d18o from parameterization
END MODULE ism_switches
```

Figure A.9: *The `switches.f90`-file for Examples 'Present-day oxygen isotopes' and 'Oxygen-isotopes in the Middle Miocene'. Important for this example experiment are computation in the vertical direction (`isw2 = 1`), thermomechanical coupling (`isw7 = 1`) and computation of temperature and $\delta^{18}O_{ice}$ in the ice layers (`isw10 = 1`). Furtheron, the insolation should be varying and therefore the orbital parameters should be read from the Laskar direct access file (`isw4 = 0`).*

Output

The history of this example experiment is written to the file `history_oxygen_isotopes_PD.dat`. More detailed information about the elevation, velocities, temperatures and $\delta^{18}O_{ice}$ per grid cell can be found in the snapshot-files (`h0002*`). The present-day $\delta^{18}O_{snow}$ (and other parameters) is stored in `oxygen_isotopes_ snow_present-day.dat`. For figures showing model parameters in time, see the previous example (Section A.5.1).

a

```
&contrl
orb_fname    = '../input/SOLCLI50Ma.BIN',
co2_fname    = '../input/CO2/co2scenario280ppm.asc',
hst_fpath    = '../output/Example_oxygen_isotopes_PD'
hst_froot    = 'h0002'
orb_origin   = 0.D0,
orb_dt       = 1000.D0,
date_initial = -1.0D0,
date_final   =  0.0D0,
/
```

b

```
&contrl
hst_fpath  ='../output/Example_oxygen_isotopes_PD'
hst_froot  = 'h0002'
proc_froot = 'pproc'
plot_froot = 'tplot'
/
```

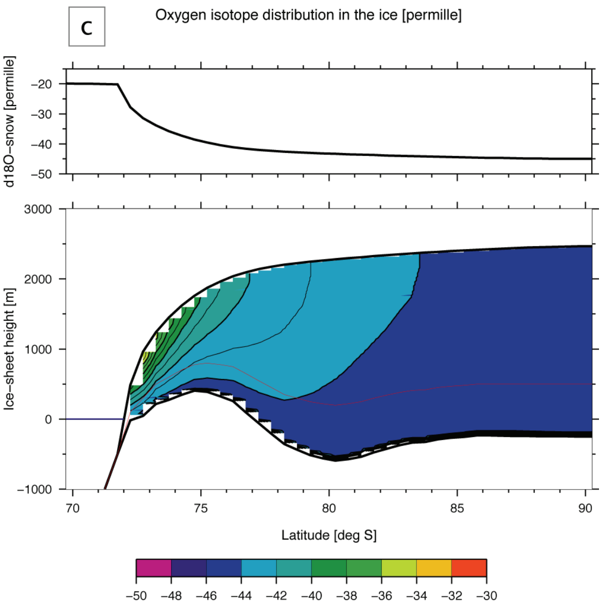

Figure A.10: *Post-processing files and velocity profile for Example 'Present-day oxygen isotopes'.* ***(a)*** *The namelist file* `pcm_namelist.contrl` *contains a list of important boundary conditions. The direct access file for the orbital elements and the* pCO_2 *file are located in the* `input`*-directory. All results are written to* `output/Example_oxygen_isotopes_PD`*. Computation time is from 1 Ma until present.* ***(b)*** *The* `proc_namelist.contrl`*-file states the paths and roots for post-processing. The model results to be processed are read from* `hst_fpath` *and will be written to the same directory with the specified roots.* ***(c)*** *Present-day oxygen-isotope profile. Again post-processing needs to be accomplished succesfully before producing this figure with* `d18o_colour.script` *in GMT.*

Post-processing

The post-processing works similar to the previous example (Section A.5.1), in which the temperature and velocity distribution for one snapshot were processed. Here we show the same technique, but for $\delta^{18}O_{ice}$. For post-processing a cross-section, `proc_namelist.contrl` needs to be adjusted (see Fig. A.10b). After compiling the `cmp_proc.lnx` file and the consequent `proc_isotopes_PD.lnx`, the relevant data can be written to the screen. Because we are interested in the present-day situation, `0` can be typed. In the output directory the GMT script `d18o_colour. script` contains the settings to create a nice figure with $\delta^{18}O_{ice}$ in the ice-sheet model. In a panel above, the $\delta^{18}O_{snow}$ information from `oxygen_isotopes_PD.dat` is used to plot the present-day $\delta^{18}O_{snow}$ profile (Fig. A.10c).

A.5.3 Oxygen-isotopes in the Middle Miocene

Target: distribution of $\delta^{18}O_{ice}$ during glaciation event

Forcing: step-wise decrease in pCO_2 and varying orbital parameters

Present-day $\delta^{18}O_{snow}$ forcing: *Giovinetto and Zwally* (1997)

Temporal $\delta^{18}O_{snow}$ forcing: *Lhomme* (2004) (α_c=0.8 ‰/°C; β_δ=-11.2 ‰/km)

Time period: 14.2-13.6 Ma

This example is a combination of the previous two recipes (Sections A.5.1 and A.5.2). Here the ice-sheet extension in the Middle Miocene is computed, again with the pCO_2 forcing set to `co2scenario410_390ppm_13.902-13.898Ma.asc`. Additionally, the $\delta^{18}O$ is computed within the ice sheet. Using a constant surface area of the ocean and the densities of ice and water, ice volume can converted into sea level. This Antarctica volume-equivalent sea level, together with $\delta^{18}O_{ice}$, is related to $\delta^{18}O_{sw}$ (see Section 2.4 and Chapter 4 for equations). This recipe shows how to compute ice volume, $\delta^{18}O_{ice}$ and related sea level and $\delta^{18}O_{sw}$ in the Middle Miocene.

Set-up and execute

The model set-up is very similar to the previous example (Section A.5.2). The main files to adjust are: `ice_driver.f90`, `cmp_ice.lnx`, `pcm_namelist.contrl` and `ism_switches.f90`. This latter list of switches is equivalent to the preceding recipe (Fig. A.9). In `pcm_namelist.contrl`, the pCO_2 forcing, output directory and model dates should be changed appropriate for this example (Fig. A.11) and `cmp_ice.lnx` needs compile the proper executable file (`ice_isotopes_MMIO.lnx`). Again the history is written to the file specified in `ice_driver.f90` (`history_oxygen_isotopes_MMIO.dat`), which can be found in `output`. The type of $\delta^{18}O_{snow}$ forcing needs to be set in `ice_driver.f90` as well as in `ism_tracer` (in `ism_procedures.f90`). The present-day distribution of $\delta^{18}O_{snow}$is referred to in the former script and the temporal parameterization is set in `ism_tracer`. In this recipe present-day forcing of *Giovinetto and Zwally* (1997) is used (`input/d18o/PD_1Ma_280ppm_sp_GZ1997_hsfc_d18o_tsat.dat`) and the temporal relation of *Lhomme et al.* (2005) is applied for α_c=0.8 ‰/°C and β_δ=-11.2 ‰/km.

Output

Annual-mean results are saved in `history_oxygen_isotopes_MMIO.dat`. Ice-sheet geometry and internal temperatures, velocities and $\delta^{18}O_{ice}$ per time-step are written to `h0003*`-files. An example of how to plot the pCO_2 forcing, sea level, bulk $\delta^{18}O_{ice}$ and $\delta^{18}O_{sw}$ in GMT (Fig. A.12) can be found in `plot_transition_MMIO.script`.

```
&contrl
orb_fname         = '../input/SOLCLI50Ma.BIN',
co2_fname         = '../input/CO2/co2scenario410_390ppm_13.902-13.898Ma.asc',
hst_fpath         = '../output/Example_oxygen_isotopes_MMIO'
hst_froot         = 'h0003'
orb_origin        = 0.D0,
orb_dt            = 1000.D0,
date_initial      = -1.42D1,
date_final        = -1.36D1,
/
```

Figure A.11: *The* `pcm_namelist.contrl`*-file for Example 'Oxygen-isotopes in the Middle Miocene'. The direct access file for the orbital elements and the* pCO_2 *file are located in the* `input`*-directory. All results are written in* `output/Example_oxygen_isotopes_MMIO`*. Computation time is from 14.2 to 13.6 Ma.*

Post-processing

For post-processing, the `proc_namelist.lnx` file should be adjusted and executed. In this recipe we do not show any examples of this, but for further explanations we refer to the previous two sections (Sections A.5.1 and A.5.2).

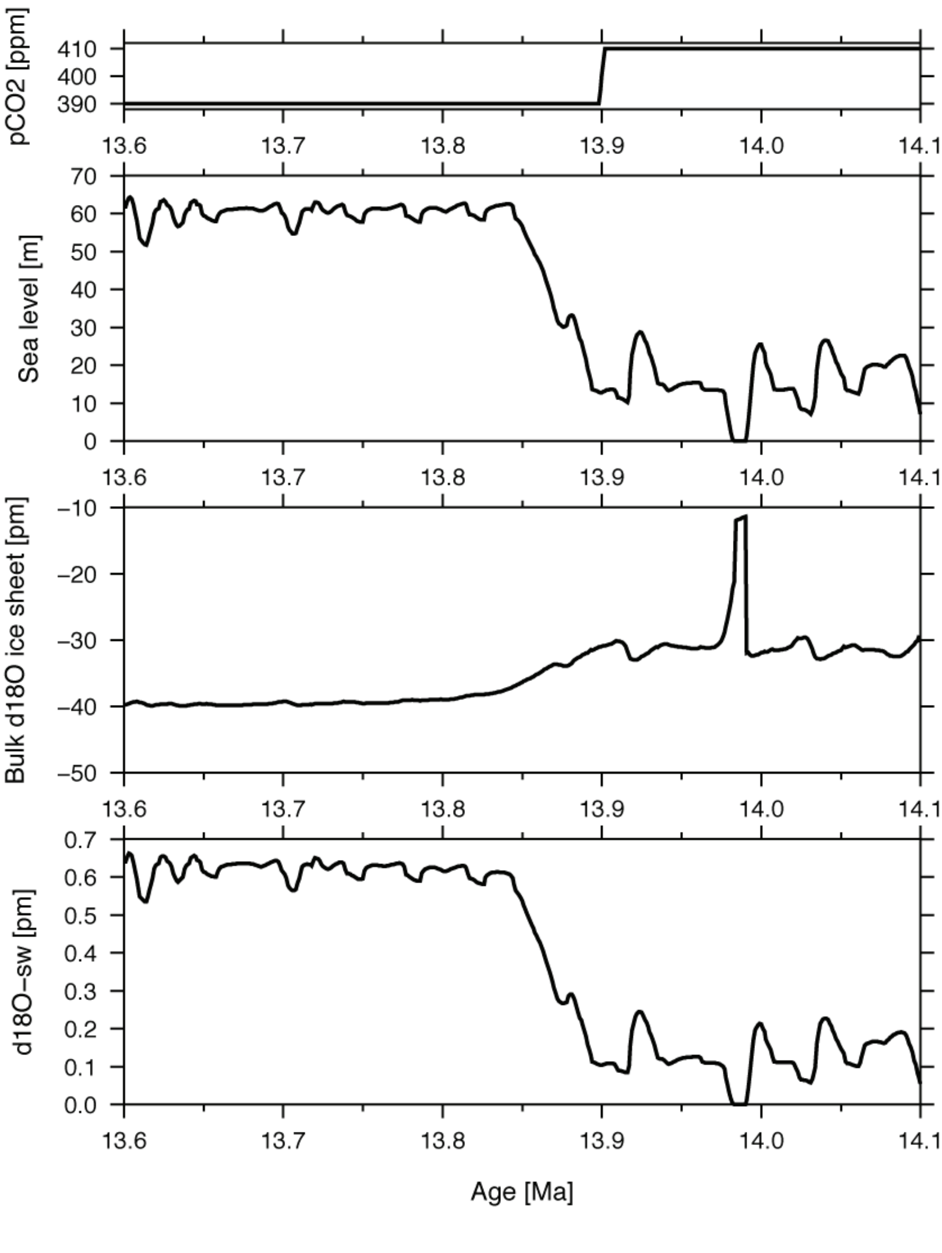

Figure A.12: *Modelled Middle Miocene transition.* ***(a)*** pCO_2 *(ppm),* ***(b)*** *ice volume in sea-level equivalents (m),* ***(c)*** *bulk* $\delta^{18}O_{\mathrm{ice}}$ *(‰) and* ***(d)*** $\delta^{18}O_{\mathrm{sw}}$ *(‰). Model is forced by parameterizations of Giovinetto and Zwally (1997) and Lhomme et al. (2005) (α_c=0.8 ‰/°C and β_δ=-11.2 ‰/km). Figure results from GMT-script* `plot_transition_MMIO.script`.

A.5.4 Bedrock

Target: test another ice-free initial bedrock topography

Bedrock: initial topography from *Van Tuyll et al.* (2007)

Forcing: constant pre-industrial pCO_2 and varying orbital parameters

Time period: last 500 ka

Here we show how to apply a different ice-free initial bedrock topography. Instead of the initial topography derived from the BEDMAP project (*Lythe et al.*, 2000), we use the bedrock stated in *Van Tuyll et al.* (2007). Although $\delta^{18}O_{ice}$ is computed, the focus is on the bedrock, so we will ignore the $\delta^{18}O_{ice}$ values.

Set-up and execute

Again, the main files to be modified are: `ice_driver.f90`, `cmp_ice.lnx`, `pcm_namelist.contrl`. The switches (`ism_switches.f90`) are not relevant in this recipe. In `pcm_namelist.contrl`, the pCO_2 forcing should be set to `co2scenario280ppm.asc`, the output path to `Example_bedrock`, for example, and the initial and final dates, such that the last 500 ka are computed (Fig. A.13a). The `cmp_ice.lnx`-file needs compile the proper executable file (`ice_bedrock.lnx`). The history file is again specified in `ice_driver.f90` (`history_bedrock.dat`). Here also the initial bedrock topography file is changed to `topog_vanTuyll_2007.asc`.

Output

Annual-mean results are saved in `history_bedrock.dat`. Ice-sheet geometry and temperatures, velocities and $\delta^{18}O_{ice}$ per time-step are written to `h0004*`-files. Examples of how to plot these variables in time can be found in recipes A.5.1 and A.5.3.

Post-processing

For post-processing a cross-section, the `proc_namelist.lnx` file should be adjusted and executed (Fig. A.13b). After compiling the `cmp_proc.lnx` file and the consequent `proc_bedrock.lnx`, `0` can be typed for a present-day cross-section. In the output directory the GMT script `temp_colour.script` contains the settings to create a temperature profile with *Van Tuyll et al.* (2007)'s initial bedrock topography (Fig. A.13c).

a

```
&contrl
orb_fname     = '../input/SOLCLI50Ma.BIN',
co2_fname     = '../input/CO2/co2scenario280ppm.asc',
hst_fpath     = '../output/Example_bedrock'
hst_froot     = 'h0002'
orb_origin    = 0.D0,
orb_dt        = 1000.D0,
date_initial = -0.5D0,
date_final    =  0.0D0,
/
```

b

```
&contrl
hst_fpath  ='../output/Example_bedrock'
hst_froot  = 'h0004'
proc_froot = 'pproc'
plot_froot = 'tplot'
/
```

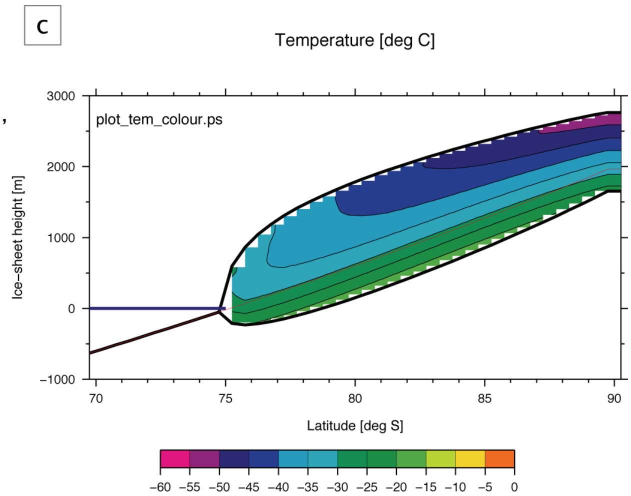

Figure A.13: *Post-processing files and temperature profile for Example 'Bedrock'.* ***(a)*** *The namelist file* `pcm_namelist.contrl` *contains a list of important boundary conditions. The direct access file for the orbital elements and the* $p\mathrm{CO_2}$ *file are located in the* `input`*-directory. All results are written to* `output/Example_bedrock`*. The last 500 ka are computed.* ***(b)*** *The* `proc_namelist.contrl`*-file states the paths and roots for post-processing. The model results to be processed are read from* `hst_fpath` *and will be written to the same directory with the specified roots.* ***(c)*** *Present-day temperature profile. Post-processing needs to be accomplished succesfully before producing this figure with* `temp_colour.script` *in GMT.*

A.6 Final remarks and acknowledgements

The ISCM is developed for a UNIX/LINUX environment, but can be used also under Windows or on a Macintosh, if there is a possibility to execute FORTRAN programs.

GMT (*Wessel and Smith*, 1988) is an open source mapping tool and can be downloaded from *http://gmt.soest.hawaii.edu*. On this website also an extensive manual can be found containing many examples showing how to plot what type of data.

MATLAB is a numerical computing environment and programming language. Among others, it allows for easy matrix manipulation and plotting of data. A large user community has its basis at the website *http://www.mathworks.com*, where many solutions to MATLAB problems can be found.

Finally, we would like to acknowledge Adriana Sima for all the work she performed on the ice-sheet model that was used as basis for the here described ISCM.

Index

Bibliography

Abels, H., F. Hilgen, W. Krijgsman, R. Kruk, I. Raffi, E. Turco, and W. Zachariasse (2005), Long-period orbital control on middle Miocene global cooling: Integrated statigraphy and astronomical tuning of the Blue Clay Formation on Malta, *Paleoceanography*, *20*, 2362–2367.

Adkins, J. F., and D. P. Schrag (2001), Pore fluid constraints on deep ocean temperature and salinity during the last glacial maximum, *Geophys. Res. Let.*, *28*, 771–774.

Archer, D. E., P. A. Martin, J. Milovich, V. Brovkin, G. Plattner, and C. Ashendel (2003), Model sensitivity in the effect of Antarctic sea ice and stratification on atmospheric $p\mathrm{CO_2}$, *Paleoceanogr.*, *18*, 1012, doi:10.1029/2002PA000760.

Arthern, R. J., D. P. Winebrenner, and D. G. Vaughan (2006), Antarctic snow accumulation mapped using polarization of 4.3-cm wavelength microwave emission, *J. Geophys. Res.*, *111*, D06,107, doi: 10.1029/2004JD005667.

Bartoli, G., M. Sarnthein, M. Weinelt, H. Erlenkeuser, D. Garbe-Schonberg, and W. Lea (2005), Final closure of Panama and the onset of Northern Hemisphere glaciation, *Earth Planet. Sci. Lett.*, *237*, 33–44.

Berger, A. L. (1978a), Long term variations of caloric insolation resulting from the Earth's orbital elements, *Quat. Res.*, *9*, 139–167.

Berger, A. L. (1978b), Long term variations of daily insolation and Quaternary climatic changes, *J. Atmos. Sci.*, *35*(12), 2362–2367.

Berggren, W. A., and C. D. Hollister (1974), Paleogeography, paleobiogeography, and the history of circulation of the Atlantic Ocean, in *Studies in Paleoceanography*, edited by W. W. Hay, pp. 126–186, Spec. Publ. Soc. Econ. Paleontol. Mineral. 20.

Bintanja, R. (1999), The Antarctic ice sheet and climate, Ph.D. thesis, University of Utrecht, The Netherlands.

Coplen, T. (1996), Editorial: More uncertainty than necessary, *Paleoceangraphy*, *11*, 369–370.

Coxall, H. K., P. A. Wilson, H. Pälike, C. H. Lear, and J. Backman (2005), Rapid stepwise onset of Antarctic glaciation and deeper calcite compensation in the Pacific Ocean, *Nature*, *443*, 53–57.

Crowley, T. J. (1992), North Atlantic Deep Water cools the Southern Hemisphere, *Paleoceanogr.*, *7*, 489–497.

Cuffey, K. (2000), Methodology for use of isotope forcings in ice sheet models, *Geophys. Res. Let.*, *27*, 3065–3068.

Cuffey, K., G. Clow, R. Alley, M. Stuiver, E. Waddington, and R. Saltus (1995), Large Arctic temperature change at the Wisconsin-Holocene glacial transition, *Science*, *270*, 455–458.

Dansgaard, W. (1964), Stable isotopes in precipitation, *Tellus*, *16*, 436–468.

DeConto, R., and D. Pollard (2003), Rapid Cenozoic glaciation of Antarctica induced by declining atmospheric CO_2, *Nature*, *42*, 245–249.

DeConto, R., D. Pollard, and D. Harwood (2007), Sea ice feedback and Cenozoic evolution of Antarctic climate and ice sheets, *Paleoceanogr.*, *22*, PA3214, doi:10.1029/2006PA001350.

DeConto, R., D. Pollard, P. Wilson, H. Pälike, C. Lear, and M. Pagani (2008), Thresholds for Cenozoic bipolar glaciation, *Nature*, *455*, 652–657.

Delaygue, G., J. Jouzel, V. Masson, R. Koster, and E. Bard (2000), Validity of the isotopic thermometer in central Antarctica: limited impact of glacial precipitation seasonality and moisture origin, *Geophys. Res. Let.*, *27*, 2677–2680.

Demicco, R., T. Lowenstein, and L. Hardie (2003), Atmospheric pCO_2 since 60 Ma from records of seawater pH, calcium, and primary carbonate mineralogy, *Geology*, *31*, 793–796.

Dowsett, H., J. Barron, and R. Poore (1996), Middle Pliocene sea surface temperatures: a global reconstruction, *Mar. Micropal.*, *27*, 13–26.

EPICA community members (2004), Eight glacial cycles from an Antarctic ice core, *Nature*, *429*, 623628.

Fairbanks, R. G., and R. K. Matthews (1978), The marine oxygen isotope record in Pleistocene coral, Barbados, West Indies, *Quat. Res.*, *10*, 181–196.

Flower, B., and J. Kennett (1995), Middle Miocene deep-water paleoceanography in the Southwest Pacific relations with East Antarctic ice-sheet development, *Paleoceanography*, *10*, 1095–1112.

Fox Maule, C., M. Purucker, N. Olsen, and K. Mosegaard (2005), Heat flux anomalies in Antarctica revealed by satellite magnetic data, *Science*, *309*, 464–467.

Fraedrich, K., H. Jansen, E. Kirk, and F. Lunkeit (2005), The Planet Simulator: towards a user friendly model, *Meteor. Zeitschrift*, *14*, 299–30.

Gallée, H., J. P. Van Yperselb, T. Fichefet, I. Marsiat, C. Tricot, and A. Berger (1992), Simulations of the Last Glacial Cycle by a coupled, sectorially averaged climate-ice sheet model: 2. Response to insolation and CO_2 variations, *J. Geophys. Res.*, *96*, 15,713–15,740.

Gat, J., W. Mook, and H. Meijer (2001), Atmospheric water, in *Environmental isotopes in the hydrological cycle, Principles and applications, Vol. 2*, edited by W. Mook, p. 7, UNESCO, Paris, France.

Giovinetto, M., and H. Zwally (1997), Areal distribution of the oxygen-isotope ratio in Antarctica: an assessment based on multivariate models, *Ann. Glaciol.*, *25*, 153–158.

Giovinetto, M., and H. Zwally (2000), Spatial distribution of net surface accumulation on the Antarctic ice sheet, *Ann. Glaciol.*, *31*, 171–178.

Gonfiantini, R. (1978), Standards for stable isotope measurements in natural compounds, *Nature*, *271*, 534–536.

Hansen, J., et al. (2008), Target atmospheric CO_2: Where should humanity aim?, *Atmos. Ocean. Phys., in press*, arXiv:0804.1126v2 [physics.ao-ph].

Hartmann, D. L. (1994), *Global Physical Climatology*, 411 pp., Academic Press, San Diego.

Haug, G. H., and R. Tiedemann (1998), Effect of the formation of the Isthmus of Panama on Atlantic Ocean thermohaline circulation, *Nature*, *393*, 673–676.

Haug, G. H., R. Tiedemann, R. Zahn, and A. C. Ravelo (2001), Role of Panama uplift on oceanic freshwater balance, *Geology*, *29*, 207–210.

Helsen, M. (2006), On the interpretation of stable isotopes in Antarctic precipitation, Ph.D. thesis, University of Utrecht, The Netherlands.

Helsen, M., R. van de Wal, and M. van den Broeke (2007), The isotopic composition of present-day Antarctic snow in a Lagrangian atmospheric simulation, *J. Climate*, *20*, 739–756.

Hill, D. J., A. M. Haywood, R. C. A. Hindmarsh, and P. J. Valdes (2007), Characterizing ice sheets during the pliocene: evidence from data and models, in *Deep-Time Perspectives on Climate Change: Marrying the Signal from Computer Models and Biological Proxies*, edited by M. Williams, A. Haywood, F. Gregory, and D. Schmidt, pp. 517–538, The Micropalaeontological Society, Special Publications, The Geological Society, London, United Kingdom.

Hillenbrand, C.-D., and G. Cortese (2006), Polar stratification: A critical view from the Southern Ocean, *Palaeogeogr., Palaeoclimatol., Palaeoecol.*, *242*, 240–252.

Hodell, D. A., and D. A. Warnke (2006), Climatic evolution of the Southern Ocean during the Pliocene epoch from 4.8 to 2.6 million years ago, *Quat. Sci. Rev.*, *10*, 205–214.

Hoffmann, G., J. Jouzel, and S. Johnsen (2001), Deuterium excess records from Greenland over the last millennium: Hints of a North Atlantic signal during the Little Ice Age, *J. Geophys. Res.*, *106*, 14,265–14,274.

Holbourn, A., W. Kuhnt, M. Schulz, and H. Erlenkeuser (2005), Impacts of orbital forcing and atmospheric carbon dioxide on Miocene ice-sheet expansion, *Nature*, *438*, 483–487.

Holbourn, A., W. Kuhnt, M. Schulz, J.-A. Flores, and N. Anderson (2007), Orbitally-paced climate evolution during the middle Miocene 'Monterey' carbon-isotope excursion, *Earth Planet. Sci. Lett.*, *261*, 534–550.

Huybrechts, P. (2004), Antarctica, in *Mass balance of the cryosphere: observations and modelling of contemporary and future changes*, edited by B. J.L. and A. Payne, pp. 491–523, Cambridge University Press, Cambridge, United Kingdom.

Huybrechts, P., T. Payne, and EISMINT Intercomparison Group (1996), The eismint benchmarks for testing ice-sheet models, *Ann. Glaciol.*, *23*, 1–12.

Huybrechts, P., D. Steinhage, F. Wilhems, and J. Bamber (2000), Balance velocities and measured properties of the Antarctic ice sheet from a new compilation of gridded data for modeling, *Ann. Glaciol.*, *30*, 52–60.

Imbrie, J., et al. (1993), On the structure and origin of major glaciation cycles: 2. The 100,000-year cycle, *Paleoceanography*, *8*, 699–735.

IPCC (2007), in *Climate Change 2007: The Scientific Basis. Contribution of Working Group 1 to the Fourth Assessment Report of the Intergovernmental Panel on Climate Change*, edited by S. Solomon, D. Qin, M. Manning, Z. Chen, M. Marquis, K. Averyt, M. Tignor, and H. Miller, p. 996, Cambridge University Press, Cambridge, United Kingdom and New York, NY, USA.

Jentsch, V. (1987), Cloud-ice-vapor feedbacks in a global climate model, in *Irreversible Phenomena and Dynamical Systems Analysis in Geosciences*, edited by C. Nicolis and G. Nicolis, p. 578, Reidel Publishing Company, Dordrecht, The Netherlands.

Jentsch, V. (1991), An energy balance climate model with hydrological cycle: 1. Model description and sensitivity to internal parameters, *J. Geophys. Res.*, *96*(D9), 17,169–17,179.

Kalnay, E., et al. (1996), The NCEP/NCAR 40-year reanalysis project, *Bull. Amer. Meteor. Soc.*, *77*, 437–470.

Keigwin, L. (1982), Isotopic paleoceanography of the Caribbean and East Pacific: Role of Panama uplift in late Neogene time, *Science*, *217*, 350–353.

Kleiven, H. F., E. Jansen, T. Fronval, and T. M. Smith (2002), Intensification of Northern Hemisphere glaciations in the circum Atlantic region (3.5–2.4 Ma) – ice-rafted detritus evidence, *Palaeogeogr., Palaeoclimatol., Palaeoecol.*, *184*, 213–223.

Klocker, A., M. Prange, and M. Schulz (2005), Testing the influence of the Central American seaway on orbitally forced Northern Hemisphere glaciation, *Geophys. Res. Lett.*, *32*, L03,703, doi: 10.1029/2004GL021564.

Kürschner, W., J. van der Burgh, H. Visscher, and D. Dilcher (1996), Oak leaves as biosensors of late Neogene and early Pleistocene paleoatmospheric CO_2 concentrations, *Mar. Micropaleontology*, *27*, 299–312.

Kürschner, W., Z. Kvacek, and D. Dilcher (2008), The impact of Miocene atmospheric carbon dioxide fluctuations on climate and the evolution of terrestrial ecosystems, *Proc. Nat. Acad. Sci. USA*, *106*, 449–453.

Larsen, H. C., A. D. Saunders, P. D. Clift, J. Beget, W. Wei, and S. Spezzaferri (1994), Seven million years of glaciation in Greenland, *Science*, *264*, 952–955.

Laskar, J., F. Joutel, and F. Boudin (1993), Orbital, prececcional, and insolation quantities for the Earth from -20 Myr to +10 Myr, *Astron. & Astrophys.*, *270*, 522–533.

Laskar, J., P. Robutel, F. Joutel, M. Gastineau, A. Correia, and B. Levrard (2004), A long-term numerical solution for the insolation quantities of the earth, *Astron. & Astrophys.*, *428*, 261–285.

Le Meur, E., and P. Huybrechts (1996), A comparison of different ways of dealing with isostasy: examples for modeling the Antarctic ice sheet during the last glacial cycle, *Ann. of Glaciol.*, *23*, 309–317.

Lear, C., H. Elderfield, and P. Wilson (2000), Cenozoic deep-sea temperatures and global ice volumes from Mg/Ca in benthic foraminiferal calcite, *Science*, *287*, 269–272.

Lear, C. H., T. R. Bailey, P. N. Pearson, H. K. Coxall, and Y. Rosenthal (2008), Cooling and ice growth across the Eocene-Oligocene transition, *Geology*, *36*, 251–254.

Lhomme, N. (2004), Modelling water istopes in polar ice sheets, Ph.D. thesis, University of British Columbia, Vancouver, Canada.

Lhomme, N., K. Clarke, and C. Ritz (2005), Global budget of water isotopes inferred from polar ice sheets, *Geophys. Res. Let.*, *32*, doi:10.1029/2005GL023774.

Lisiecki, L., and M. Raymo (2005), A Plio-Pleistocene stack of 57 globally distributed benthic δ^{18}O records, *Paleoceanography*, *20*, 522–533, doi:10.1029/2004PA001071.

Lowenstein, T., and R. Demicco (2006), Elevated Eocene atmospheric CO_2 and its subsequent decline, *Science*, *313*, 1928.

Lunt, D., G. Foster, A. Haywood, and E. Stone (2008a), Late Pliocene Greenland glaciation controlled by a decline in atmospheric CO_2 levels, *Nature*, *454*, 1102–1105.

Lunt, D., P. J. Valdes, A. M. Haywood, and I. Rutt (2008b), Closure of the Panama Seaway during the Pliocene: implications for climate and Northern Hemisphere Glaciation, *Climate Dyn.*, *30*, 1–18.

Lythe, M., D. Vaughan, and the BEDMAP Consortium (2000), *BEDMAP - bed topography of the Antarctic. 1:10,000,000 scale map*, British Antarctic Survey, Cambridge, United Kingdom.

Marshall, S., L. Tarasov, G. Clarke, and W. Peltier (2000), Glaciological reconstruction of the Laurentide Ice Sheet: physical processes and modeling challenges, *Canadian J. Earth Sci.*, *37*, 769–793.

Maslin, M. A., G. Haug, M. Sarnthein, and R. Tiedemann (1996), The progressive intensification of Northern Hemisphere Glaciation as seen from the North Pacific, *Geol. Rundsch.*, *85*, 452–465.

Masson-Delmotte, V., et al. (2008), A review of Antarctic surface snow isotopic composition: observations, atmospheric circulation, and isotopic modeling, *J. Climate*, *21*, 3359–3387.

MATLAB (2006), The MathWorks Inc., Natick, Massachusetts, USA.

Mercer, J. H. (1976a), Glacial history of southernmost South America, *Quat. Res.*, *6*, 125–166.

Mercer, J. H. (1976b), Cenozoic glaciation in the Southern Hemisphere, *Ann. Rev. Earth Planet. Sci.*, *11*, 99–132.

Miller, K., G. Mountain, J. Browning, M. Kominz, P. Sugarman, N. Christie-Blick, M. Katz, and J. Wright (1998), Cenozoic global sea level, sequences, and the New Jersey transect: results from coastal plan and continental slope drilling, *Rev. Geophys.*, *36*, 569–601.

Miller, K. G., et al. (2005), The Phanerozoic record of global sea-level change, *Science*, *310*, 1293–1298.

Mix, A. C., and W. F. Ruddiman (1984), Oxygen-isotope analysis and Pleistocene ice volumes, *Quat. Res.*, *21*, 1–20.

Molnar, P. (2008), Closing of the Central American Seaway and the Ice Age: A critical review, *Paleoceanogr.*, *23*, PA2201, doi:10.1029/2007PA001574.

Mudelsee, M., and M. E. Raymo (2005), Slow dynamics of the Northern Hemisphere Glaciation, *Paleoceanogr.*, *20*, PA4022.

Myhre, G., E. J. Highwood, K. P. Shine, and F. Stordal (1998), New estimates of radiative forcing due to well mixed greenhouse gases, *Geophys. Res. Lett.*, *25*, 2715–2718.

Nisancioglu, K. H., M. E. Raymo, and P. H. Stone (2003), Reorganization of Miocene deep water circulation in response to the shoaling of the Central American Seaway, *Paleoceanogr.*, *18*, 1006, doi:10.1029/2002PA000767.

North, G. R. (1975), Theory of Energy Balance Climate Models, *J. Atmos. Sci.*, *32*, 2033–2043.

Oerlemans, J. (2001), Glaciers and climate change, in *Modeling glacier mass balance*, edited by J. Oerlemans, chap. 4, Balkema, The Netherlands.

Oerlemans, J. (2002), Global dynamics of the Antarctic ice sheet, *Clim. Dynam.*, *19*, 85–93.

Oerlemans, J. (2004), Antarctic ice volume and deep-sea temperature during the last 50 Myr: a model study, *Ann. Glaciol.*, *39*, 13–19.

Oerlemans, J., and C. van der Veen (1984), *Ice sheets and climate*, p. 217, D. Reidel Publishing Company, Dordrecht, The Netherlands.

Pagani, M., J. C. Zachos, K. H. Freeman, B. Tipple, and S. Bohaty (2005), Marked decline in atmospheric carbon dioxide concentrations during the Paleogene, *Science*, *309*, 600–603.

Pälike, H., R. D. Norris, J. O. Herrle, P. A. Wilson, H. K. Coxall, C. H. Lear, N. J. Shackleton, A. K. Tripati, and B. S. Wade (2006), The heartbeat of the Oligocene Climate System, *Science*, *314*, 1894–1898.

Payne, A. J., and P. W. Dongelmans (1997), Self-organization on the thermomechanical flow of ice sheets, *J. Geophys. Res.*, *106*, 12,219–12,233.

Pearson, P. N., and M. R. Palmer (2000), Atmospheric carbon dioxide concentrations over the past 60 million years, *Nature*, *406*, 695–699.

Pekar, S. F., and R. M. DeConto (2006), High-resolution ice-volume estimates for the early Miocene: Evidence for a dynamic ice sheet in Antartica, *Paleogeography, Paleoclimatology, Paleoecology*, *231*, 101–109.

Pekar, S. F., N. Christie-Blick, M. A. Kominz, and K. G. Miller (2002), Atmospheric carbon dioxide concentrations over the past 60 million years, *Geology*, *30*, 903–906.

Petit, J. R., et al. (1999), Climate and atmospheric history of the past 420,000 years from the Vostok ice core, *Nature*, *399*, 429–436.

Pillans, B., and T. Naish (2004), Defining the Quaternary, *Quat. Sci. Rev.*, *23*, 2271–2282.

Pollard, D. (1982), A simple ice sheet model yields realistic 100 kyr glacial cycles, *Nature*, *296*, 334–338.

Pollard, D. (1983a), A coupled climate-ice sheet model applied to the Quaternary ice ages, *J. Geophys. Res.*, *88*(C12), 7705–7718.

Pollard, D. (1983b), Ice-age simulations with a calving ice-sheet model, *Quat. Res.*, *20*, 30–48.

Pollard, D., and R. M. DeConto (2005), Hysteresis in Cenozoic Antarctic ice-sheet variations, *Glob. Planet. Change*, *45*, 9–21.

Prange, M. (2008), The low-resolution CCSM revisited: new adjustments and a present-day control run, *Ocean Sci.*, *4*, 151–181.

Prange, M., and M. Schulz (2004), A coastal upwelling seesaw in the Atlantic Ocean as a result of the closure of the Central American Seaway, *Geophys. Res. Lett.*, *31*, L17,207, doi: 10.1029/2004GL020073.

Quinn, T., S. Tremaine, and Duncan (1991), A 3 million year integration of the Earths orbit, *Astron. J.*, *101*(6), 2287–2305.

Raffi, I., J. Backman, E. Fornaciari, H. Pälike, D. Rio, L. Lourens, and F. Hilgen (2006), A review of calcareous nannofossil astrobiochronology encompassing the past 25 million years, *Quat. Sc. Rev.*, *25*, 31133137.

Raymo, M. E. (1994a), The Himalayas, organic carbon burial, and climate in the Miocene, *Paleoceanography*, *9*, 399–404.

Raymo, M. E. (1994b), The initiation of Northern Hemisphere Glaciation, *Ann. Rev. Earth Planet. Sci.*, *22*, 353–383.

Raymo, M. E., B. Grant, M. Horowitz, and G. H. Rau (1996), Mid-Pliocene warmth: stronger greenhouse and stronger conveyor, *Mar. Micropaleontology*, *27*, 313–326.

Raymo, M. E., L. Lisiecki, and K. Nisancioglu (2006), Plio-Pleistocene ice volume, Antarctic climate, and the global δ^{18}o record, *Science*, *313*, 492–495.

Rebesco, M., and A. Camerlenghi (2008), Late Pliocene margin development and mega debris flow deposits on the Antarctic continental margins: Evidence of the onset of the modern Antarctic Ice Sheet?, *Palaeogeography, Palaeoclimatology, Palaeoecology*, *260*, 149167.

Royer, D. L. (2006), CO_2-forced climate thresholds during the Phanerozoic, *Geochimica et Cosmochimica Acta*, *70*, 56655675.

Royer, D. L. (2008), Linkages between CO_2, climate and evolution in deep time, *Proc. Nat. Acad. Sci. USA*, *105*, 407–408.

Royer, D. L., S. L. Wing, D. J. Beerling, D. W. Jolley, P. L. Koch, L. J. Hickey, and R. A. Berner (2001), Paleobotanical evidence for near present-day levels of atmospheric CO_2 during part of the Tertiary, *Science*, *292*, 2310–2313.

Schrag, D. P., G. Hampt, and D. W. Murray (1996), Pore fluid constraints on the temperature and oxygen isotopic composition of the Glacial Ocean, *Science*, *272*, 1930–1932.

Sellers, W. D. (1970), A global climate model based on the energy balance of the earth-atmosphere system, *J. Appl. Meteorol.*, *8*, 392–400.

Shackleton, N. J. (1974), Attainment of isotopic equilibrium between ocean water and the benthoic foraminifera genus Unigerina: isotopic changes in the ocean during the last glacial, *Cent. Natl. Sci. Colloq. Int.*, *219*, 203–209.

Shackleton, N. J. (1986), Paleogene stable isotope events, *Palaeogeography, Palaeoclimatology, Palaeoecology*, *57*, 9–102.

Shackleton, N. J. (2000), The 100,000-year ice-age cycle identified and found to lag temperature, carbon dioxide, and orbital eccentricity, *Science*, *289*, 1897–1902.

Shevenell, A., J. P. Kenneth, and D. W. Lea (2004), Middle Miocene Southern Ocean cooling and Antarctic cryosphere expansion, *Science*, *305*, 1766–1770.

Shevenell, A., J. P. Kenneth, and D. W. Lea (2008), Middle Miocene ice sheet dynamics, deep-dea temperatures, and carbon cycling: A Southern Ocean perspective, *Geochem. Geophys. Geosyst.*, *9*, doi:10.1029/2007GC001736.

Shevenell, A. E., and J. P. Kennett (2004), Paleoceanographic change during the Middle Miocene climate revolution: an Antarctic stable isotope perspective, in *The Cenozoic Southern Ocean: Tectonics, Sedimentation and Climate Change between Australia and Antarctica. Geophysical Monograph Series, vol. 151*, edited by N. Exon, J. Kennett, and M. Malone, American Geophysical Union, Washington, DC, USA.

Sima, A. (2005), Modeling oxygen isotopes in ice sheets linked to Quaternary ice-volume variations, Ph.D. thesis, University of Bremen, Germany.

Sima, A., A. Paul, M. Schulz, and J. Oerlemans (2006), Modeling the oxygen-isotope composition of the North American Ice Sheet and its effect on the isotopic composition of the ocean during the last glacial cycle, *Geophys. Res. Let.*, *33*, doi:10.1029/2006GL026923.

Staley, D. O., and G. M. Jurica (1970), Flux emissivity tablesfor water vapor carbon dioxide and ozone, *J. Appl. Meteorol.*, *9*, 365–372.

Steph, S., R. Tiedemann, M. Prange, J. Groeneveld, D. Nürnberg, L. Reuning, M. Schulz, and G. Haug (2006), Changes in Caribbean surface hydrography during the Pliocene shoaling of the Central American Seaway, *Paleoceanogr.*, *21*, PA4221, doi:10.1029/2004PA001092.

Stephens, B. B., and R. F. Keeling (2000), The influence of Antarctic sea ice on glacial-interglacial CO_2 variations, *Nature*, *404*, 171–174.

Sugden, D. E. (1996), The East Antarctic Ice Sheet: unstable ice or unstable ideas?, *Transact. Inst. British Geogr.*, *21*, 443–454.

Toggweiler, J. R. (2008), Origin of the 100,000-year timescale in Antarctic temperatures and atmospheric CO_2, *Paleoceanography*, *23*, PA2211.

Van Tuyll, C., R. van de Wal, and J. Oerlemans (2007), The response of a simple Antarctic ice flow model to temperature and sea level fluctuations over the Cenozoic era, *Ann. of Glaciol.*, *46*, 69–77.

Waelbroeck, C., L. Labeyrie, E. Michel, J. C. Duplessy, J. F. McManus, K. Lambeck, E. Balbon, and M. Labracherie (2002), Sea-level and deep water temperature changes derived from benthic foraminifera isotopic records, *Quat. Science Rev.*, *21*, 295–305.

Wang, Z., and L. A. Mysak (2000), A simple coupled atmosphere-ocean-sea ice-land surface model for climate and paleoclimate studies, *J. Climate*, *13*, 1150–1172.

Wessel, P., and W. Smith (1988), *Generic Mapping Tool*, National Science Foundation and GNU General Public License, Soest, Hawaii, USA.

Weyl, P. K. (1968), The role of the oceans in climatic change: A theory of the ice ages, in *Causes of Climate Change*, edited by J. M. Mitchell, pp. 37–62, Meteorol. Monogr.

Whitehead, J. M., and S. M. Bohaty (2003), Pliocene summer sea surface temperature reconstruction using silicoflagellates from Southern Ocean ODP Site 1165, *Paleoceanogr.*, *18*, 1075, doi: 10.1029/2002PA000829.

Zachos, J. C., L. D. Stott, and K. C. Lohmann (1994), Evolution of early Cenozoic marine temperatures, *Paleoceanogr.*, *9*, 353–387.

Zachos, J. C., M. Pagani, L. Sloan, E. Thomas, and K. Billups (2001), Trends, rythms, and aberrations in global climate 65 Ma to present, *Science*, *292*, 686–693.

Zachos, J. C., G. R. Dickens, and R. E. Zeebe (2008), An early Cenozoic perspective on greenhouse warming and carbon-cycle dynamics, *Nature*, *451*, 279–283.

Zwally, H. J., M. Giovinetto, M. Craveb, V. Morgan, and I. Goodwin (1998), Areal distribution of the oxygen-isotope ration in Antarctica: comparison of results based on field and remotely sensed data, *Ann. Glaciol.*, *27*, 583–590.